DOKUZ EYLÜL UNIVERSITY
GRADUATE SCHOOL OF NATURAL AND APPLIED SCIENCES

COMPREHENSIVE DESING FOR CONTROLLING AND MODELLING OF AN OFF-GRID PV SYSTEM AT MAXIMUM POWER OUTPUT

by
Sinan KIVRAK

August, 2008
İZMİR

COMPREHENSIVE DESING FOR CONTROLLING AND MODELLING OF AN OFF-GRID PV SYSTEM AT MAXIMUM POWER OUTPUT

A Thesis Submitted to the
Graduate School of Natural and Applied Sciences of Dokuz Eylül University
In Partial Fulfillment of the Requirements for the Degree of Doctor of Philosophy in Electric and Electronic Engineering

by
Sinan KIVRAK

August, 2008
İZMİR

Ph.D. THESIS EXAMINATION RESULT FORM

We have read the thesis entitled **"COMPREHENSIVE DESING FOR CONTROLLING AND MODELLING OF AN OFF-GRID PV SYSTEM AT MAXIMUM POWER OUTPUT"** completed by **SİNAN KIVRAK** under supervision of **PROF. DR. MUSTAFA GÜNDÜZALP** and we certify that in our opinion it is fully adequate, in scope and in quality, as a thesis for the degree of Doctor of Philosophy.

Prof. Dr. Mustafa GÜNDÜZALP
Superviser

Prof. Dr. Haldun KARACA
Committee Member

Prof. Dr. Ali GÜNGÖR
Committee Member

Jury member

Jury member

Prof.Dr. Cahit HELVACI
Director
Graduate School of Natural and Applied Sciences

ACKNOWLEDGEMENT

I wish to express deep gratitude to all people and firms that contributed to the work presented in this thesis. Particularly, I thank my advisor, Prof Dr. Mustafa GÜNDÜZALP, for his guidance and unwavering support during my Ph. D. studies. I would like to thank Prof. Dr. Ali GÜNGÖR, and Prof Dr. Haldun KARACA for serving on my doctoral committee and providing helpful comments. Besides, I am sincerely grateful to Prof Dr. İrfan Alan, Assoc. Prof. Dr. E. Şahin ÇONKUR, H. Kemal ÖZTÜRK, Serdar İPLİKCİ, Asst. Prof. Dr. Ahmet ÖZEK and Selim BÖREKCİ for their help during my research.

I am deeply debited to all the team members from Temiz Enerji Evi, VEGA MAKINE, KAYACANLAR MAKINE, TÜRKER PRINT and PAMSOLAR AS that made the completion of the project possible.

I am grateful to my parents and family who always stand behind me and particular to my mother and mother in law for their support and blessing.

Finally, I would like to express a great amount of gratitude to my wife for being most supportive of my efforts.

Sinan KIVRAK

This work has been supported by the Milli Prodüktivite Merkezi.

COMPREHENSIVE DESING FOR CONTROLLING AND MODELLING OF AN OFF-GRID PV SYSTEM AT MAXIMUM POWER OUTPUT

ABSTRACT

Using conventional energy sources causes air pollution and global warming at the present time. Many countries have conflict in sharing fossil-fuel-based sources. However, the sun has been a major energy source since the world exists. The energy that comes from the sun is to such a degree that it makes it meaningless to fight for the energy. The only thing to be considered is to find how to use it properly.

Today, the solar energy is used widely in water boiling-heating and electricity generation. We are not interested in boiling and heating water, but the sun tracker that was designed and constructed in this study can be used for such operations.

It is well known that the efficiency of photovoltaics that produces electric energy from solar energy is significantly low. The cost of photovoltaic systems is quite high. Considering all these disadvantages, doing work on photovoltaic systems that gets the most efficient results will decrease the cost of the systems while it increases the interest in these sources.

This dissertation focuses on three significant subjects:

First, the maximum power point of PV (Photovoltaic) panels was tracked using the linear region characteristic of semiconductor switches on a dc-dc chopper (Boost converter). Being so different from classical methods, this work presents a simple method that determines maximum power point without adding any additional circuit to power systems. In this method, the real MPP (Maximum Power Point) of the system is always determined in a precise manner by eliminating local MMPs. Being stable, fast and compatible with all the systems will increase its widespread usage.

Second, a new tracker classification was developed considering advantages and disadvantages of existing trackers. Open and closed-loop methods were implemented separately on the prototype with a microcontroller. In open-loop, sun tracking is achieved by using geographical location, date and time information while sun tracking is achieved in closed-loop by evaluating the panel open circuit voltage. In addition, fixed and two-axis trackers were compared in performance with the measurements taken in sunny days. The correctness of the results was verified by means of a computer simulation. An important aspect of the work is that the tracker system in this prototype was implemented in an industrial type PV system with 1.75 kWp power.

Third, battery types were mentioned shortly. The structure of the battery types and various charging techniques used widely in today's PV systems were explained in detail. After the control system determines the maximum power level, batteries are fed from the chopper in the way that they get the most appropriate power from PV using various charging techniques.

Keywords: Photovoltaic Panel, MPPT (Maximum Power Point Tracking), Sun Tracking, Boost Converter, Battery Charging.

ŞEBEKEDEN BAĞIMSIZ BİR PV SİSTEMİNİN MAKSİMUM ÇIKIŞ GÜCÜNDE ÇOK YÖNLÜ KONTROL VE MODELLENME DİZAYNI

ÖZ

Günümüzde fosil tabanlı geleneksel yakıtların kullanımı hava kirliliğine ve küresel ısınmaya sebep olurken bu yakıtların paylaşımı ülkeler arasında savaşlara sebep olmaktadır. Halbuki dünya var olduğundan bu yana en önemli enerji kaynağı güneştir. Güneşten gelen enerji, enerji için yapılan savaşları anlamsız kılacak kadar çoktur. Yeter ki ondan uygun şekilde faydalanalım.

Günümüzde güneş enerjisi yaygın olarak su ısıtılmasında, kaynatılmasında ve elektrik üretiminde kullanılmaktadır. Su ısıtılması ve kaynatılması bizim çalışmamızın dışındadır fakat çalışmamızda tasarlanan ve kurulan güneş izleyicisi prototipi ve kontrol sistemi bu işlemler için kullanılabilir.

Bilindiği üzere güneş enerjisinden elektrik üreten fotovoltaiklerin enerji dönüşüm verimi oldukça düşüktür. Ayrıca bugünkü şartlarda fotovoltaik sistem maliyetleri çok yüksektir. Bu gibi dezavantajlar göz önünde bulundurularak fotovoltaik sistemlerden en verimli şekilde faydalanılacak çalışmaların yapılması sistem maliyetlerini düşürürken bu kaynaklara olan ilgiyi artıracaktır.

Bu amaçla yapılan çalışmamız 3 önemli konu üzerinde odaklanmıştır.

İlk olarak; DC-DC bir kıyıcının yarı iletken anahtarının lineer bölgesindeki çalışma karakteristiğinden faydalanılarak PV panellerin maksimum güç noktası takibi yapılmıştır. Bu çalışma klasik yöntemlerden çok farklı olarak güç sistemlerine ilave devre eklemeden mevcut yapı üzerinde maksimum güç noktasını bulmayı sağlayan basit bir yöntem sunmaktadır. Bu yöntemde yerel MPP'ler elimine edilerek sistemin gerçek MPP'si kesin olarak bulunmaktadır. Kararlılığı, hızlı oluşu ve her sisteme uygulanabilirliği bu yöntemin kullanılmasını yaygınlaştıracaktır.

İkinci olarak mevcut izleyicilerin avantaj ve dezavantajları üzerinde durulup yeni bir izleyici sınıflandırılmasına gidilmiştir. Mikrodenetleyici kontrollü prototip üzerinde kapalı çevrim ve açık çevrim metotları ayrı ayrı uygulanmıştır. Açık çevrimde; coğrafi konum, tarih ve zaman bilgisinin kullanılması ile güneş takibi yapılırken, kapalı çevrim yönteminde panel açık devre voltajının değerlendirilmesi ile güneş takibi gerçekleştirilmiştir. Ayrıca sabit ile iki eksenli izleyiciler, güneşli günlerde yapılan ölçümler ile performans açısından karşılaştırılmış olup sonuçların doğruluğu simülasyon ile ispatlanmıştır. En önemlisi ise bu prototip çalışmasındaki izleyici sisteminin 1.75kWp'lik sanayi tipi bir PV sisteminde uygulanmasıdır.

Üçüncü adımda ise; Batarya çeşitlerinden kısaca bahsedilirken günümüzdeki PV sistemlerinde yaygın olarak kullanılan kurşun asit akülerin yapısı ve çeşitli şarj teknikleri detaylı bir şekilde anlatılmıştır. Kontrol sistemi maksimum güç tespitini yaptıktan sonra çeşitli şarj teknikleri kullanarak aküler PV'den en uygun gücü çekecek şekilde kıyıcıdan beslenmiştir.

Anahtar kelimeler: Fotovoltaik Panel, MPPT, Güneş Takibi, Bust Konvertör, Akü Şarjı.

CONTENTS

Page

CHAPTER ONE
INTRODUCTION

1.1 Solar Energy

Many countries produce electricity by burning fossil fuel such as coal, oil, and natural gas. Also some of them use nuclear fuel as an energy source. Using these fuels causes pollution in various forms in the environment and atmosphere such as nuclear waste, carbon dioxide which is an important component of greenhouse gas emissions, nitrogen oxide, and sulfur dioxide. Burning these fuels causes acid rain, smog, and the global warming.

Increase in oil price and oil shortage were firstly seen in the 1970s, today oil price approaches to 140$ per gallon and it is estimated that its price will rise to over 200 $. Furthermore, petrol can be embargoed or controlled by any one nation. Therefore, renewable energy sources are getting more and more important for all countries.

The surface temperature of the sun is 5800 K and it radiates 1.6 x 10^7 watts of power per square meter from its surface at all wavelengths. The sun is almost 150 million kilometers from the Earth, the energy density per unit time of the sunlight reaching the upper atmosphere of the Earth is 1366 W/m^2 (solar constant). Solar intensities are commonly normalized with respect to full sun solar radiation at sea level with average humidity and aerosol particulate concentration atmospheric conditions commonly referred to as “air mass 1.5” (*AM 1.5*). The Air Mass is a measure of how absorption in the atmosphere affects the spectral content and intensity of the solar radiation reaching the Earth’s surface. The Air Mass number is given by;

$$Air\ Mass = 1/\cos\theta \text{ or defined as; } Air\ Mass = \sqrt{1+(S/H)^2}$$

Where θ is the angle of incidence and S is the length of a shadow cast by an object of height H. The solar radiation at AM1.5 is approximately 1000 W/m^2, significantly less than the 1350 W/m^2 of radiant energy bathing the earth at AM0 (on the outer

edge of the earth's atmosphere). The sun radiates more energy to the earth in one second than the total energy used during one year.

The sun is the most important energy source which is environmentally friendly. It makes no contribution to air, water, or noise pollution, does not pose a health hazard, and produces no harmful waste products to the environment. The combustion of fossil fuels releases more than 6 billion tons of carbon into the atmosphere each year. Clean energy sources, such as solar energy, can help meet rising energy demands while reducing pollution and preventing damage to the environment and public health at the same time. For example; a 1-kilowatt home solar system will prevent approximately 77.11 kg of coal from being burned, 136 kg of CO_2 from being released into the atmosphere and 397.5 liter of water from being consumed each month! *http://www.nineplanets.org/sol.html, August 4, 2006.*

Photovoltaic cells have been used in order to generate electric power since 1950s. Photovoltaic (PV) arrays produce electric power directly from sunlight with no fossil-fuel consumption, no noise, and posing no health and environmental hazards. PV systems can help reduce dependence on fossils fuels. Therefore, they can help to reduce emissions, and financial risks associated with large capacity additions and fuel price fluctuations. PV cells are being used in space and terrestrial applications where they are economically competitive with alternative sources. This fact, together with the continuing decline in the world's conversional sources of energy, implies a promising role for PV power-generation systems in the near future.

Present PV cells have not been very efficient yet. Today's commercial PV cells convert only about 14 to 18 percent of the radiant energy into electrical energy. Therefore, as in this thesis, optimum power harvesting methods could be applied for taking most energy from PVs. Fossil fuel plants, on the other hand, convert from 30-40 percent of their fuel's chemical energy into electrical energy. The cost of one kilowatt-hour electricity produced from PV cells is at the present time three to four times higher than the cost of the electricity produced from conventional sources. However, PV cells make sense for many uses today, such as providing power in

remote areas or other areas where electricity is difficult to provide. *http:// sa.colorado.edu.essencetextssolar.htm.*

The cost of the 1.75kWp Off-Grid PV system setup in our country is 16050$+VAT (VAT=1.18) as seen in Table 2.1. Amortization of a PV system set up in the country where the cost of electricity per kW is 16 cent including all taxes can be calculated in this way. A system with 1.75kWp produces approximately 10kWh energy per day, 3650 kWh per year. If the energy was bought from the network, the amount of charge paid for the energy per year would be 3650x0.16=584$. Consequently, amortization time for a system that produces energy at the value of 584$ is 16050$x1.18/584$=32 years.

However, if we take the replacement of the batteries into account every 5 years (the batteries should be replaced 6 times within 32 years), considering battery values in Table 2.2, the cost of the battery 2640$/5=528$ per year is added to amortization time. Therefore, amortization time turns out to be very long. Nevertheless, if temporary 100% increase in lead prices due to lead crisis is lifted and better batteries with 10 year life are used, amortization time will be reduced to a reasonable value.

It should be noted that off-grid systems are used in areas where there is no electricity network. If the cost of getting energy from the network is assumed to be the cost of the system, the cost of the PV system is reduced to almost zero. For example, the cost of the wiring to get energy from the network to the farm in which the 1.75kWp Off-Grid PV system was constructed in the countryside is 16840$+VAT.

Furthermore, the PV industry has demonstrated high growth rates over recent years, 30% per year in the late 1990s. By the year 2010, it is assumed that modules will cost 1.50 €/Wp and systems 3.00 €/Wp. (*V. Salas, E. Olı´as, A. Barrado, A. La´zaro 2005)*

Nowadays, the price of Off-Grid PV system components per watt in Turkey was illustrated in Table 1.1

Tablo 1.1 The Cost of PV system component per Watt

Component of PV System	The Cost Per Watt
PV Panel(polycrystal)	5.43 $
Charge Regulator	0.16 $
Battery (Gel)	0.18 $
Inverter(sinus)	0.48 $
Tracker(two-axis)	1.00 $
Total	7.25 $

The cost of Off-Grid PV system for 1.75kWp in Turkey was given Table 1.2. This system has both two days autonomy and two-axis tracker.

Tablo 2.2 The cost of 1.75kWp Off-Grid PV system

Component Of PV System	Pcs	The Cost Components/Unit	Total	Percentage %
175Wp Polycrystal Panel	10	950 $	9500$	59.19
12-24V/40A Charge Regulator	2	155$	310$	1.93
12/230A AGM Battery	6	440$	2640$	16.44
Two-axis Tracker	1	2000$	2000$	12.46
2500W modified Inverter	2	300$	600$	3.73
Others(cable, fuse, transportation etc.)	1	1000$	1000$	6.23
TOTAL			16050$	

According to Enslin J. H. R, (1991-95), in a PV system, the PV array contributes to 57% of the total cost, with the battery storage the second major contributor, at 30%. Other components in the systems, i.e., inverters and regulators/maximum power point tracker (MPPT) contribute to a smaller portion, at 7%. The cabling and installation costs can also form another 6% of the total capital cost.

Our work and the work mentioned above show that the cost of off-grid PV systems between 1991-1995 and the cost in Turkey at the present time are almost the same.

Today renewable energy sources and among them photovoltaic panels is now widely used. PV panel output power varies depending mainly on the level of solar radiation and ambient temperature corresponding to a specific weather condition.

An important consideration in achieving high efficiency in PV power systems is to match the PV source and load impedances properly for any weather conditions, thus usage of maximum power is obtained.

1.2 Characteristic of the Solar Cell

Photovoltaic energy conversion in solar cells consists of two essential steps. First, absorption of light generates an electron-hole pair. The electron and hole are then separated by the structure of the device - electrons to the negative terminal and holes to the positive terminal - thus generating electrical power. A solar cell is simply a semiconductor diode that has been carefully designed and constructed to efficiently absorb and convert light energy from the sun into electrical energy. A simple conventional solar cell structure is depicted in Figure 1.1.

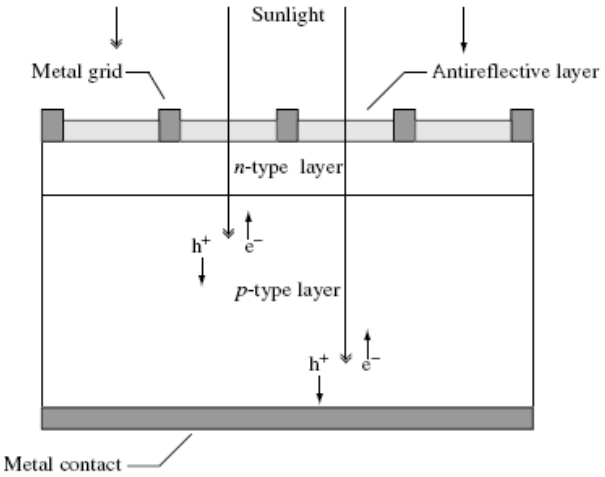

Figure 1.1 A schematic of a simple conventional solar cell. Creation of electron–hole pairs, respectively, is depicted. Luque A. & Hegedus S. (2003)

Sunlight is incident from the top on the front of the solar cell. A metallic grid forms one of the electrical contacts of the diode and allows light to fall on the semiconductor between the grid lines and thus be absorbed and converted into

electrical energy. An antireflective layer between the grid lines increases the amount of light transmitted to the semiconductor. The semiconductor diode is fashioned when an *n*-type semiconductor and a *p*-type semiconductor are brought together to form a metallurgical junction. *Luque A. & Hegedus S. (2003)*

$$I = I_{sc} - I_{o1}(e^{qV/kT} - 1) - I_{o2}(e^{qV/2kT} - 1) - \frac{(V + IR_S)}{R_{Sh}}$$

In the given above formula which was obtained from two diode model, k is the Boltzmann constant, T is the absolute temperature, q is the electron charge, and V is the voltage at the terminals of the cell, I_{SC} is the short-circuit current when there are no parasitic resistances. I_{o1} is the dark saturation current due to recombination in the quasi-neutral regions, I_{o2} is the dark saturation current due to recombination in the space-charge region. R_{Sh} is shunt resistance which has no effect on the short circuit current, but reduces the open-circuit voltage. R_S is the series resistance which has no effect on the open-circuit voltage, but reduces the short-circuit current. (*Markvart T. & Castafier L. 2003)*

From the above formula, it is apparent that a solar cell can be modeled by an ideal current source (I_{SC}) in parallel with two diodes (1, 2), and series and parallel (shunt) parasitic resistors as shown in Figure 1.2. Note that the direction of the current source is opposed to the current flow of the diodes that is, it serves to forward-bias the diodes.

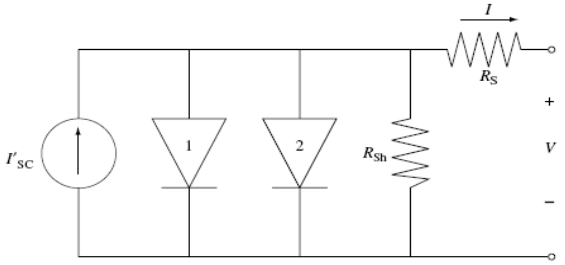

Figure 1.2 Solar cell circuit model with the parasitic series and shunt resistance

In Figure1.3; I-V characteristic and maximum voltage and current (V_{mp} and I_{mp}) points of a PV cell is illustrated.

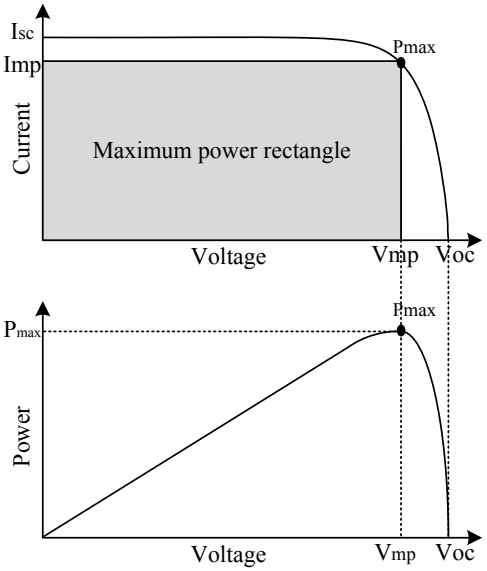

Figure.1.3 Demonstrating PV's voltage versus current curve and maximum power is equal to the shaded rectangle.

The I_{sc} and V_{oc} values can be measured to be short circuit and open circuit test respectively but the I_{mp} and V_{mp} can be found (basically adjusting rheostat) with the help of special test and circuits. The I_{mp} and V_{mp} are the current and voltage produced under maximum power conditions and is more representative than I_{sc} and V_{oc} of operational performance. The Fill Factor (FF) is performance parameter, and commonly used to collectively describe the degree to which V_{mp} matches V_{oc} and I_{mp} matches I_{sc}. Ideally FF value is required to be near 1 but generally is 0.8 or 0.9. Fill factor efficiency are given by the following formulas:

$$FF = \frac{V_{max} \times I_{max}}{V_{oc} \times I_{sc}}, \quad \eta = \frac{P_{mp}}{P_{in}} = \frac{FF \times V_{oc} \times I_{sc}}{P_{in}} \quad \textit{Master, Gilbert M. (2004)}$$

The power of solar cells depends on the cell temperature and it is called temperature coefficient. Fore example, for crystalline silicon cells, Isc increases by approximately 0.05%, Voc drops by about 0.37% for each degree Celsius increase in cell temperatures. Similarly, MPP slides slightly upwards and toward the left with a decrease in maximum power about 0.5% for each degree Celsius increase in cell temperatures. Figure 1.4 a, b, c, d show respectively; the typical P-V curve and I-V curve with respect to change of irradiation, and P-V curve and I-V curve with respect to change of temperature.

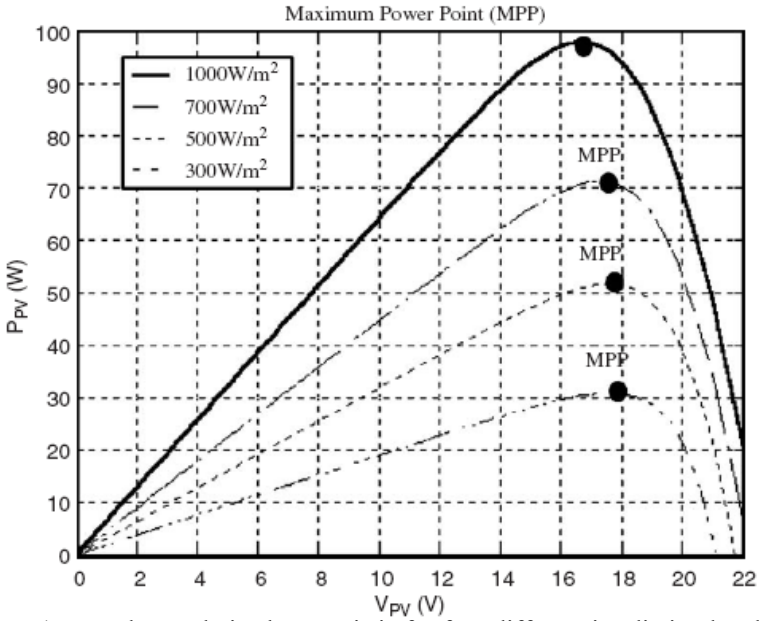

a.) P–V photovoltaic characteristic for four different irradiation levels.

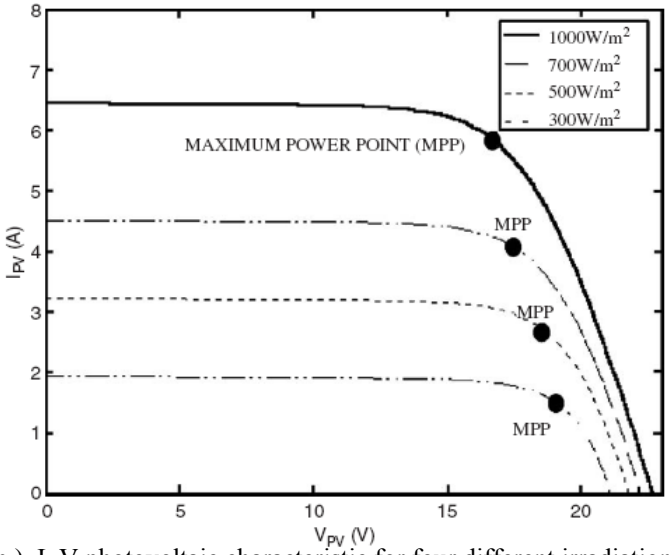

b.) I–V photovoltaic characteristic for four different irradiation levels.

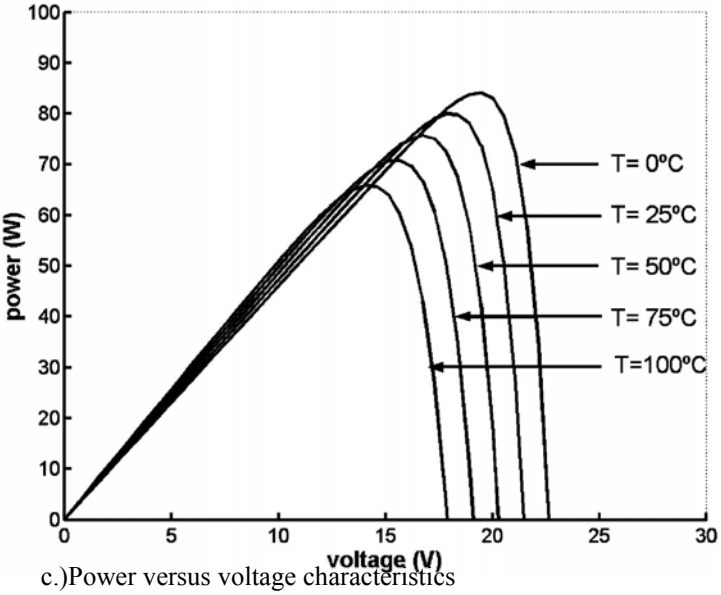

c.)Power versus voltage characteristics

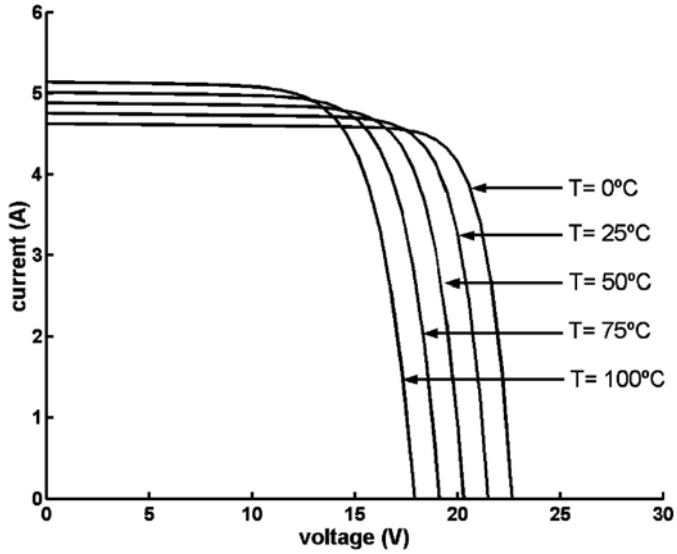

d.) Current versus voltage characteristics

Figure 1.4 a, b, c, d Typical P-V curve and I-V curve vs. irradiation, and P-V curve and I-V curve vs. change of temperature.

In Figure1.5.a below, the temperature effect on the PV's power is illustrated for Kyocera's 125W polycrystalline panel and the effect of irradiance on the panel power is denoted in Figure1.5.b.

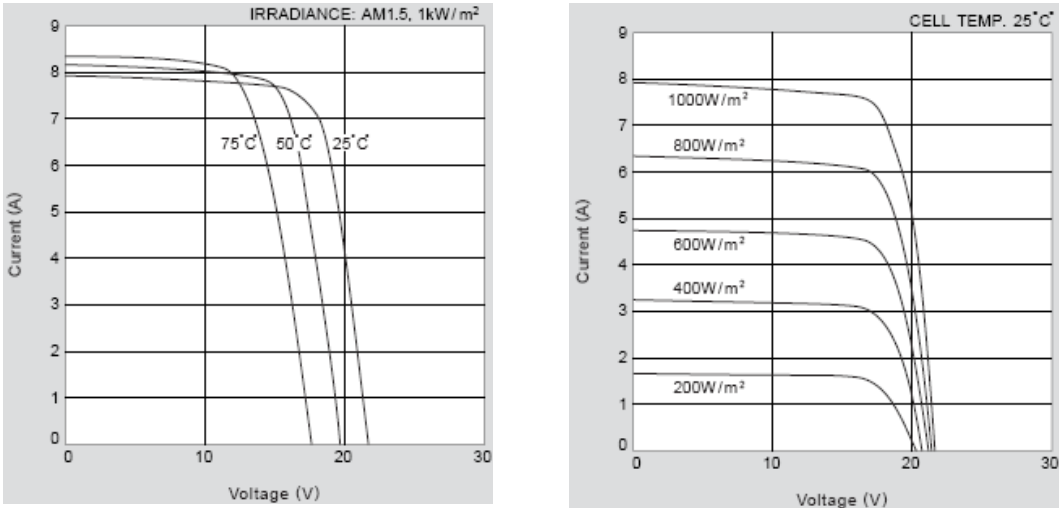

(a) (b)

Figure 1.5 (a) Current-Voltage characteristics of Photovoltaic Module KC125GHT-2 at various cell temperatures. (b) Current-Voltage characteristics at various irradiance levels.

The effects of temperature and irradiance on the panel power must be taken into consideration on PV applications. While the maximum power point is tracked, these effects must also be taken into consideration.

1.4 Maximum Power Point Tracking

While meteorological conditions change, the output power of PV panels changes. In addition to power variation, the output characteristics (voltage and current relationship) of the photovoltaic module vary with variation in insolation level as well as temperature. The power control system must track the changes in PV power level.

As Enslin J. H. R, (1991-95) was mentioned and will be proved in our work, the cost of maximum power point tracking systems contributes a little to the cost of the whole system while it considerably increases energy harvesting efficiency.

To harvest maximum power from PV capability, PV module characteristics must be adopted to load characteristics. Using MPP tracker can increase the output power of PV up to 25%. For this reason, to decrease the cost of PV System and to use PV in maximum efficiency, the MPP tracker should be used.*(Arias J.& others 2004)*

Finding MPP characteristic of PV panel, several methods have been used in the literature. In this thesis, all of them were discussed and some of them were applied by the circuit we designed. One important aspect of this study is the invention of a new MPP tracking method (finding MPP with triggering semiconductor in linear region).

1.5 Sun Tracking System

The studies indicated that sun tracking increases energy production by 37% to 40% annually (Messenger, R. A., & Ventre, J. 2004). To Neville R.C., (1978) the energy available to the ideal tracker is higher by 5–10% and 50% than the east–west tracker and the fixed surface, respectively. By keeping the PV modules perpendicular to the incoming sunlight, trackers maximize energy production. Using trackers results in increasing the overall system efficiency. The cost of tracker systems is lower than the cost of PV panes. When a tracker is used, the overall system cost is reduced since fewer number of panel needed. Considering all these facts, two axis

open-loop and closed-loop controlled tracker systems with microcontrollers were chosen to be implemented in this study.

1.6 Battery Charge Control

There are various types of batteries used in industrial applications. For autonomy, the batteries must be used in a stand alone system. Batteries react as a nonlinear element. Each of them has different charge and discharge characteristics.

Charging and discharging characteristics of batteries are very important for efficiency and to reduce the cost of the system. For this reason, charge and discharge characteristics of batteries were detailed and two batteries (12V, 18A) were charged by the PV panel with the help of a boost converter.

1.7 Research Objective

The objective of our research is the design and implementation of a solar energy control system with maximized conversion efficiency and high reliability. This work is intended to contribute to the knowledge of solar energy systems. Since prototyping and experimental work in this subject lack in our country, application and recommendations made here directly address the real-world issues associated with the implementation of such systems. New design and implementation challenges are shown, explained and analyzed.

1.8 Thesis Outline

In Chapter 1, a brief introduction to solar energy, photovoltaic solar cell model and its characteristics are provided and the subjects of other chapters are explained briefly.

In Chapter 2, conventional MPPT techniques are reviewed. Some of them are implemented. A new MPPT technique is developed and constructed on a boost converter by means of a microcontroller.

Chapter 3 contains information about types of batteries and explains their charging and discharging characteristics. Two AGM (Absorbed Glass Mat) lead acid batteries were charged with respect to optimum charge techniques by the boost converter at issue.

In Chapter 4, tracking of sun systems for PV are reviewed and a new classification is done. A new two axes tracker prototype are developed. Open-loop and closed-loop control techniques are implemented on it. Tracking of sun in an exact manner is achieved by using a microcontroller and it is shown that the cost of tracking system can be reduced.

Chapter 5 contains conclusions of this work and proposals for future work.

In Figure 1.6, 1.7 and 1.8 below, the proposed control circuit's simulations models, the produced control circuits and the prototype tracker are all illustrated.

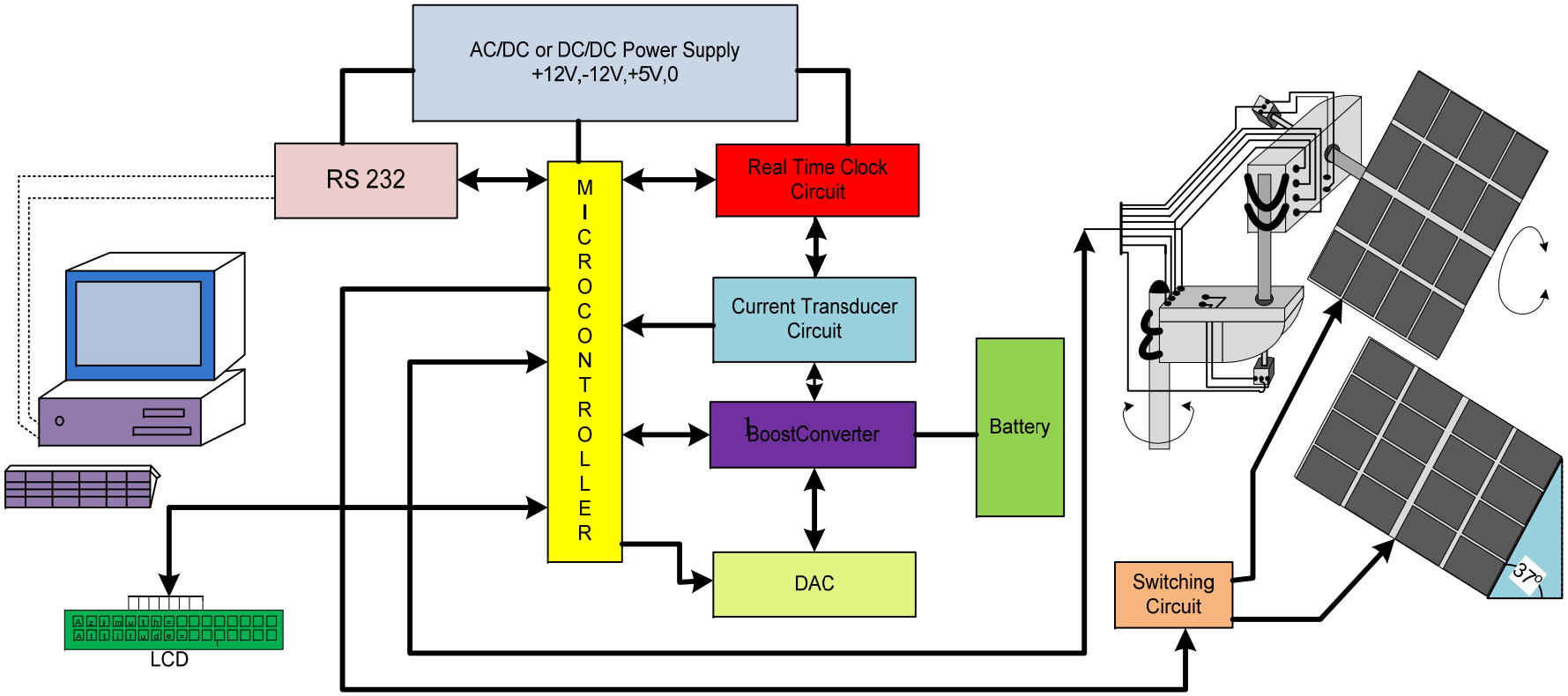

Figure 1.6 Overall system model

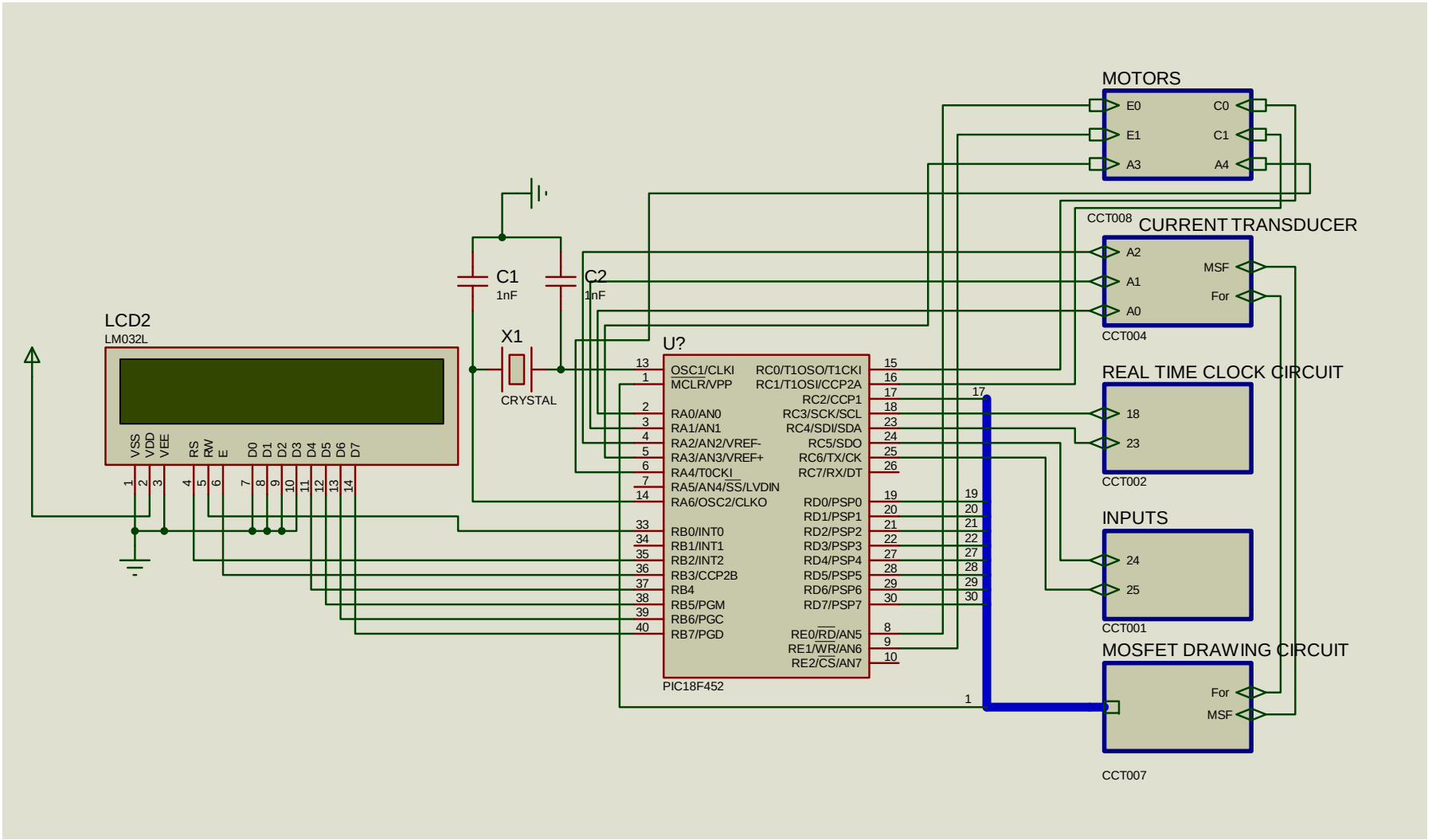

Figure 1.7 Overall system block simulation model

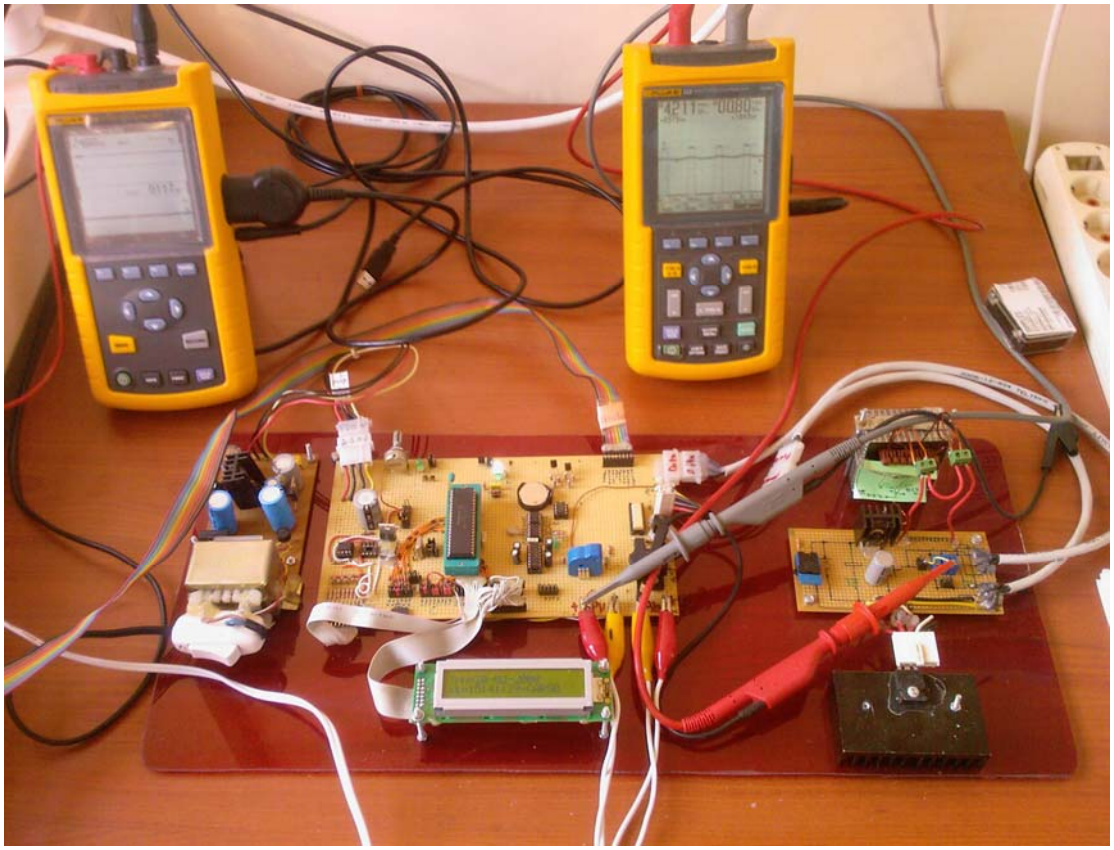

a)

(b)

Figure 1.8.a,b Prototype control circuit and tracker, realized in the thesis

CHAPTER TWO
EXISTING RESULTS AND NEW SOLUTION FOR MPP

2.1 Review and Literature Survey of The MPPT Techniques

The output characteristics of PV-modules alter nonlinearly under changing atmospheric conditions or when the PVs are shaded by any object i.e. dust. Thereby, for maximum efficiency the maximum power point (MPP) of PV modules must be tracked. The use of MPP trackers increases power of PVs up to 25%. Tracking MPP methods of PV modules are classified by many authors in many different ways. In this chapter, first, existing MPPT classification methods will be discussed, explained. Then, our MPPT technique and particularly its implementation (based on "using linear region of semiconductor switch as rheostat method") will be explained.

Lee et al. (2003) classified MPPT techniques largely into two groups. The first group consists of large scale PV-power systems based on digital signal processor DSP, which includes the hill-climbing, short circuit current methods etc. The second group includes small-scale PV-power systems without using DSP, i.e. open circuit method.

Accocording to Masoum M. A. S. & others; classification of MPPT techniques can be categorized into three groups;

Look-up table methods: In this method, the measured values of the PV generator's voltage and current are compared with those stored in the control system, which suits the operation in the maximum point, under concrete climatological conditions. This method has as the disadvantage that a large capacity of memory is required for storage of the data. Moreover, the implementation must be adjusted for a panel PV specific. The nonlinear and time-varying nature of solar cells and their great dependency on radiation and temperature levels as well as degradation (aging, dirt) effects, make it difficult to record and store all possible system conditions.

Perturbation and observation (P&O) methods: Measured cell characteristics (current, voltage, power) are employed along with an online search algorithm to compute the corresponding maximum power point independent of insolation, temperature, or degradation levels. Major problem with this approach is the undesired measurement errors that can especially be significant for current since it strongly affects tracker accuracy.

Computational methods: In this method, the nonlinear *V–I* characteristics of solar panel is modeled using mathematical equations or numerical approximations. The model must be valid under different insolation, temperature, and degradation conditions to work properly. Based on the modeled *V–I* characteristics, the corresponding maximum power points are computed for different load conditions as a function of cell open-circuit voltages or cell short-circuit currents.

On the other hand, MPPT control methods can be grouped with respect to the control variables (one variable and two variables) measured in the seeking process. One variable method contains the feedback voltage, open-voltage PV generator, open-voltage PV cell as well as the short circuit current method. Two variables method includes the voltage measurements, V_{PV}, and current, I_{PV} of the PV output power. Among others, the differentiation, perturbation and observation (P&O) and the conductance incremental (C.I.) methods can be cited.

The MPPT's classification method of Salas V. & others is one of the most detailed classifications. Their classification method of MPPT techniques can be summarized by the following excerpt:

The indirect control: the ''quasi seeking''

- Curve-fitting method
- Look-up table method
- Open-circuit voltage photovoltaic generator method

- Short-circuit photovoltaic generator method
- Open-circuit voltage photovoltaic test cell method

Direct control: the ‘‘true seeking’’

- Sampling methods
- Methods by modulation

Other methods: artificial intelligence methods

2.1.1 The Indirect Control the ‘‘Quasi Seeking’’

The indirect methods are based on the use of a database that includes parameters and data such as curves typical of the PV generator for different irradiances and temperatures and the use of the mathematical functions obtained from empirical data to estimate the MPP. In most cases, a prior evaluation of the PV generator is required, or the mathematical relationship obtained from empirical data is used, which does not meet all climatologic conditions. The following methods belong to this category: curve fitting, look-up table, open circuit voltage PV generator, short circuit current PV generator and open circuit voltage cell. These will be explained below in detail.

2.1.1.1 Curve-Fitting Method

The nonlinear characteristic of PV generator can be modeled off-line, from conventional single-diode, two-diode and modified two diode model using mathematical equations or numerical approximations *Phang J.C.H et al. (1984) K. Nishioka, et al. (2003)*. However, their solution is impossible by analogue control and very difficult by conventional digital control. Hence, their applications do not seem to be suitable for obtaining the MPPs. Nevertheless, other model based approaches can be used according to *M.A. Hamdy, (1994) N. Takehara, S. Kurokami, (1997).*

According to Ref. *N. Takehara, S. Kurokami, (1997).,* in the first equation below express the P–V characteristic of a PV generator where a, b, c and d are coefficients determined by the sampling of *m* values of PV voltage V_{PV}, PV current I_{PV}, and PV

power P_{PV} in the required intervals. Thus, the voltage at which the power becomes maximum is obtained by means of the second formula below.

$$P_{PV} = aV^3{}_{PV} + bV^2{}_{PV} + cV_{PV} + d$$

$$V_{MPP} = b\sqrt{\frac{(b^2\text{-}3ac)}{3a}}$$

This process should be repeated every few milliseconds in order to find a fine MPP. The accuracy will depend on the number of samples. The disadvantage is that either it requires accurate knowledge of the physical parameters related to the cell material or manufacturing specifications or the expressions used that are not valid for all climatologically conditions. In addition, it might require a large memory capacity for calculations of the mathematical formulations. *(V. Salas_, E. Olı´as, A. Barrado, A. La´zaro, (2005))*

2.1.1.2 Look-Up Table Method

In this method, the measured values of the PV generator's voltage and current are compared with those stored in the control system, which correspond to the operation in the maximum point *(H.E.-S.A. Ibrahim, et al., 1999),* under concrete climatologically conditions. Then, this algorithm has as the disadvantage that a large capacity of memory is required for storage of the data. Moreover, the implementation must be adjusted for a panel PV specific. In addition, it is difficult to record and store all possible system conditions.

2.1.1.3 Open-Circuit Voltage Photovoltaic Generator Method

This algorithm is based on the voltage of PV generator at the MPP which is approximately linearly proportional, k_1, to its open-circuit voltage, Voc. The proportional constant depends on the fabrication technologies solar cells technology, fill factor and the meteorological conditions, mainly.

$$k_1 = (V_{MPP} / V_{OC}) = \text{Constant} < 1.$$

PV generator's open-circuit voltage is measured by interrupting the normal operation of the system, with a certain frequency, storing the measured value. Later, the MPP is calculated, according to above equation and the operation voltage is adjusted to the maximum voltage point.

This process will be repeated periodically. Although this method is apparently simple, it is difficult to choose an optimal value of the constant k_1. However, the literature *(Ela M. A., Roger J.,(1984), Andersen M., Alvsten T.B.(1995), Schoeman J.J., Wyk J.D.,(1982)),* reports k_1 values ranging from 0.73 to 0.80, for polycrystalline PV modules, as well as a typical interval of sampling of 15 ms *(Masoum M.A.S., et al, (1999)).*

Since adjustment of the reference voltage of V_{oc} is chosen as a fixed value, assuming that it remains constant for a wide variation of temperature and insolation, and does not change significantly with the aging of the array, this method cannot be integrated in one of the 'true seeking methods' of the MPP. The exactitude of the adjustment of the voltage operation to the maximum voltage, V_{MPP}, depends on the choice of this fraction, compared with the real relation that exists between V_{MPP} and V_{oc}.

In this method, very simple control circuit is used, which is low-priced and uses only one feedback loop. But between sampling periods the reference voltage of open circuit is constant. So this method may result in considerable error in power because the output voltage of PV module only follows the unchanged reference voltage during one sampling period. In addition, the interrupted system operation yields power losses when scanning the entire control range. Thus, the actual power generated by the panels never reaches its full potential. That is, as it is assumed that for given open-circuit voltage the maximum point is determined if the operation point is incorrect, or slightly inexact, the

extracted power will not be the maxima. In this study the MPP is tracked using an open circuit voltage control.

2.1.1.4 Short-Circuit Photovoltaic Generator Method

This method is similar to the above method. The operation current at MPP of PV module is linearly proportional to short circuit current of PV module. The I_{MPP} is determined from multiplying I_{sc} with the proportional parameter *k* and it can be seen that the relationship between I_{MPP} and I_{sc} is still proportional even though the temperature changes from 0 to 60^{o}C. The relationship is given with the equation below. As does the previous method, the proportional constant depends on fabrication technologies, solar cells technology, fill factor and the meteorological conditions, mainly.

$$k_2 = I_{MPP}/ I_{SC} = \text{Constant}<1.$$

According to the study of *NOGUCHI Toshihiko, and TOGASHI Shigenori, NAKAMOTO Ryo.(2000)* the proportional parameter *k* is estimated to be approximately 0.92. In the same study, researchers conducted experiments using different PV panels in order to confirm generality of this relation. The experiments show that investigated two different panels have a similar proportional characteristic and that the proportional parameter *k* is 0.91 in both cases. However, *k* is not always constant and should rather be regarded as a variable because it is affected to a great extend by surface conditions of the PV panel, especially by shades partially covering the panel. For instance in the study of *Alghuwainem, S. M. (1994) k* is called as M_c "current factor" and is equal to 0.86 for another silicon panel. This demonstrates that *k* or M_c changes from PV to PV.

All the experimental results obtained from reference *(Noguchi T., at al.,(2000),, Alghuwainem, S. M. (1994))* rationalize that the short-current based MPPT is effective and useful to determine the optimum operating point without complicated algorithms and hardware.

However, in many cases, the way of determining k_2 is more complicated than only a fixed value, as in reference *T. Noguchi, et al. (2002)*. In that paper, a PV scanning is performed every several minutes in order to calculate k_2. After k_2 is obtained, the system remains with the approximation, until the next calculation of k_2. The flow chart of the control is then, similar to the open-circuit voltage method. This method tracks MPP rapidly, under rapidly changing atmospheric conditions but the control circuit is complex and the conduction loss occurs during short circuits in addition extra components (diode, switch etc.) are added to MPPT's circuit. Therefore, this method offers the same advantages and disadvantages as the above control.

2.1.1.5 Open-Circuit Voltage Photovoltaic Test Cell Method

In order to avoid possible drawbacks related to the frequent interruption of the system, Refs. (*D. Lafferty,(1993), Schaefer J.F., Hise L., (1984), Louis A.U., (1972)*) proposed, as an alternative, an additional use of a cell test. Thus, the PV generator's open-circuit voltage is measured from the single cell, which is electrically independent from the rest of the PV array. The resulting values of the k_3 will be applied to the main PV generator.

$$k_3 = V_{MPP} / V_{OC,\text{cell test}} = \text{Const} < 1.$$

This method's advantage is that it is simple and economical; it uses only one feedback loop control. Moreover, it avoids the problems caused by the interruptions of the operation of the PV described in the previous method. As a disadvantage, it supposes that the test cell has properties identical to each cell of the PV generator main.

Therefore, V_{oc} of the test cell is considered proportional to V_{oc} of the PV unit used in the selection of the MPP. If the assumption is incorrect, maximum power will not be extracted. And, finally, it can be an unsuitable method for applications with surface limitations (i.e. solar vehicles).

2.1.2 Direct Control: The ‘‘True Seeking’’

Direct methods include those methods that use PV voltage and/or current measurements. From those, taking into account the variations of the PV generator operating points, the optimum operating point is obtained. These algorithms have the advantage of being independent from a priori knowledge of the PV generator characteristics. Thus, the operating point is independent of insolation, temperature or degradation levels. The main problem is the issue of undesired errors that strongly affect tracker accuracy. The methods belonging to this group include the differentiation, feedback voltage (current), P&O, C.I., auto-oscillation as well as fuzzy logic. Other types of classification methods which distinguish between sample and modulation methods can also be included within this group.

2.1.2.1 Sampling Methods

In these procedures, a sample is made up of the PV’s voltage and current. Afterwards, using diverse strategies in every sampling, the PV output power, P_{PV} (t) is gathered. Such sampling has the objective for determining of the relative time evolution of the abovementioned variable. So, firstly, the P_{PV}(t) is computed. At the stage two, the PV power $P_{PV}\ (t+D_t)$ is computed again. After gathering the past and the present information on the P_{PV}, the controller makes a decision depending on the location of the operating point. This tracking process repeats itself indefinitely until the peak power point is reached. The following methods (sections 2.1.2.1.1 to 2.1.2.1.6) are based on the principle of sampling methods.

2.1.2.1.1 Differentiation method. This technique is presented in Refs. *(David J.H., (1968), Bavaro L.T.W., (1988))* and is based on the property in which the MPP is located by solving below equation.

$$\frac{dP_{PV}}{d_t} = V_{PV}\frac{dI_{PV}}{d_t} + I_{PV}\frac{dV_{PV}}{d_t} = 0$$

However, in order to provide real time adjustments of the operating point, this equation must be solved quickly. This is difficult because solving this equation requires at least eight calculations and measurements: a determination of present array voltage V_{PV}; a determination of present array current I_{PV}; a measure of the change in voltage, dV_{PV}, in the face of a given operating point perturbation (dt); a measure of the change in current, dI_{PV}, corresponding to the operating point perturbation; a calculation of the product V_{PV} times dI_{PV}; a calculation of the product I_{PV} times dV_{PV}; a calculation of the resulting sum $V_{PV}\, dI_{PV} + I_{PV}\, dV_{PV}$; and a comparison of this sum to an equal perturbation on the opposite side of the operating point or the operating point power. Furthermore, if the final sum is not zero, a ninth determination must be made of the sign of the dP_{PV} sum. This sign indicates the direction that the operating point must be adjusted to reach the MPP.

2.1.2.1.2 Feedback Voltage (Current) Method. If there is no battery present in the system, in order to tie the bus voltage at a nearly constant level, a simple control can be applied as in refs. *(Maheshappa H.D.,at al, (1998), Hua Ch., Shen Ch., (1998))*. Thus, the feedback of the PV voltage (current) and the comparison with a constant voltage (current) can be used to continuously adjust the duty cycle (D) of a DC/DC converter, to operate the PV panel at a predefined operating point close to the MPP. The disadvantages of this configuration are the same as the ones for the method of direct connection (PV generator + load profile). That is, the system is not able to adapt to changeable environmental conditions, such as irradiance and temperature. However, if batteries are present in the system, a common technique is to compare with a reference constant voltage, where it is assumed that it corresponds to the V_{MPP}, under environmentally specific conditions. The resultant signal differentiation (error signal) is used to control the DC/DC converter. Although the implementation of this variant is not relatively simple, it fails as well to fulfill the proposed objective because it does not take into account the effects of irradiation and temperature variations. The advantages of this method are the same as the previous methods: It is a simple and economical method and uses only one feedback-loop control. Nevertheless, as mentioned before, it presents the

following disadvantages: It can not be applied in a generalized fashion in systems which do not consider the effect of variations of the irradiation and temperature of the PV panels. It can not be applied to the systems with batteries.

2.1.2.1.3 Perturbation and Observe (''P&O'') Method. This method tracks MPP by continuously increasing and decreasing the output voltage at MPP of PV module. This method is simple and can track simply MPP of PV when the atmospheric conditions are constant or slowly changed but those are rapidly changed this methods fail to track MPP.

It is an iterative method of obtaining MPP. It measures the PV array characteristics, and then perturbs the operating point of PV generator to encounter the change direction. The maximum point is reached when $dP_{PV}/dV_{PV} = 0$. Doing so, the operating voltage of the PV generator is perturbed by a small increment dV_{PV}, and the resulting change, ΔP_{PV}, in power is measured. If ΔP_{PV} is positive, the perturbation of the operating voltage should be in the same direction of the increment. However, if it is negative, the system operating point obtained moves away from the MPPT and the operating voltage should be in the opposite direction of the increment. If the PV power has increased, the operating point should be increased as well. However, if the PV power has decreased, the voltage should do the same. Nevertheless, a disadvantage of this method, described by *Hussein et al. (1995)* appears in the case of a sudden increase of irradiance, Figure 2.1, where the algorithm reacts as if the increase occurred as a result of the previous perturbation of the operating voltage. In order to better understand this phenomenon, see Figure 2.1. Thus, the case is considered in which the irradiance is such that it generates the P–V curve characteristics, curve 3. In this way, the operating voltage initially oscillates around the maximum point, from A to A1. Now, an increase in the power will be measured because the solar irradiation has increased from curve 3 to curve 2. Then, if one assumes that being in point A, that it comes from a diminution of the voltage, and before the following disturbance takes place, the irradiance is increased, with the curve characteristic being now curve 2, and the operation point will occur at B1.

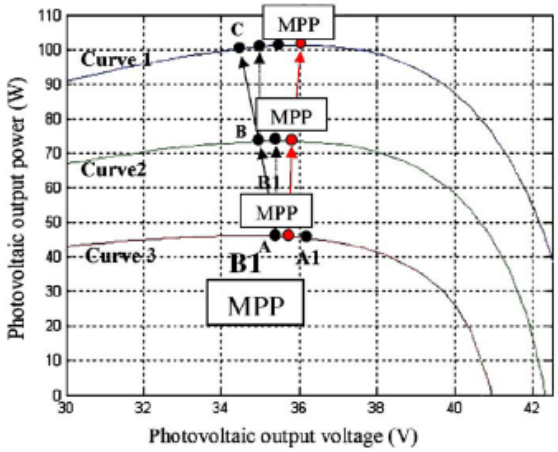

Figure 2.1 Deviation from the MPP with the Perturbation and Observation algorithm under rapidly changing insolation levels. *(Salas.V at all. (2005))*

Indeed, since there has been a positive increase in power, the disturbance will continue in the same direction. In other words, the voltage will diminish and go to point B. Furthermore, if the irradiance is increased again quickly to curve 1, there will be another increase in positive power, with which the operation point will now be C. That is, due to two increases of irradiance, the operation point has been transferred from A to C, moving away from the maximum point. This process remains until the increase of the irradiance slows or stops. The advantages of this method can be summarized as follows: A previous knowledge is not required of PV generator characteristics; it a relatively simple method. Nevertheless, in their most simple form, at a steady state, the operating point oscillates around the MPP, giving rise to the wasting of some amount of available energy. In addition, it is an unsuitable method with rapidly changing atmospheric conditions. Hussein K.H, at al. (1995).

2.1.2.1.4 Conductance Incremental Method (''C.I.''). When the atmospheric conditions are changed rapidly, incremental conductance methods track the MPP of PV. But complicated control algorithms, delay caused by these algorithms and the slow response speed of finding MPP can be treated as disadvantage.

An alternative to the ‘‘P&O’’ method was proposed by Hussein at al (1995), developing the ‘‘C.I.’’ method. It is based on the first equation below, that is, differentiating the PV power with respect to voltage and setting the result to zero,

$$\frac{dP_{PV}}{dV_{PV}} = I_{PV}\frac{dV_{PV}}{dV_{PV}} + V_{PV}\frac{dI_{PV}}{dV_{PV}} = I_{PV} + V_{PV}\frac{dI_{PV}}{dV_{PV}} = 0,$$

$$-\frac{I_{PV}}{V_{PV}} = \frac{dI_{PV}}{dV_{PV}}$$

The left-hand side of the above second equation represents the opposite of the instantaneous conductance, $G = I_{PV}/V_{PV}$, whereas the right hand side of the above second equation represents its incremental conductance. On the other hand, the incremental variations, dV_{PV} and dI_{PV}, can be approximated by the increments of both the parameters, ΔV_{PV} and ΔI_{PV}, with the aim of measuring the actual value V_{PV} and I_{PV} with the values measured in the previous instant, the following expressions respectively.

$$dV_{PV}(t2) \approx \Delta V_{PV}(t2) = V_{PV}(t2) - V_{PV}(t1)$$
$$dI_{PV}(t2) \approx \Delta I_{PV}(t2) = I_{PV}(t2) - I_{PV}(t1)$$

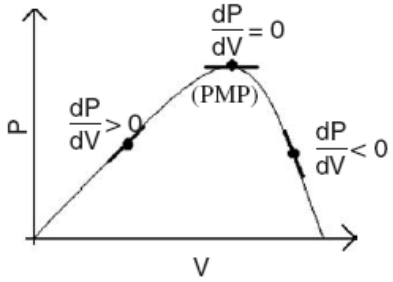

Figure 2.2 Characteristics curve of the P–V photovoltaic generator. Variation of the dP/dV.

Therefore, analyzing the derivative one can test whether the PV generator is operating at its MPP or far from it. The main advantage of this technique is that it offers a good yield method under rapidly changing atmospheric conditions. Also, it achieves lower oscillation around the MPP than the P&O method, even though, when the P&O method is optimized, the MPPT efficiencies of the incremental conductance and P&O

MPPT algorithms are, essentially, the same (*Hohm D.P., Ropp M.E., (2003), Liu X., Lopes L.A.C., (2004)*). Nonetheless, it has a drawback of requiring complex control circuit. Such circuits had a high cost 10 years ago. However, today there are many options for doing it much more cheaply.

2.1.2.1.5 Parasitic Capacitance Method. This method was developed by *Branbrilla at al., (1999)* and is similar to the incremental conductance method, except that the effect of the PV cell's parasitic union capacitance, C_{PV}, is included. The analysis is carried out with instantaneous PV output power, and the current can be expressed as a time function of PV output voltage. The incremental conductance and instantaneous conductance are defined by suitable formulas. The disadvantage of this method is that it requires two multiplications with the complexity of the control circuit.

2.1.2.1.6 The Only Current Photovoltaic Method. To finding MPP in direct methods, the PV voltage and current are required to measure so far. However, it is possible to find a method that only uses the PV current, *(Salas V., et al., (2005))* based on Figure 2.3.

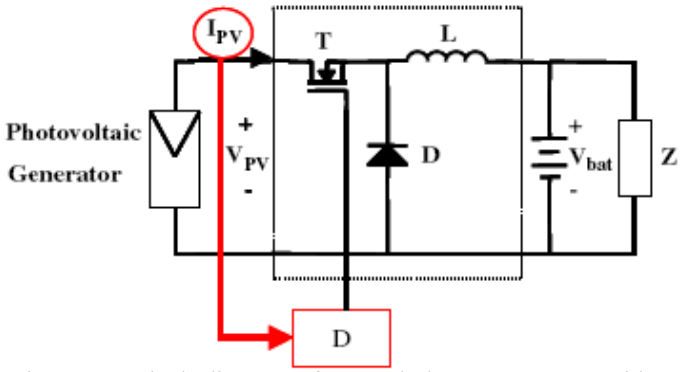

Figure 2.3 Block diagram of a stand-alone PV system with the only current PV algorithm

The nonlinear PV array can be modeled (*M.A. Hamdy, (1994)*) as $I_{PV} = f(V_{PV}, I_{PV})$, in the below formula;

$$I_{PV} = I_{PV}(V_{PV}, I_{PV}) = I_L - I_O(e(V_{PV} + I_{PV} R_S / mv_t) - 1) \quad \frac{V_{PV} + I_{PV} R_S}{R_{sh}}$$

operating current PV; V_{PV} *= operating voltage PV;*

Rs = cell series parasitic resistance; R_P *= cell shunt parasitic resistance;*

m = junction constant; I_0 *= cell reverse saturation current;* I_L *= cell photocurrent.*

It can be rearranged to obtain I_{PV} as a sole function of V_{PV}, $I_{PV} = f(V_{PV})$, which can be used in the expressions for the power converters. In our case, this first analysis will be based on the buck converter, with the known below first and second equations, where; Vbat = battery voltage (which is assumed with constant voltage for every Δt) and D = duty cycle.

$$V_{bat} = \frac{t_{on}}{T} V_{PV},$$

$$P_{in} = V_{PV} I_{PV} = V_{bat} \frac{I_{PV}}{D} = V_{bat} P^*, \quad P^*_{Buck} = \frac{I_{PV}}{D}$$

It can be demonstrated that input power to the converter, P_{in}, versus duty cycle, D, and P^*_{Buck} versus D present the same maximum points for the same duty cycle values as illustrated in Figure 2.4 for constant battery voltage.

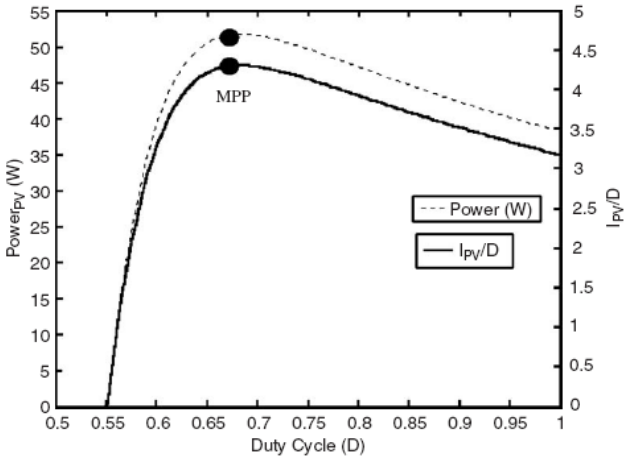

Figure 2.4 The relation of PV power curve and I_{PV}/D curve.

The algorithm, for this method, can be explained as follows: the tracking process is started with an initial duty ratio. Firstly, the PV current $I_{PV}(t)$ is measured and computed $P^*(t)$. Then, the duty cycle is increased, ΔD1. At the stage two, the PV current $I_{PV}(t+\Delta t)$

is measured and computed $P^*(t+\Delta t)$ again. After gathering the past and the present information on the P^*, the controller makes a decision on whether to increase or decrease the duty ratio (sign of the incremental duty ratio) depending on the location of the operating point. This tracking process repeats itself indefinitely until the peak power point is reached.

This method has as a major advantage, when compared with other direct methods, of using the measurement of the variable, PV current. In addition, this algorithm operates successfully even in cases of rapidly changing atmospheric conditions and different sky conditions (*Salas V., et al., (2005))*. Furthermore, even though this description is made for a step-down DC/DC converter, it can be proven that this method is suitable for any DC/ DC topology, step-down and step-up, as is reported in reference *(Salas V., et al., (2005).*

2.1.2.2 Methods by Modulation

In the methods discussed earlier, the sampling methods, the appropriate adjustment for the maximum voltage point leads to a point close to and oscillating around the maximum point. These oscillations are generated automatically by the feedback control used. However, there are many other methods that add an oscillation. These algorithms are known as forced oscillation methods.

2.1.2.2.1 Forced Oscillations Methods. Several articles have dealt with this subject *(Cocconi A., Rippel W.,(1990), Tse K.K., Chung H.S.H., Hui S.Y.R., Ho M.T., (2001))* For example, reference (*Tse K.K., et al. (2001))*) introduces a small voltage, 100 Hz, which is added to the voltage of operation voltage of the PV generator. This leads to a ripple power, whose phase and amplitude are dependent on the relative location of the operation point to the MPP, as can be seen in Figure 2.5. Curve P–V for a PV generator with the power ripple is constructed by the photovoltaic voltage modulation. Point ‘‘A’’ denotes the area of operation, on the left of the MPP, and point ‘‘B’’ the area on the

right of the MPP. If this modulation occurs in zone ‘‘A’’, at the left side of the MPP, the ripple voltage of the power will be perfectly in phase.

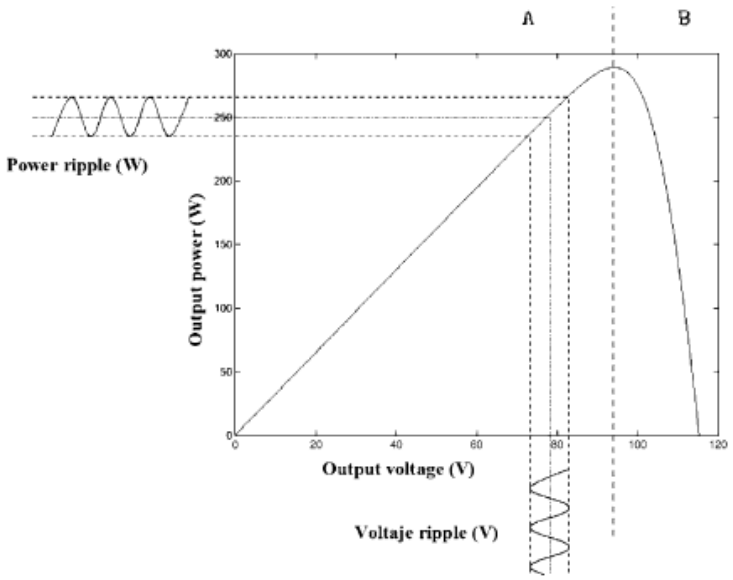

Figure 2.5 Curve P–V for a PV generator with the power ripple caused by the photovoltaic voltage modulation. Point ‘‘A’’ denotes the area of operation, on the left of the MPP, and point ‘‘B’’ the area on the right of the MPP.

However, if the modulation occurs in a point of operation of zone ‘‘B’’, to the right side of the MPP, the curling of the power output will be 180^{o} out of phase with respect to the voltage. In case that the operation point is exactly the MPP, the curling of power output will have twice the frequency of the curling of the voltage, with very small amplitude. The advantage of this method is that analysis of the amplitude and the phase provides information on the location of the MPP. In addition, the exit signal converges slowly towards zero, when the point of operation approaches the MPP. This allows the operating voltage to be adjusted slowly to the MPP voltage. With it, there will be no continuous oscillation around the MPP caused by a fixed width of passage of converter MPPT. The only oscillation that happens with this method is 100Hz of modulation of the voltage operation. Nevertheless, it has as a disadvantage of having the greater complexity of its implementation as well as the evaluation of the signals of very low amplitude.

2.1.3 Other Methods: Artificial Intelligence Methods

In recent years, the fuzzy logic controllers (FLCs) and neural network methods have received attention and used very successfully in the implementation of MPP searching. The fuzzy controllers improve control robustness and have advantages over conventional ones. They do not need exact mathematical models; they can work with vague inputs and they can handle nonlinearities and are adaptive, in nature; likewise, their control gives them robust performance, under parameter variation, load and supply voltage disturbances. Based on their heuristic nature and fuzzy rule tables, these methods use different parameters to predict the maximum power output: the output circuit voltage and short circuit current (*N. Femia, G. Petrone, G. Spagnuolo, M. Vitelli, (2005));* the instantaneous array voltage and current; instantaneous array voltage and reference voltage (obtained by an offline trained neural network) *(Liu X., Lopes L.A.C., (2004));* instantaneous array voltage and current of the array and short circuit current and open circuit voltage of a monitoring cell (Tse K.K., Chung H.S.H., Hui S.Y.R., Ho M.T., *(2001), Cocconi A., Rippel W.,(1990),)* and solar radiation, ambient temperature, wind velocity and instantaneous array voltage and current, used in reference (*M. Veerachary, T. Senjyu, K. Uezato, (2003),)*. Finally, it is of note that other methods have been implemented such as those that are based on the use of the Fibonacci series *(Wilamowski B.M., et al., (2001))*, although, once again, two variables are measured: output voltage and current of the DC/DC converter.

2.2 Review of Boost Converter

Boost converter generally is used in regulated dc power supplies and the regenerative braking of dc motors applications. The output voltage (battery charge voltage V) of boost converter is always greater than the input voltage (PV voltage V_g). Theoretically, conventional boost converters are able to achieve high step-up voltage gain in heavy duty load conditions. In practice, however, the voltage gain of the boost converter is limited owing to the losses associated with the inductor, filter capacitor,

main power switch and rectifier diode. *Erickson, R.W., & Maksimovic, D (1950), Mohan, N., Undeland, T.M., & Robbins,W.P 1995, Hart, D.W.1964.*

When the very high duty ratio is used the output rectifier conducts for only a very short time during each switching cycle, thus resulting in serious reverse-recovery problems and an increase in the rating of the rectification diode. The switch-off loss due to the rectifier diode will degrade the efficiency. In addition, the EMI (electromagnetic interference) problem is severe under this condition. These are disadvantage of conventional boost converters but are not analyzed in the proposed thesis.

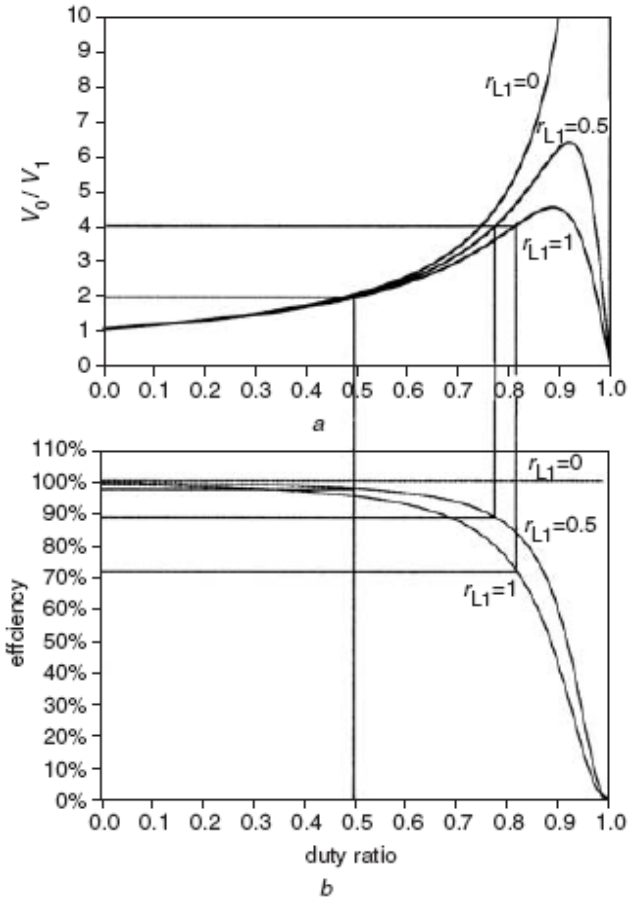

Figure 2.6 a) Voltage gain against duty ratio
b) Efficiency against duty ratio for various r_{L1}

In practice, to boost up the output of converter voltage more than 4-5 times is difficult since the inductor has a series resistance (r_{L1}); therefore this resistance

impresses the efficiency and voltage gain. As shown in the figure 2.6 extreme duty ratios dramatically degrade the efficiency. *K.C. Tseng & T.J. Liang (2004)*

The converter which is used in this thesis does not need voltage gain higher than 2 or 3, therefore these problems are not analyzed and the inductor can be accepted without resistance.

2.2.1 Analysis of Boost Converter

The analysis of Boost Converter can be done by examining the inductor voltage and current during the converter's switch on and off positions. As seen below when the switch is on, the diode is reversed biased, so the battery or load is insolated from the input PV voltage. When the switch is on interval, the PV supplies energy only to the inductor so, inductor current rises and energy is stored in inductor L. When the switch is off, the energy stored in the inductor is transferred to the output stage (Batteries, load) by way of fast diode and the inductor current falls.

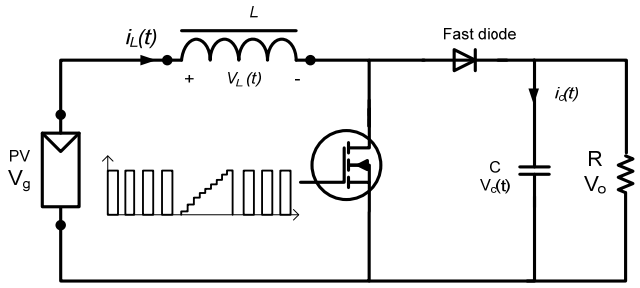

Figure 2.7 a) General Boost

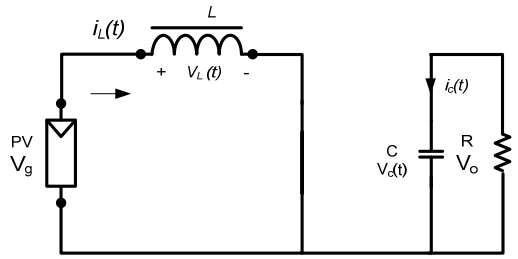

Figure 2.7 b) When the Switch is on

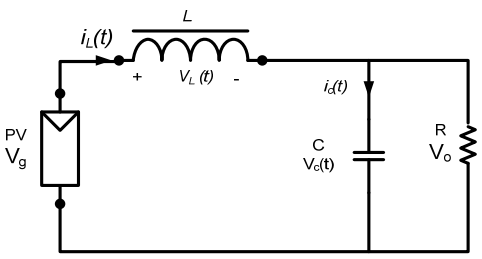

Figure 2.7 c) When the Switch is off

When the system analyzed, the steady-state condition is considered and the capacitor value, which is used as output filter, is assumed to be very large to ensure a constant output voltage, namely $v_0(t) \cong V_o$

2.2.1.1 First Switching (On) Position

When the switch is on, the rate of change of current becomes a constant. So the current increases linearly. Inductor voltage, capacitor current and small ripple approximation formula for first switching position is given in the following figure and formulas.

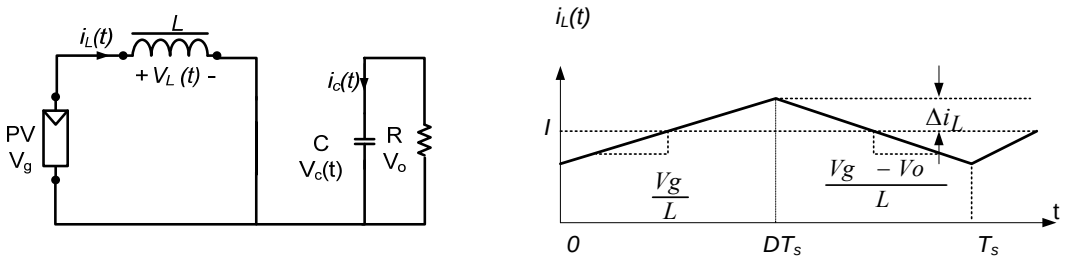

Figure 2.8 Switch on position and current wave shape of boost converter (subinterval1).

$$v_L(t) = V_g = L\frac{di_L(t)}{dt} \Leftrightarrow \frac{V_g}{L} = \frac{di_L(t)}{dt}, \quad i_C = \frac{v_o}{R}$$

When the lie a ripple appoximati on is used $v_o \approx Vo$

$$v_L(t) = V_g, \quad i_C = \frac{V_o}{R}$$

Inductor current slope during subinterval (0 - DT_s) 1:

$$v_L(t) = L\frac{di(t)}{dt} = V_g \Rightarrow \frac{di(t)}{dt} = \frac{V_g}{L}$$

The change in current, $2\Delta i_L$, is equal to the slope (the applied inductor voltage divided by L) times the length of the first subinterval (DTs).

Change in $i_L(t)$ = (slope)x(length of subinterval)

$2\Delta i_L = \frac{Vg}{L} DTs$ Solve for peak ripple: $\Delta i_L = \frac{Vg}{2L} DTs$

Typical values of Δi_L lie in the range of 10% to 20% of the full-load value of the dc component I_L. *Erickson, R. W.(2000).*

Determination of capacitor voltage ripple;

$$i_C(t) = C\frac{dv_C(t)}{dt} = \frac{Vo}{R} \Rightarrow \frac{dv_C(t)}{dt} = \frac{Vo}{RC} = \frac{ic(t)}{C}$$

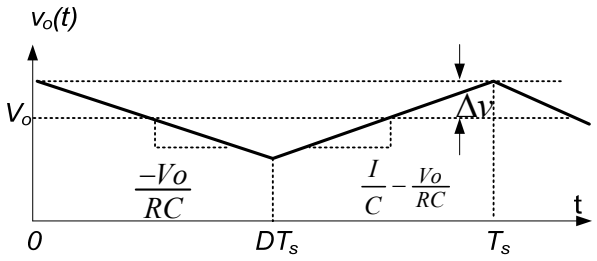

Figure 2.9 Voltage wave shape of boost converter

$$D = \frac{t_{on}}{T_s}, \quad D' = \frac{t_{off}}{T_s}, \quad T_s = t_{on} + t_{off}$$

During subinterval 1, the change in capacitor voltage, $-2\Delta v$, is equal to the slope multiplied by the length of the subinterval (DTs):

$$2\Delta v_C = \frac{V_O}{RC} DTs \Leftrightarrow \Delta v_C = \frac{V_O}{2RC} DTs$$

To obtain a given output voltage ripple peak magnitude, the above expression can be used for selecting the capacitor value C. In practice, capacitor equivalent series resistance leads to increased voltage ripple.

2.2.1.2 Second Switching (Off) Position

Inductor voltage, capacitor current and small ripple approximation formula for second switching position is given below.

$$v_L = V_g - v_o, \quad i_C = i_L - \frac{v_o}{R}$$

When the small-ripple approximations $v_o \approx V_o$ and $i_L = I$ are used

$$v_L = V_g - V_o, \quad i_C = I - \frac{V_o}{R}$$

Inductor current slope during subinterval 2 (DT_s-T_s):

$$v_L(t) = L\frac{di_L(t)}{dt} = V_g - V_o \Rightarrow \frac{di_L(t)}{dt} = \frac{V_g - V_o}{L}$$

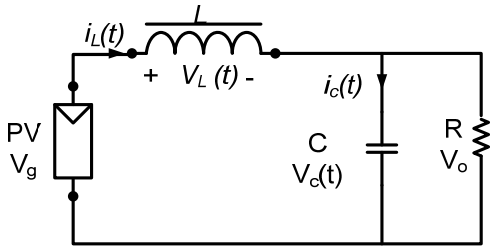

Figure 2.10 Turn off switch position

$$2\Delta i_L = \frac{V_g - V_o}{L}(1-D)Ts \Leftrightarrow \Delta i_L = \frac{V_g - V_o}{2L}(1-D)Ts$$

Capacitor voltage slope during subinterval 2:

$$I_C(t) = i_L(t) - i_R(t)$$

$$\frac{dv_c(t)}{dt} = \frac{ic(t)}{C} = \frac{I}{C} - \frac{Vo}{RC}$$

2.2.2 Conduction Modes of Boost Converter

The boost converter works in two modes (Continuous-Conduction Mode, and Discontinuous-Conduction Mode) with respect to the inductor current $i_L(t)$;

2.2.2.1 Continuous-Conduction Mode.

In this mode the inductor current ($i_L(t)>0$) flows continuously in steady-state condition. The hint is there that the time integral of the inductor voltage over one time period must be zero.

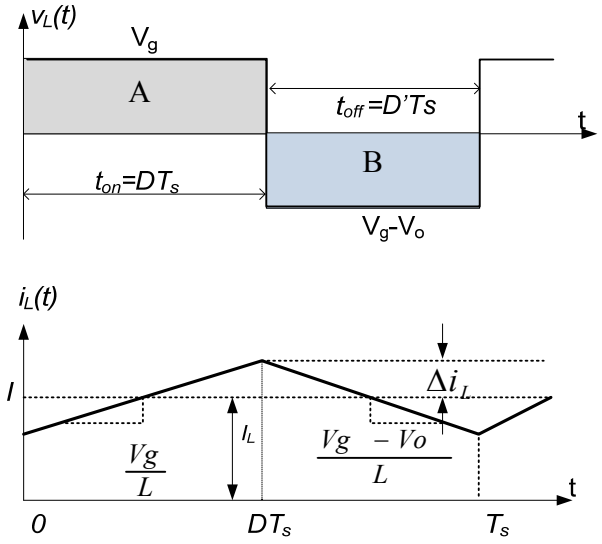

Figure 2.11 Current and Voltage wave shape of boost inductor

$$A + B = 0 \Rightarrow V_g \times ton = (Vg - Vo) \times toff \Rightarrow \frac{V_g \times ton}{Ts} = \frac{(Vg - Vo) \times toff}{Ts}$$

$$D = \frac{ton}{Ts} \Leftrightarrow D' = \frac{toff}{Ts} \Rightarrow ton + toff = Ts \Rightarrow D + D' = 1$$

$$D' = 1 - D$$

$$V_g \times DTs + (Vg - Vo) \times D' Ts = 0 \Rightarrow V_g \times D + (Vg - Vo) \times D' = 0$$

$$V_g \times D = (Vo - Vg) \times D' \Rightarrow \frac{D}{1 - D} = \frac{Vo - Vg}{Vg} = \frac{Vo}{Vg} - 1$$

$$\frac{Vo}{Vg} = \frac{D}{1 - D} + 1 = \frac{1}{1 - D} = \frac{Ts}{toff}$$

If the circuit is assumed as a lossless one

$$Pg = Po \Rightarrow Vg \times Ig = Vo \times Io \Rightarrow \frac{Vo}{Vg} = \frac{Ig}{Io} = \frac{1}{1-D}$$

Figure 2.12 shows $\frac{V_{g\,ave}}{V_{o\,ave}} \leftrightarrow I_{L\,ave}$ characteristic of a step-up converter in the continuous and discontinuous conduction modes of operation. *Mohan, N., Undeland, T. M., & Robbins, W. P.(1995),*

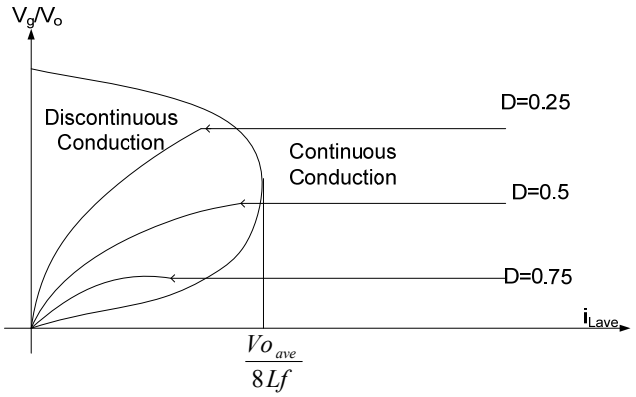

Figure 2.12 Vg/Vo-I_L characteristic of a boost converter.

2.2.2.2 Discontinuous Conduction Mode.

When the output power is required to be decreased with unchanged input and output voltage (D would vary in order to keep V_o constant), the converter must work in the discontinuous mode. The discontinuous mode of operation occurs when the value of the load current is less than or equal to zero at the end of a given switching period, in other words in this mode i_L goes to zero at the end or before the off interval. The boundary point between continuous and discontinuous current conduction occurs when the average inductor current over one switching period is half of the maximum peak value, as illustrated in Figure 2.13.

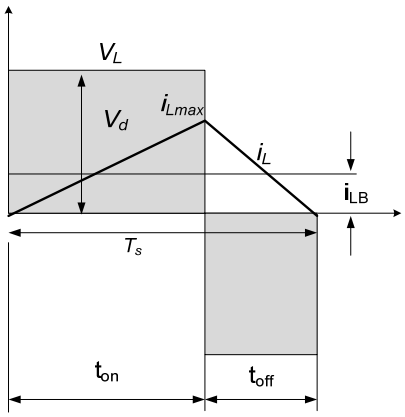

Figure 2.13 Inductor current at boundary point for discontinuous mode of boost converter.

From calculating triangle shaped area and dividing by *Ts,* the average inductor current at the boundary can be found.

$$\frac{(\frac{T_s i_{L\,max}}{2})}{T_s} = I_{LB} = \frac{i_{L\,max}}{2}$$

$$V_L = L\frac{di_L}{dt} \Rightarrow \int_0^{t_{on}} V_L dt = \int_0^{i_{l\,max}} L di_L \Leftrightarrow V_g t_{on} = L\, i_{L\,max} \Leftrightarrow i_{L\,max} = \frac{t_{on} V_g}{L}$$

$$I_{LB} = \frac{V_g\, t_{on}}{2L}, \quad D = \frac{t_{on}}{Ts}, V_g = (1-D)V_o$$

$$I_{LB} = \frac{(1-D)V_o\,(DT_s)}{2L} = \frac{T_s V_o}{2L} D(1-D)$$

I_{LB} reaches a maximum value at D=0.5 $\qquad I_{LB\,max} = \frac{T_s V_o}{8L}$

The average output boundary current is found as below;

$$I_o = I_g(1-D) \quad from \quad I_g = I_{LB}$$

$$I_{o\,B} = \frac{T_s V_o}{2L} D(1-D)(1-D) \Leftrightarrow I_{oB} = \frac{T_s V_o}{2L} D(1-D)^2 \Rightarrow I_{oB\,max} = 0.074\frac{T_s V_o}{L}$$

Finding suitable continuous conduction mode value of inductor the below formula is used;

$$L_{boundary} = \frac{T_s V_o}{2I_{oB}} D(1-D)^2$$

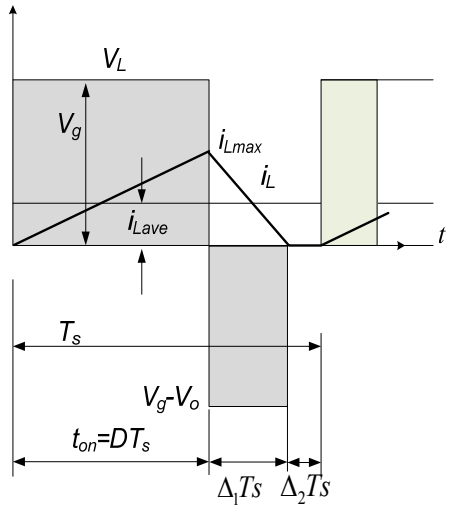

Figure 2.14 Inductor current and voltage wave form for at discontinuous mode of boost converter.

In the above figure the discontinuous conduction occurs due to decreased output power (P_o) and, hence a lover inductor current (I_L) but constant input voltage. Since i_{Lmax} is the same in both modes. A lower value of I_L is possible only if V_o goes up. If the inductor voltage integral over one time period is equated to zero,

$$V_g D T_s + (V_g - V_o)\Delta_1 T_s = 0$$
$$V_g D + V_g \Delta_1 = V_o \Delta_1$$
$$V_g D + V_g \Delta_1 = V_o \Delta_1$$
$$\frac{V_o}{V_g} = \frac{\Delta_1 + D}{\Delta_1} \quad \Leftrightarrow \quad \frac{I_o}{I_g} = \frac{\Delta_1}{\Delta_1 + D}$$
$$I_g = I_L = \frac{Field}{T_s} = \frac{T_s(\Delta_1 + D) i_{L\,max}}{2T_s} = \frac{(\Delta_1 + D) i_{L\,max}}{2}$$

$$V_L = L\frac{di_L}{dt} \Rightarrow \int_0^{t_{on}} V_L dt = \int_0^{i_{L\,max}} L di_L \Leftrightarrow V_g t_{on} = L\ i_{L\,max} \Leftrightarrow i_{L\,max} = \frac{t_{on} V_g}{L}$$

$$I_g = \frac{(\Delta_1 + D)t_{on} V_g}{2L}$$

$$I_o = (\frac{T_s V_d}{2L})\Delta_1 D$$

$$D = \sqrt{\frac{4}{27}\frac{V_o}{V_g}\ \frac{V_o}{V_g} - L\ \frac{I_o}{I_{oB\,max}}}$$

Not to be forgotten that during each switching time period $\frac{1}{2} L\, i_{L\,max}^2$ energy is transferred from the input to the output capacitor and to the load. If the load is very light, not connected or is not able to absorb this energy the capacitor voltage (output voltage) V_o would increase until an energy balance is established. When this occurs high V_o voltage may cause a capacitor breakdown or a dangerously high voltage to occur. *Mohan, N., Undeland, T.M., and Robbins,W.P (1995).*

Therefore in the proposed study the output voltage is controlled in each cycle and while the D is changed, this is taken into consideration.

All of the equations above demonstrate that the Boost converter works as a DC/DC transformer. The Boost converter do not need low voltage capacitor because the inductor L is used as an energy store instead of low voltage capacitor which is used for storing energy during turn off time in the Buck converter.

The boost converters can be used as a dc motor breaking controller and while the motor is in electric breaking mode, they operate as dc generators, whose terminal voltage falls as the machine speed decreases. In this mode, the boost converter transfers power to the fixed source. *Rashid M. H. (1993).*

The boost converter in continuous conduction draws a continuous source current, but the load current will be discontinuous. This continuous source current may be

advantageous for PV applications as it reduces the filtering required between the PV and the converter. Again the converter may be operated in discontinuous mode, when the load voltage will depend on both duty ratio and switching current. With the boost (or book-buck) converter the voltage may reach to a very high value if there is no load current, unless active measures are taken to prevent this from happening. *Markvart T. and Castafier L. (2003).*

2.2.3 Inductor Volt-Second Balance

Net volt-seconds applied to inductor over one switching period:

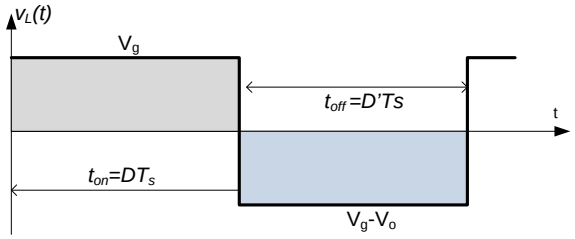

Figure 2.15 Inductor voltage wave form.

$$\int_0^{T_S} v_L(t)\,dt = (V_g)\,DT_s + (V_g - V_o)\,D'\,T_s$$

In periodic steady state, the net change in inductor current is zero. So equate to zero and collect terms:

$$V_g(D + D') - V_0 D' = 0 \quad solve\ for V_o$$

$$V_o = \frac{V_g}{D'} = \frac{V_g}{1 - D}$$

So, the voltage conversion ratio is conversion ratio *M(D)* of the boost converter

$$M(D) = \frac{V_O}{Vg} = \frac{1}{D'} = \frac{1}{1 - D}$$

2.2.4 Capacitor Charge Balance

In periodic steady state, the net change in capacitor voltage is zero. So collect terms and equate the result to zero:

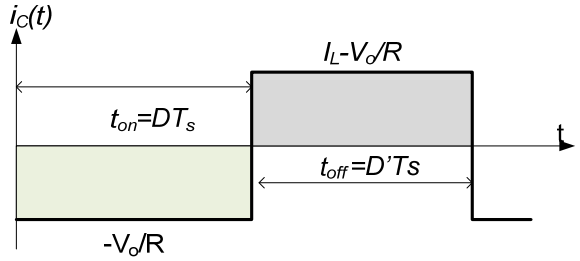

Figure 2.16 Capacitor current wave form

$$\int_0^{Ts} i_C(t)\,dt = (\frac{-Vo}{R})\,DT_S + (I_L - \frac{Vo}{R})\,D'T_S$$

$$D + D' = 1$$

$$\frac{Vo}{R}D = I_L D' - \frac{Vo}{R}D'$$

$$\frac{Vo}{R}(D + D') = ID' \Rightarrow I_L = \frac{Vo}{RD'}$$

This demonstrates that the dc component of inductor current I_L is equal to the load current eliminated V_o to express in terms of Vg:

$$I_L = \frac{Vg}{RD'^2} = \frac{Vg}{R(1-D)^2}$$

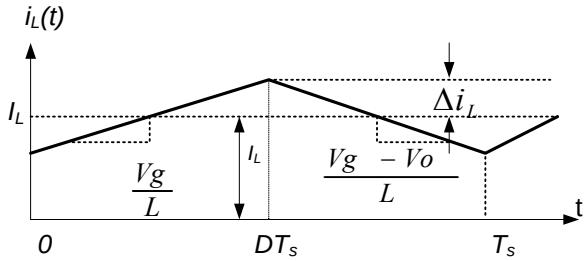

Figure 2.17 Current wave shape of boost inductor

Maximum and minimum inductor currents are determined by using the average value and change in current Δi_L. *Hart D. W. (1997).*

$$Imax = I_L + \Delta i_L = \frac{Vs}{(1-D)^2 R} + \frac{V_S DT_S}{2L}$$

$$Imin = I_L - \Delta i_L = \frac{Vs}{(1-D)^2 R} - \frac{V_S DT_S}{2L}$$

2.2.5 Computing and Manufacturing of Boost's Inductor

Computational formulas of an inductor are given in the previous section. In this section computational manufacturing of an inductor is released for boost converter to work in continuous or noncontinuous mode. After the inductor value is determined, manufacturing of this inductor is started. But, first, some important relations must be given. Ampere's law;

$$\oint H\,dl = I_{net}$$

H=Magnetic field intensity vector produced by the current I_{net}, I is measured as Ampere and H is measured ampere-turns per meter. Composed from Ferromagnetic material core is wrapped N turns winding and its mean path length is called l_c. The I_{net} is then NI which produces all the magnetic field in the core.

$$H\,l_c = NI$$

So, the magnitude of magnetic field intensity is;

$$H = \frac{NI}{l_c}$$

Produced field flux in the core depends on the material of the core. The relationship between the H (magnetic field intensity) and resulting B (magnetic flux density) within a material is given by

$$B = \mu H$$

B= Resulting magnetic flux density (also called the magnetic induction, its units are webers per square meter, Teslas, T).

H=Magnetic field intensity (its units are ampere turns per meter).

Permeability (its units are henrys per meter),

$$\mu = \mu o\, \mu r$$

μ_o =Free space permeability and its value is 4π x 10^{-7} H/m

μ_r=Relative permeability which is used for comparing permeability of any material with permeability of free space.

The material core permeability is very important for flux density. The great majority of flux remains inside the high permeability core and little flux travel through the surrounding air which its permeability is lowest. This little flux is important for determining the flux linkages between coils and the self-inductances of coils in transformers and motors. The total flux in an area is;

$$\Phi = \int_A B\, dA \Rightarrow \Phi = B\, A,\ \textit{(For constant area)}$$

A is cross-sectional area of the core and B is assumed constant throughout the area. The total flux in the core;

$$\Phi = B\ A = \frac{\mu N i A}{l_c}$$

Magnetomotive force (*F amper-turns*) is any physical cause that produces magnetic flux and is equal to the effective current flow applied to the core. It is analogous to electromotive force or voltage in electricity. In the magnetic circuit, the applied magnetomotive force (mmf) causes flux Φ to be produced.

$$F = N\, i = \Phi R$$

In the above formula *R* is reluctance of circuit and its units are ampere-turns per Weber.

$$R = \frac{l_c}{\mu A}$$

The general characteristic of a magnetic circuit are similar to electric circuits as the expressions for reluctance and resistance are similar. For example series reluctances are summed to obtain total reluctance and resultant parallel reluctance are obtained like as parallel resistors.

$$R_{eq}=R_1+R_2+R_3+R_4+\ldots\ldots$$

$$\frac{1}{R_{eq}} = \frac{1}{R_1} + \frac{1}{R_2} + \frac{1}{R_3} + \frac{1}{R_4} + \ldots..$$

B-H figure below shows that it is necessary to increase the reluctance of inductor to have no saturation in the core. Thus, when the current drawn by coil is increased, the saturation does no occur in the core, in other words B-H curve becomes a linear one.

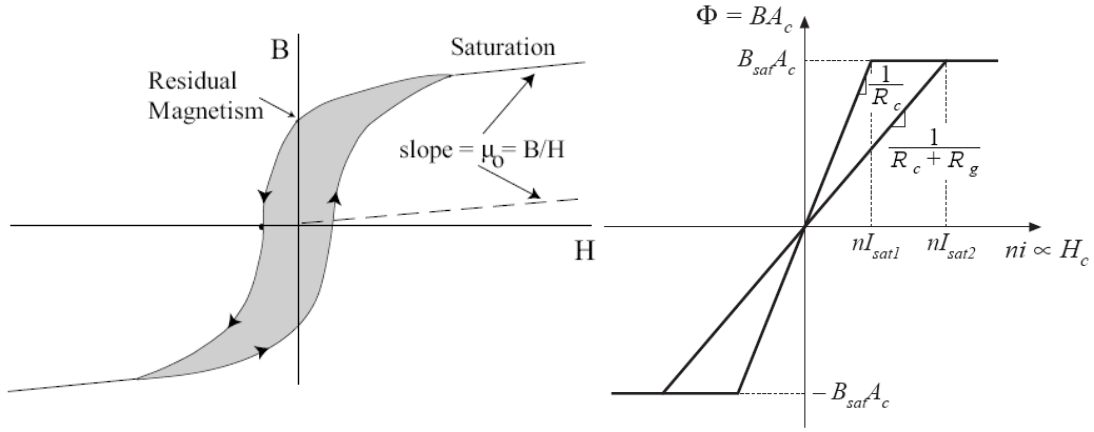

Figure 2.18 B-H curves and saturation characteristic of core.

$$e = N\frac{d\varphi}{dt} = \frac{d\lambda}{dt} = L\frac{di}{dt}$$

λ, is flux linkage of the winding and equal to;

$$\lambda = N\varphi = L\,i$$

$$L = \frac{\lambda}{i} = \frac{N}{i} = \frac{N}{F/N} = \frac{N^2}{F} = \frac{N^2}{R_{tot}} = \frac{N^2}{R_{gap}+R_{core}} = \frac{N^2}{R_{tot}}$$

The succeeding formulas are given to be used in the computation of the value of inductance; (http://en.wikipedia.org/wiki/Inductor)

$$L = \mu_0 \mu_r \frac{N^2 r^2}{D}$$

Basic inductance formula for a cylindrical coil (http://en.wikipedia.org/wiki/Inductor):

$$L = \mu_0 \mu_r \frac{N^2 A}{l}$$

Inductance formula for any iron cored inductor (Charles, 1997):

$$L = \frac{3.19 N^2 A_c 10^{-8}}{l_g + \frac{l_c}{\mu_\Delta}}$$

L = Inductance in henries (H)

μ_0 = Permiability of free-space = $4\pi \times 10^{-7}$ H/m

μ_r = Relative permeability of core material

N = Number of turns

r = Radius of coil winding in meters

D = Overall diameter of toroid in meters

$A = A_c$= Area of cross-section of the coil in squaremeters (m^2)

l = Length of coil in meters (m)

l_c=Lenght of the core gap

l_g=Lenght of the core magnetic path

μ_Δ=Incremental permeability

2.2.6 Using MOSFET as a Switch and Adjustable Resistor

We able to use both Power MOSFET and BJT in our power circuits but we have preferred the power MOSFET because it does not suffer from second breakdown and sharing current in parallel devices is possible. Also, the power MOSFETs do not require the large dc base-drive currents of power BJTs that requires additional power dissipated driving circuitry.

However, that the drive stage in a MOS power amplifier should be capable of supplying sufficient current to charge and discharge the MOSFET's large and nonlinear input capacitance in the time allotted. The operate speed of power MOSFET higher than the power BJT. *(Sedra, & Smith 2004)*

2.2.6.1 Characteristics of Power MOSFETs.

Generally power MOSFETs characteristics are quite similar to those of small signal MOSFETs. But the differences between them are not discussed in this study. Power MOSFETs have threshold voltages in the range of 2V to 4V. In saturation, the drain current is related to V_{GS} by the square-law characteristic of equation which is given below.

$$i_D = \frac{1}{2}\mu_n C_{ox}\left(\frac{W}{L}\right)(v_{GS} - v_t)^2$$

However as shown below in Figure 2.19, the i_d-v_{GS} characteristic becomes linear for larger values of v_{GS}

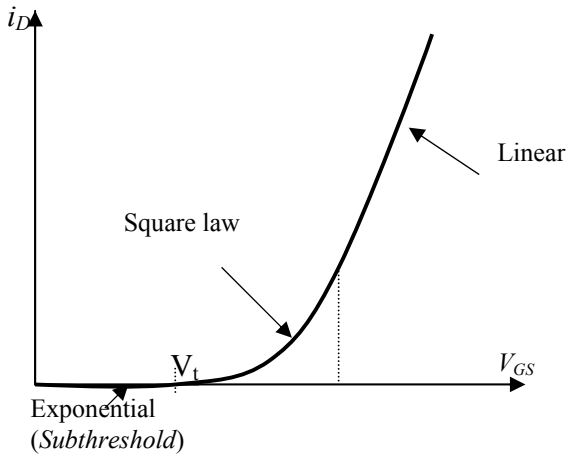

Figure 2.19 Transfer characteristic of MOSFET

To consider deeply; the MOSFET's V_{DS} versus I_D characteristic is explained in three regions (triode region, saturation region, and cut-off region). When used as a switching device, only triode and cut-off regions are used, whereas, when it is used as an amplifier, the MOSFET must operate in the saturation region, which corresponds to the active region and denoted below figure2.20. MOSFET behaves like a constant resistance R_{DS} during in the on state region (triode region). R_{DS} is linearly proportional to the change between V_{DS} and I_D. This resistor value is important for computing the dissipated power losses and voltage drop across on the MOSFET. *Rashid, M.H. (2001)*

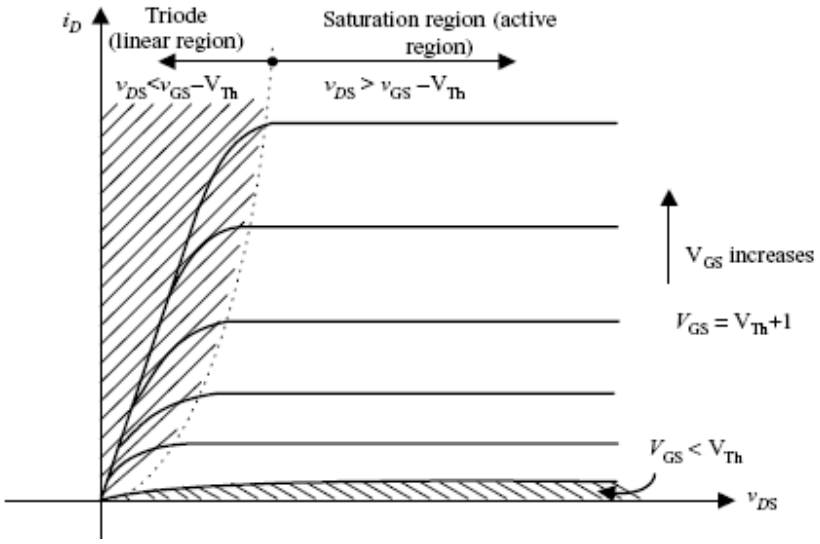

Figure 2.20 The I_D vs. V_{DS} of MOSFET Characteristic

One of the most important parameters that affect the MOSFET switching behavior are the parasitic capacitances between the device's three terminals, namely, gate-to-source, Cgs, gate-to-drain Cgd and drain-to-source (Cds) capacitances. During turn on, capacitors Cgd and Cgs must be charged through resistance R_G and the gate, hence, the design of the gate control circuit must take into consideration the variation in these capacitances. The objective of the drive circuit is to charge and discharge the gate-to-source and gate-to-drain parasitic capacitances to turn on and off the device, respectively.

$$\tau = R_G (C_{GS} + C_{GD})$$

In this study, a parallel resistor is connected to C_{GS} capacitor to discharge the C_{GS} capacitor in a short time. Additionally, to obtain MOSFET's linear characteristic the dc bias circuit is added to Mosfet driver circuit. The bias voltage value is near the threshold voltage but is not equal to it.

2.3 Finding MPP with Boost Converter

In this section Boost converter circuit is designed and MPP of PV is obtained by this circuit. The components and circuit of Boost converter were given in the previous section. Its main components are MOSFET and Inductor, so in the following section we design the Inductor for Boost converter. The MOSFET and its driving circuit which is composed of DAC (with OPAMP) are explained. The MOSFET triggering characteristics are given and on the last sections, determining MPP is given with respect to different methods (Open circuit voltage, short circuit current and triggering of MOSFET in linear region).

2.3.1 A Boost Converter Design for Charge Regulator

To minimize the ripple in the current supplied from the solar panel, the boost converter must work in Continues Conduction Mode (CCM). As mentioned before the minimum inductor's values in CCM is

$$L_{boundary} = \frac{T_S V_O}{2 I_{OB}} D(1-D)^2$$

In the proposed system, two solar panels (125W and 20W) are used as boost converter charger source, so the converter input voltage for 125W panel (V_g) varies in a wide range from 12V to 17.4V, and for 20W panel varies from 12V to 16.5V. To charging two 12Vx18A or two 12Vx200A batteries the boost output voltage (V_o) must vary from 25V to (nominally 1.22x24 = 29.28 V) 30V. The output of converter current is varied from C/4 to C/100, so if the battery capacity current is 18A, the minimum

average output current (I_{oB}) is 180 mA else if the battery capacity current is 200A, the minimum average output current (I_{oB}) is 2A. The maximum power output is restricted by maximum output power of PV; 20W or 125W. Very large capacitor is used as converter output capacitor.

From above equation; For 20W panel; with respect to $D=(V_o-V_g)/V_0$; D=(30-12)/30=0.6, D=(25-12)/25=0.52, D=(30-16.5)/30=0.45, D=(25-16.5)/25=0.34 the duty cycle D is to be in range of 0.34 - 0.6 for 20W panel and for boost converter inductance boundary value for 18Ax24V batteries is calculated as below; The PWM frequency is 5 kHz so *Ts*=0.2 ms. I_{oB}= 180 mA, D=0.6, Vo=30V

$$L_{boundary} = \frac{0.2*10^{-3}*30}{2*180*10^{-3}} 0,6(1-0,6)^2 = 1.6\,mH$$

For 200A x 24V batteries; I_{oB}= 2A, D=0.6, Vo=30V

$$L_{boundary} = \frac{0.2*10^{-3}*30}{2*2} 0,6(1-0,6)^2 = 0.144\,mH$$

For 125W panel;

D=(30-17.4)/30=0.42, D=(30-12)/30=0.6, D=(25-12)/25=0.52, D=(25-17.4)/25=0.304

I_{oB}= 180 mA, D=0.6, Vo=30V $L_{boundary}$ = 1.6mH

I_{oB}= 2 A, D=0.6, Vo=30V $L_{boundary}$ = 0.144 mH

Under solving above boundary inductor formula the minimum inductors' value must be 1.6 mH which is chosen to keep the inductor current continuous and the ripple small. The output current of converter is 125W/25V=5A, and 20W/25V=0.8A in ideally.

2.3.1.1 Design of Boost's Inductor

In this section, the inductor of boost converter whose value was calculated in previous section will be designed by using two E ferromagnetic cores.

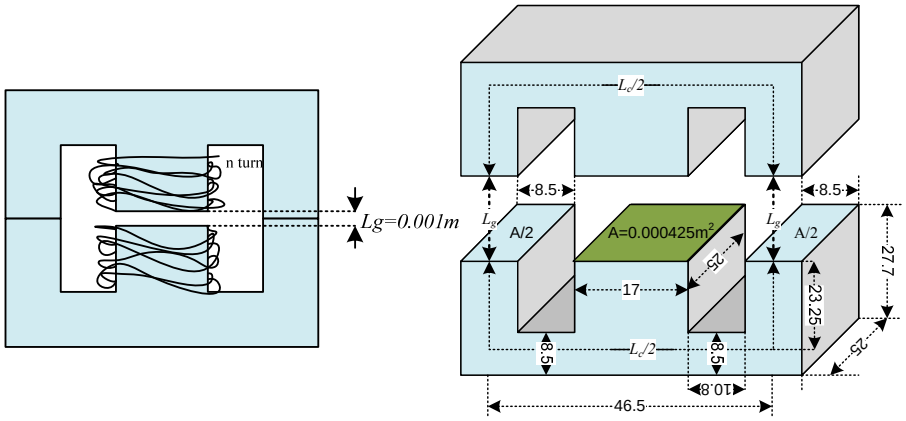

Figure 2.21 Used E core inductor and its cross-sections

The two E core with gap are used to make boost's inductor. Using previous flux formula the flux in the cores can be found.

$$\Phi = B\ A = \frac{N\,i}{R_{tot_{()}(R_{gap}+R_{core})}} = \frac{Ni}{\frac{l_c}{\mu cAc} + \frac{l_g}{\mu oAg}}$$

When μc is much bigger than μo ($lg/\mu o >> lc/\mu c$) the flux is nearly independent of the *e* core permeability, namely;

$$\Phi \approx \frac{N\ I}{R_{gap}} \approx \frac{NI}{\frac{l_g}{\mu_o Ac}}$$

If gapped cores are used the flux level and temperature do not affect the core permeability and the inductance is not changed. According to the final formula the resultant inductance is approximately independent of core properties. Past experiences have shown that, the most important reason of using gapped core is generally not known

the permeability of ferromagnetic core in the market and getting its knowledge value is hard so gapped core ferromagnetic inductor have been preferred. Its calculation is illustrated below;

$$L = \frac{N\Phi}{I} \approx \frac{N^2}{R_{gap}} = \frac{N^2}{\frac{l_g}{\mu_O A_g}}$$

In the Section 2.3.1; the inductance value was found as 1.6 mH, according to this winding number can be calculated as below for gapped core which is illustrated in Figure 2.21.

$$N = \sqrt{Lx\frac{l_g}{\mu_O x A_g}} = \sqrt{0.0016\,Hx\frac{0.001m}{4\pi 10^{-7}\frac{W}{Am}x\,0.000425m^2}} = 54.7 \approx 55\ turns$$

The diameter of magnet wire used in the inductor can be calculated with the help of WireTronic Inc's Wire Info Software program which is shareware on the internet. *http://www.wiretron.com/magnet.html.*

The boost's inductor wire diameter for 125W panels is calculated below;

$$\frac{Vo}{Vg} = \frac{Ig}{Io} = \frac{25\,V_{min\_battery}}{17.4V\,max\,PV} = \frac{7.2A\,max\,PV}{Io} \Rightarrow Io = \frac{7.2x17.4}{25} = 5.01A$$

It is multiplied by safety factor (1.25); Io_inductor current = 1.25x5.01=6.26A
According to program, the inductor diameter for 6.26A is 18 AWG= 1.0236 mm

For 20W panels is calculated below;

$$\frac{Vo}{Vg} = \frac{Ig}{Io} = \frac{25\,V_{min\_battery}}{16.5V\,max\,PV} = \frac{1.212A\,max\,PV}{Io} \Rightarrow Io = \frac{1.212x16.5}{25} = 0.8A$$

It is multiplied by safety factor (1.25); $I_{o\_inductor\ current}$ = 1.25x0.8=1A
According to program,the inductor diameter for 1A is 26 AWG= 0.4039 mm
Using these data, the needed inductors were made.

2.3.1.2 Design of DAC with OPAMPs

Necessity for driving of Boost Switch the OPAMP in the circuit must supply enough current to turn on switch. There are two OPAMP to make digital to analog conversion. The first OPAMP (741) are used to conversion and the other (OPA547) are used for inverting first OPAMP output and supply enough current to the Semiconductor Switch for triggering the MOSFET. The circuit at issue is given Figure 2.2 and the model of OPA547 is given Figure 2.23.

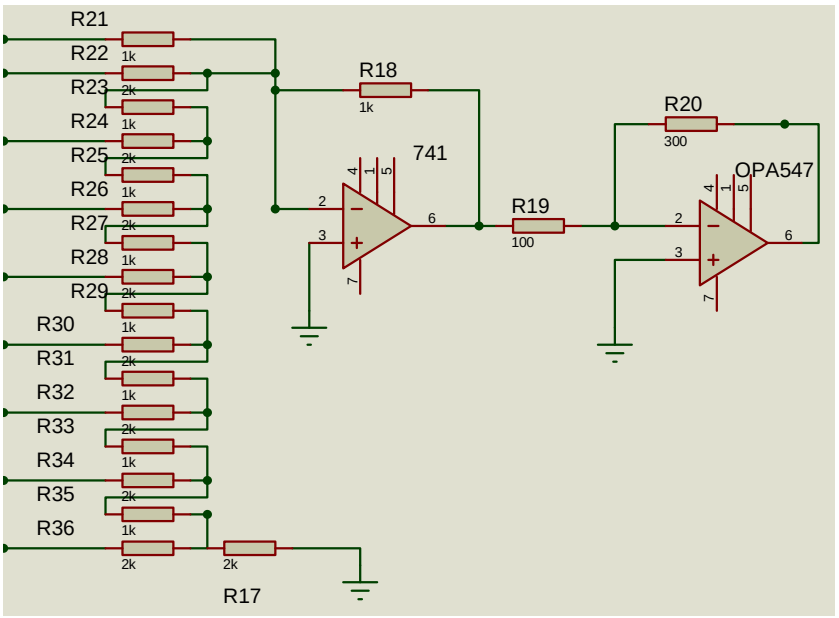

Figure 2.22 DAC with LM741 and OPA547 circuit.

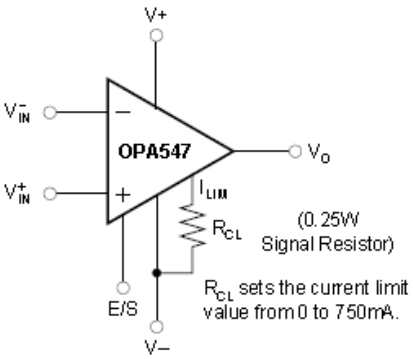

Figure 2.23 547 OPAMP model

The features of OPA547 are given below; Wide supply range; Single supply: +8v to +60v, dual supply: 4V to 30V. High output current: 500 mA continuous. Wide output voltage swing; fully protected: thermal shutdown, adjustable current limit, Output disables control, thermal shutdown indicator, high slew rate: 6v/μs, low quiescent current

2.3.1.3 Current Transducer with Differential Amplifier

Current Transducer LTSR 15 NP is used in the Circuits. Its general characteristics can be observed catalog on the web (www.lem.com). In normally, while there is no current on the primary side, the output value is 2.5V. If there is 15A on the primary current, the output of LEM is 3.125V. That is to say, the output voltage range is changed from 0 to 0.625V. This value is not enough for PIC's ADC so a Differential Amplifier must be used. Differential Amplifier firstly takes difference of output and the reference; then amplifies it.

The general definition of Differential Amplifier and its circuit are illustrated below.

$$Vout = \frac{R2}{R1}(V2 - V1)$$

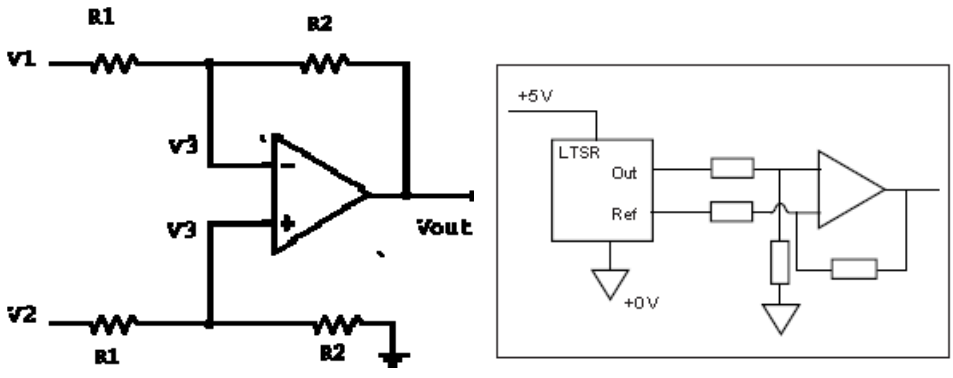

Figure 2.24 Differential Amplifier with LEM LTSR15

2.3.2 Implementation of Some MPP Methods with Designed Circuit

Generally tracking of MPP is achieved by DSP in the above 1KW large scaled PV systems but in 80-200W small scaled system using DSP loses cost efficiency. Therefore in this study, a low cost microcontroller is used for tracking of MPP. In this part; open circuit voltage and short circuit current method are performed. Constructed circuit, which is illustrated in Figure 2.25, is able to supply both methods and can be used for tracking MPP in large scaled PV systems.

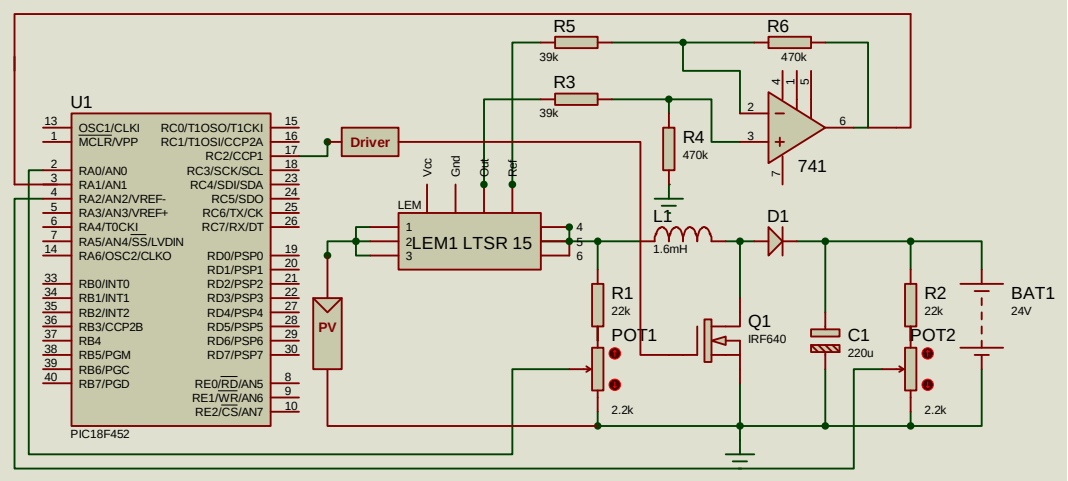

Figure 2.25 Used circuit for MPP in the Open circuit Voltage and Short Circuit Voltage methods

2.3.2.1 MPPT Technique Based on Open Circuit Voltage

Firstly, the constant *k* for using Panel (KC125T) must be founded. When the proposed circuit is used as a boost converter in order to charge the batteries, the batteries' voltages must be greater than the boost converter input (PV) voltage. When the blockage diode is blocked by the batteries voltage, the PV open voltage can be measured by the microcontroller. Then it is multiplied by constant *k* to obtain the MPP optimum voltage.

k for KC125T;

$$k = \frac{V_{MPP}}{VOC_{PANEL}} = \frac{17.4}{21.7} = 0.80$$

After finding the MPP voltage, the battery charging voltage value is calculated, the microcontroller generates PWM to control output of boost according to MPP point. Every 4 minutes later this process is repeated for finding optimum MPP. If T_s is defined as 8 bits width PWM, the t_{on} can be found binary and it is replaced onto microcontroller PWM duty register.

$$V_{battery\_Charge\_Voltage} = 1.22 \times V_{battery} = 1.22 \times 24 = 29.28 = \frac{V_{PV\_MPP}}{1\text{-}D} = \frac{0.8 \times V_{OC}}{1\text{-}D}$$

$$D = (1 \quad 0.027322 \times V_{oc}) = \frac{t_{on}}{Ts} \Rightarrow ton = Ts \times (1 \quad 0.027322 \times V_{oc}) \Rightarrow PWM_{registerr\_value} = \frac{256 \times t_{on}}{T_S}$$

For example; The PWM frequency is given 5 kHz and $V_{batteries\_voltage}$ is given 24V, read open circuit panel voltage is 21.7, and k constant is taken 0.80 so, find ton and PWM register value.

T_s=1/(5kHz)=0.0002 sec.

$V_{battery\_charge\_voltage}$= 29.28 V

V_{MPP}=0.8 x 21.7V=17.4V

29.28/17.4=1/(1-D) => D=0.4057377 so ;

t_{on}= T_sxD =0.000081147

Then it is to be written t_{on} as 8 bit register value=256x0.000081147/0.0002=103.86≈104

The T_s is known, the V_{oc} is measured and the V_{MPP} is calculated by the microcontroller. As demonstrated on the following flow chart and calculations t_{on} of PWM is computed and generated from microcontroller' PWM output pin RC2.

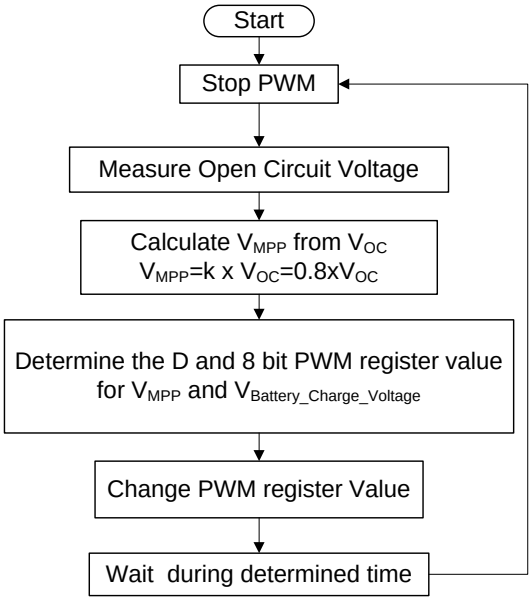

Figure 2.26 Flow chart of finding MPP with open circuit voltage control

In the below Figure 2.27-28, solar radiation and output characteristic of 125W PV panel illustrated are given, which are mounted parallel to the ground in a sunny February day. The MPPs are calculated with the help of proposed MPP methods.

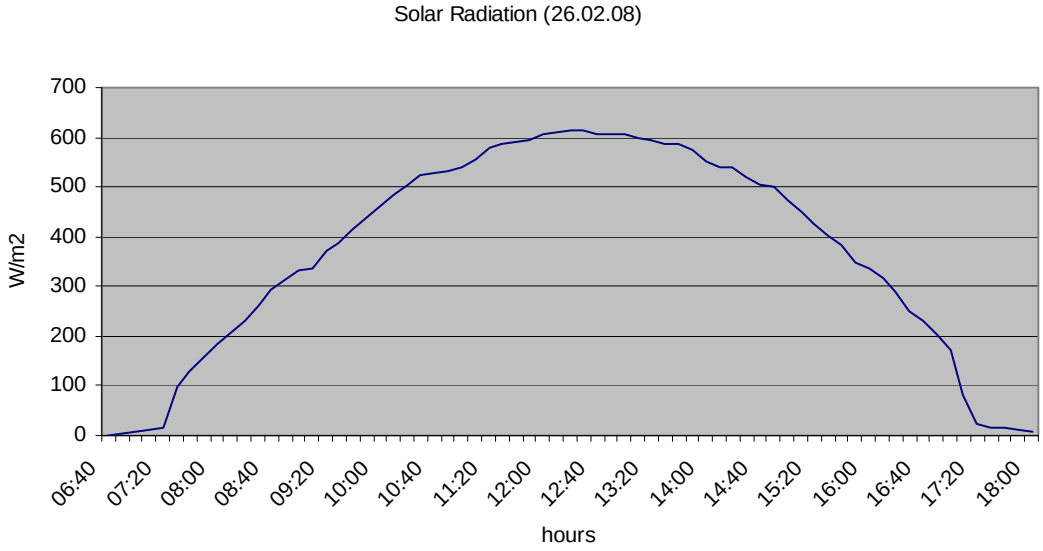

Figure 2.27 Measured solar radiation on the horizontal plane. (Measured by VANTAGE PRO2)

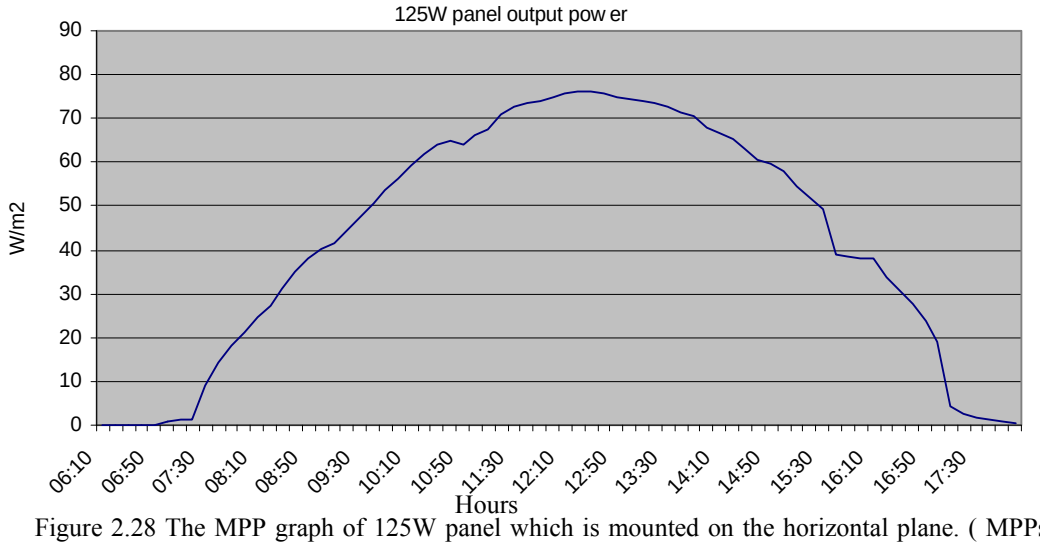

Figure 2.28 The MPP graph of 125W panel which is mounted on the horizontal plane. (MPPs were measured by our method)

2.3.2.2 MPPT Technique Based on Short Circuit Current

In the aimed study the boost converter is used, so extra components are not used in such a way that the boost main switch is used as short circuit component during sample time (2ms). The general circuit is given in the figure 2.25. The flow chart is illustrated in the below explains briefly short circuit current MPP technique.

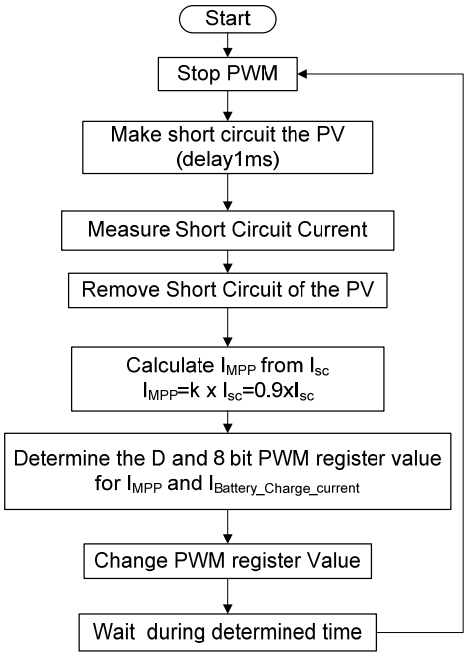

Figure 2.29 Flow chart of finding MPP with open circuit voltage control

We can use parameters (k=M_c) and calculate MPPs but short circuits current parameters given above can not be suitable for our PV panels. Therefore, firstly the control system developed must determine a suitable parameter value and then with the help of this, the system calculates the most effective maximum power point.

k for KC125T;

$$k = \frac{I_{MPP}}{I_{sc\,PANEL}} = \frac{7.2}{8} = 0.90$$

I_{MPP} = 0.9 x I_{sc}, from boost converter formulas;

$$D = 1 - \frac{I_{battery}}{kxI_{sc\,PANEL}} =$$

If battery capacity current is C/6 = 3A, and I_{sc} is 7.2A, the calculated D and t_{on} are;

$$D = 1 - \frac{3A}{0.9x7.2} = 0.53703703 = \frac{t_{on}}{Ts} \Rightarrow t_{on} = 0.0002x0.53703703 = 0.000107407$$

If we write ton as 8 bit register value = 256 x 0.000107407/0.0002 = 137.48≈137

When the t_{on} is 137, Vbattery_charge _voltage is 2.15x$Vin_{(MPP)}$ but the battery voltage bound the boost output voltage during constant current charge interval, after this interval, the system take into consideration the output voltage with respect to battery, otherwise over voltage charges is encountered.

During short circuit time (per four minutes) the panel loss energy; we calculated the loosing energy for our panel during one day (6 hour);

Day time as minutes=6x60=360 minutes

360/4=90 sampling is executed 90x0.002s=0.18s => 125Wx0.18/3600=0.00625 W is lost during one day (the panel power is assumed 125W during 6 hours)

The total power of panel is 6x125W=750W => efficiency = (750-0.00625)/750 = 0.9999916.

If sampling is taken every 200 ms, efficiency is;

6x60x60x1000=21600000ms => 21600000ms/202ms =106930 is number of sampling value. 106930x2ms=213861ms=0.05940 hour. 0.05940 hour.x125=7.42W so efficiency is (750-7.42)/750=0.99

The above results illustrate that the efficiency of our system is sufficiently high.

2.3.2.3 MPPT Technique Based on Short Circuit Current and Open Circuit Voltage

In the previous two sections, MPPs were obtained from either open circuit method or short circuit method. In this section, both methods are used together. MPP point is calculated and estimated. The comparison of this method and the new methods is given Section 2.3.3.2 .The flowchart of this method is given in Figure 2.30.

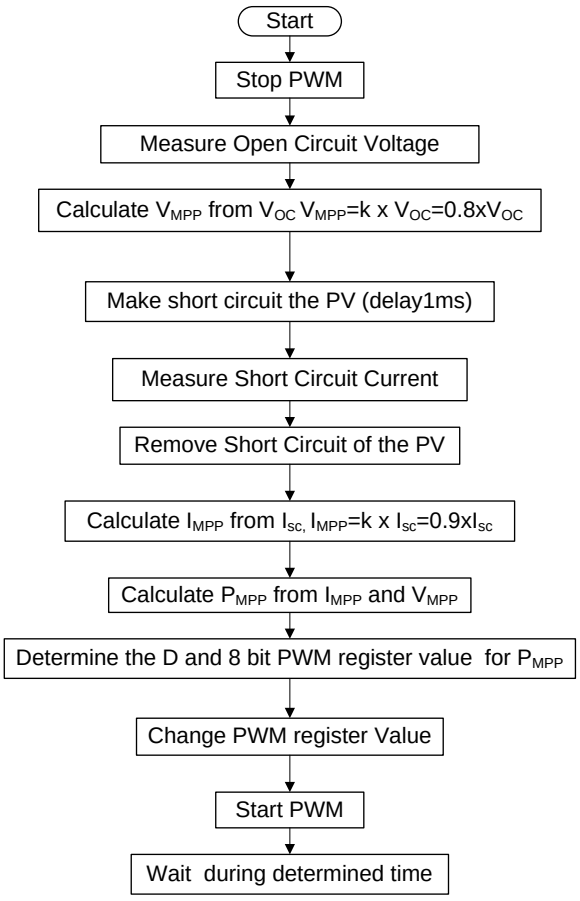

Figure 2.30 Finding MPP Based on Short Circuit Current and Open Circuit Voltage

2.3.3 Finding MPP with Converters' Working in Linear Region of MOSFET

The aim of this thesis is to find MPP with the help of a new method. The main idea is to use MOSFET as a variable resistor. For this purpose, boost converter is used and its semiconductor switch (Transistor, MOSFET) is used in three regions that are on, off and linear region. While the circuit can find the MPP of PV, at the same time it is used as charge regulators or etc. In a short time interval the circuit finds the MPP using the MOSFET as a linear component, after finding MPP, the MOSFET is used on-off switch for boost converter. In a boost converter, extra components or complex circuits are not used for finding MPP, only a simple linear driver is constructed which is controlled by microcontroller.

2.3.3.1 Using MOSFET in Linear Region

Firstly Power Transistor (2N6284) is used as a semiconductor switch in the study but experiments were shown that its behavior at linear region is affected by its thermal characteristics. Therefore use of MOSFET (IRF840) is required. Because of MOSFET's linear region is between at 4V-6V, forward biasing of MOSFET is necessary. The MOSFET is biased with a potentiometer and connected DAC's output. Experimental results are given below;

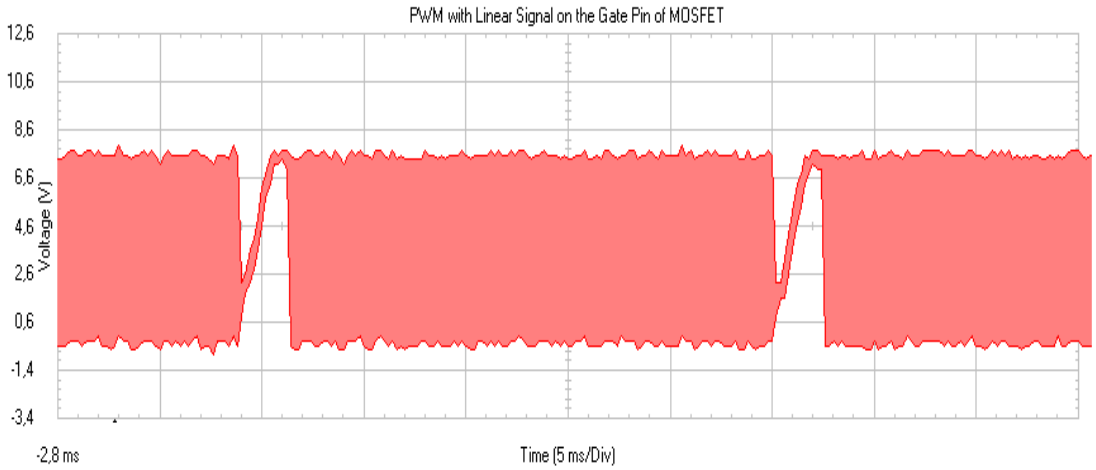

Figure 2.31 a) Applied PWM with Linear signal on the gate pin of MOSFET.

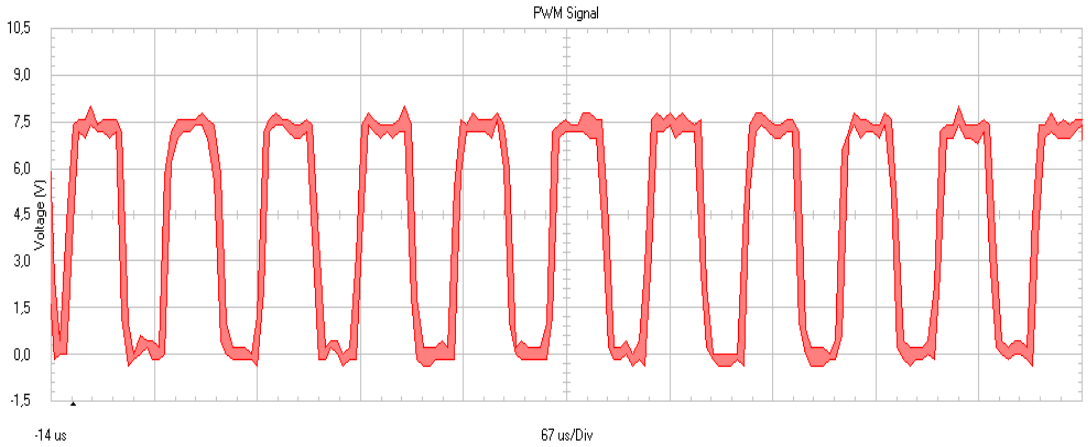

Figure 2.31 b) PWM signal applied to the gate of MOSFET

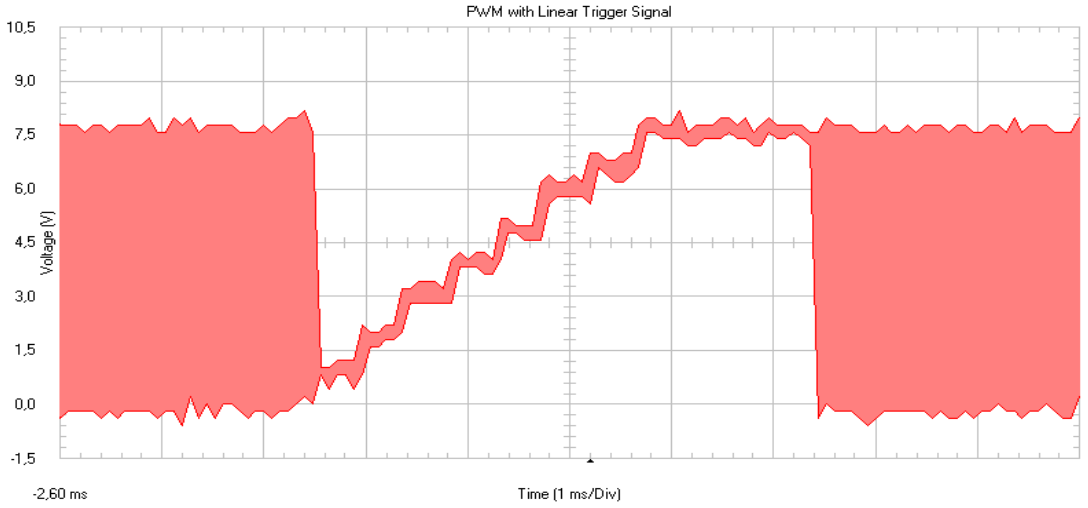

Figure 2.31 c) Extended region of linear signal

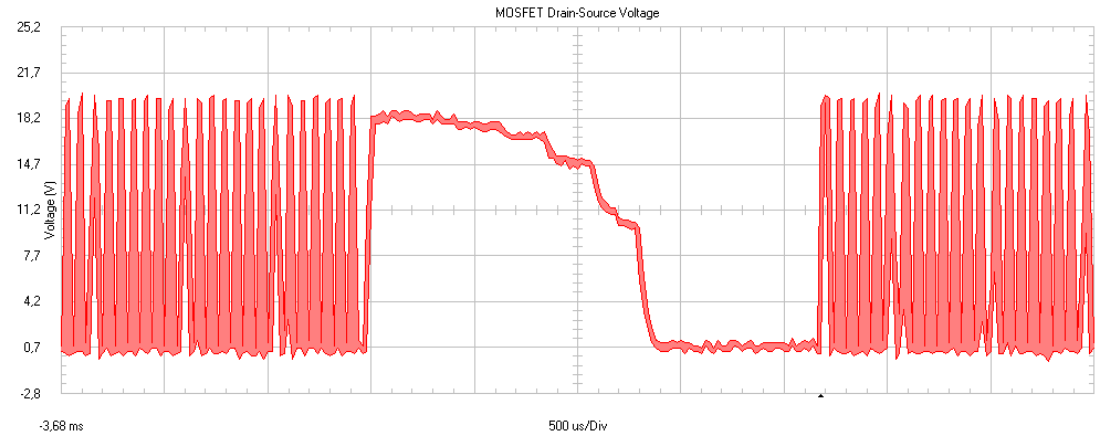

Figure 2.32 The voltage characteristic of MOSFET between the drain and source pins.

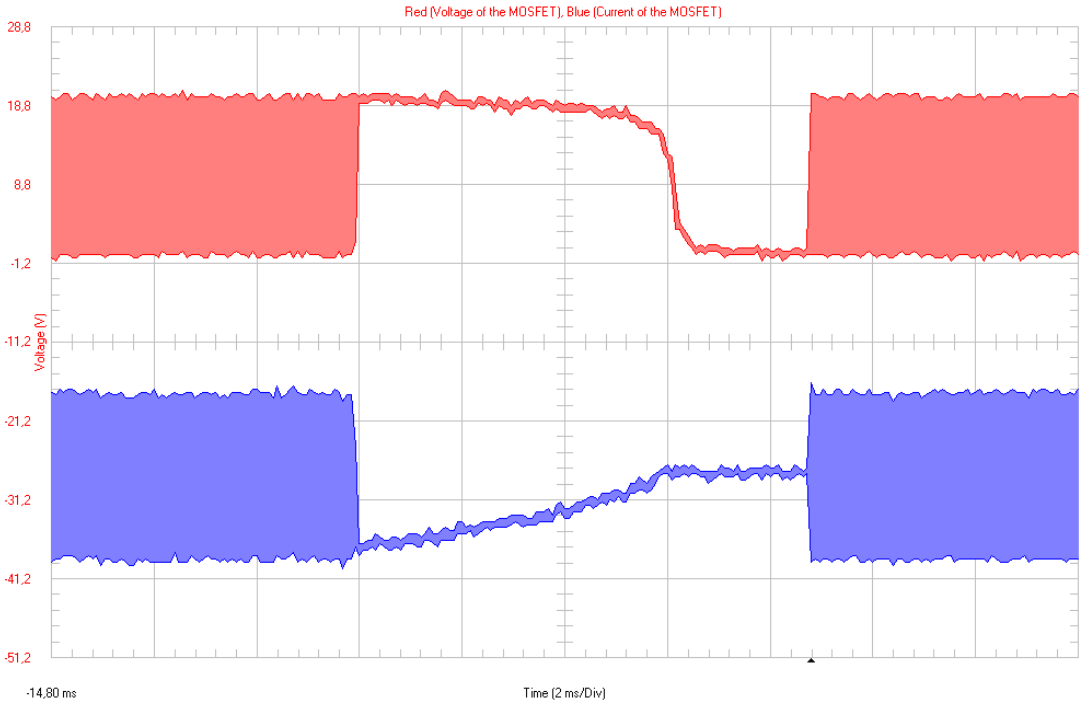

Figure 2.33 MOSFET's D-S voltage and current according to linear pulse of Gate

Every four minutes the control system stops the PWM and generates linear pulse (0-10V). When the linear pulse is applied to the gate of MOSFET, microcontroller read the panel voltage and current. After multiplying them, generated power can be calculated. Applying software program, the maximum power, maximum voltage and current can be determined. According these values, the new charge methods can be applied. Flowchart of finding MPP with MOSFET is demonstrated in Figure 2.34.

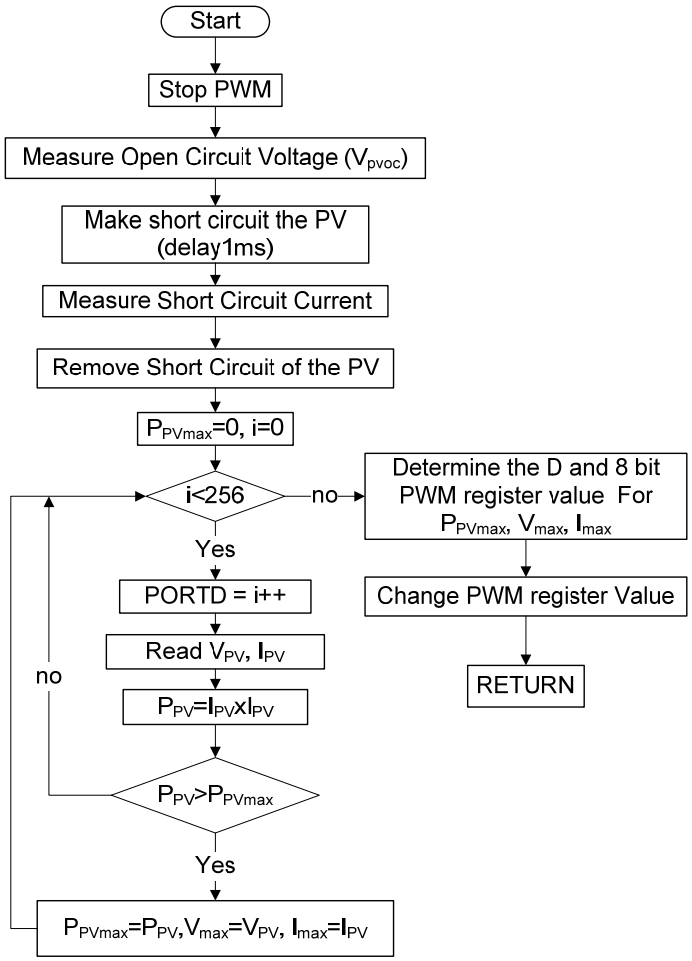

Figure 2.34 Flowchart of finding maximum power point

The comparison of the results of the new method and classical rheostat method is illustrated in Figure 2.35. These results are obtained from the 125W panel which was fixed at the orient position in 22.12.2007 (the radiation is between 345Wm^2 -240Wm^2, the temperature was +12^{o}C which is measured by Vantage PRO2 weather station instrument).

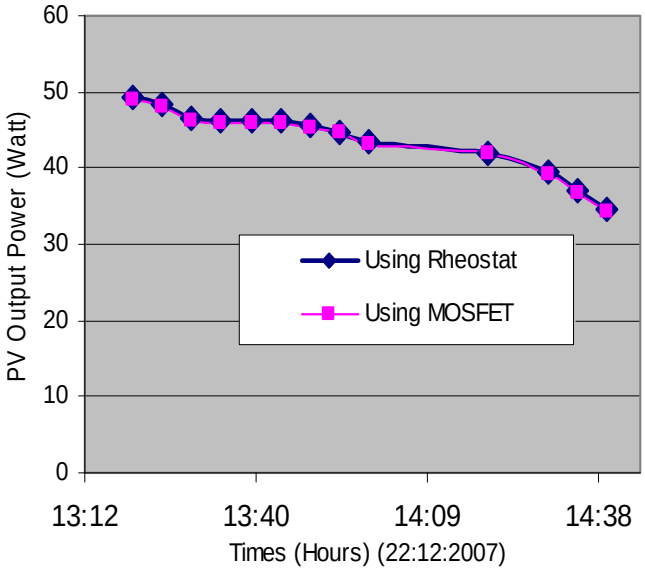

Figure 2.35 Comparison of results

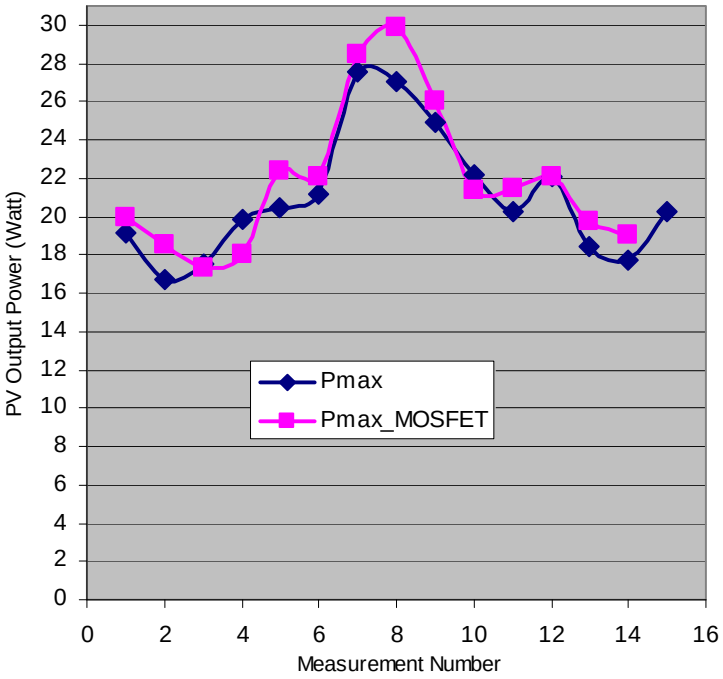

Figure 2.36 Comparison results of V_{oc}-I_{sc} with aimed method.

2.4 Conclusion

In this Chapter, first, existing MPP tracking systems and a related literature review were presented. MPP tracking techniques were classified, their working principles were explained and their advantages and disadvantages were discussed. Second, a detailed information was given on the boost type circuit and its design that is used for both MPP tracking and charging batteries in MPP. Furthermore, a detailed description of one of these circuit elements, MOFSET, was given and the design of the inductor was explained (this design work can be regarded as a basis for other work in this subject).

Working principals of other circuits (digital analogue converter, differential amplifier) used between microcontroller circuit and boost circuit were explained and designed. The circuit designed and produced is able to implement existing MPP tracking methods due to its flexible structure. For this reason, MPP values were found with respect to open circuit voltage Voc and short circuit current Isc as illustrated figure 2.36.

The essence of this chapter is to find a new tracking method for MPPs. In this method, the linear region characteristic of semiconductor switches was used as rheostat. Any boost, buck or buck-boost converters must use semiconductor switch. As a result, we track MPPs on the circuits above without an additional external circuit. When you drive a semiconductor switch (MOSFET, Transistor, etc.) in linear region, you can use it as a rheostat. For this purpose a boost converter and its semiconductor switch MOSFET were used in this thesis. This method is very useful for finding MPPs. When the output characteristics of the constructed circuit are analyzed and compared with the others, the results draw attention.

There is no need for extra elements (DSP, PLC etc.) except a microcontroller and hall effect current transducer whose costs are very low (both of them are 20$). This prototype circuit does not only work with the new method, but also works with all the methods proposed previously.

CHAPTER THREE
BATTERIES

There are a number of technical solutions to the problem of energy storage. Storing energy in the electric field of a capacitor is a solution to store energy in the time range from microseconds up to 10 s. Storing energy in the magnetic field of a coil is a technology that has been under development for many years (superconducting coils). It has, however, until today, not resulted in a product that has entered the commercial market *(Crompton C.R, 2000).* The energy can be stored too as compressed air, hydrogen or another form but today it is not common, battery makes the most sense. The batteries have been one of the most important components of energy storage system yet as in the stand alone PV system. It takes the advantage of storing energy. It also supplies huge instantaneous surges of current or power which the PV system does not support (for example a refrigerator is supplied with 300 W at steady state but initially it requires 5 times more power, that is 1500W). If the batteries with PV system are not configured correctly, the designed system does not work and leads to faults. In this chapter we aim to explain battery types, battery characteristics and their charger and discharger systems. They can be classified in accordance with substances of their structure and the areas in which they are used.

Rechargeable Battery Types used in PV Systems can be classified according to their substances.

1. Nickel batteries
2. Lithium batteries
3. Lead-Acid batteries

3.a) By application

- Conventional automobile batteries (starting, lighting and ignition SLI)
- Low-cost deep cycle batteries (golf cars)
- Stand-by (stationary) batteries
- Traction (propulsion) batteries

3.b) By production technology

- Flooded/Wet cell batteries
- Valve regulated lead acid batteries (VRLA):
- AGM Absorbed glass mat batteries
- Gel cell batteries

3.c) By construction

- Plate type
- Grid alloy
- Grid thickness

Many different types of rechargeable batteries suitable for PV applications are currently available. The lead-acid battery is still the most common for relatively economical storage of relatively large quantities of electrical energy and will probably remain so at least for the next few years. The other batteries are more expensive per joule stored than lead-acid units. It is predicted that Nickel metal hydride and several lithium technologies will provide cost effective storage in the future. For example, *Ni-Cad* batteries have common use in applications that require sealed batteries capable of operating in any position, and still require high energy density. NiCad batteries don't suffer from cold weather effects, which is the main reason why they are sometimes used instead of lead acid batteries in cold climates. It should be noted that normal methods of PV charge control are not possible for sealed nickel-cadmium, nickel-hydride or lithium batteries and these are rarely specified for smaller PV systems. *Messenger, R. A., & Ventre J. (2005).* In spite of its cost in some application (in solar powered racing car, electric vehicles, and satellite) Nickel, Lithium and the other kind of batteries have been used. So except lead-acid batteries, the other batteries will be explained briefly.

3.1 Nickel Batteries

Nickel-Cadmium: The nickel-cadmium battery system has a nominal voltage of 1.2 V/cell. The typical end voltage for discharge in PV systems is 0.9-1.0 V/cell, and the

typical end voltage for charging in PV systems varies between 1.45 and 1.6 V/cell, depending on battery, controller and system type. There is no relationship between open circuit voltage and SOC. They can survive freezing and high temperatures, can be fully discharged and are less affected by overcharging. As a result, in some applications, Ni-Cd batteries may be a better choice because their robust nature may enable the elimination of the system charge controller. Loss of charge is also temperature dependent. The loss rate is greater at higher temperatures, but at a temperature of –20 ^{o}C, there is almost no loss at all. If Ni-Cd batteries are charged and then left unused, they will lose charge at the rate of approximately 2% per day for the first few days, but then stabilize to a relatively low loss rate. Over a 6-month period, the total loss is typically about 20%, depending on whether the battery is a high, medium or low discharge rate battery. The higher the discharge rating of the battery, the greater the loss of charge overtime. The lifetime of a Ni-Cd battery depends on how it is used, but is less dependent on depth of discharge than that of lead-acid batteries. A lifetime of at least 2000 cycles can be expected for a battery when it is not used extensively at elevated temperatures. Ni-Cd batteries may be charged at either constant current, constant voltage or somewhere in between. This makes them especially useful in PV applications, since a PV array tends to act as a constant current source, depending on the cloud cover at the moment. If Ni-Cd batteries are overcharged, gassing will occur and the water in the electrolyte will decompose, creating a need for more maintenance. Normally, charging from full discharge to full charge should be accomplished in 5 to 7 hours, with a charging voltage between 1.50 and 1.65 volts per cell. The ampere-hour charging efficiency of the most efficient Ni-Cd batteries approaches 85%. If the battery discharge exceeds their capacity limit, the low capacity cells can be driven into reverse polarity (i.e. will have a voltage less than 0 V), which can shorten their life. It is therefore usual to specify that a nickel-cadmium battery in a PV system has a maximum DOD (Depth Of Discharge) of 90%. If the battery is not fully discharged prior to recharge; the battery will tend to discharge only to the point where it was most recently discharged, which is called *memory effect*, and then lose cell voltage. To cope with memory effect of NiCad batteries a remedy for restoring the full capacity is “reconditioning”, in which the battery is fully discharged to almost zero voltage once

every few months and then fully charged to about 1.55 volts per cell. Other types of batteries do not have the memory effect. *Patel, M. R.,(1999).*

Disadvantages of Ni-Cd batteries include difficulty in determining the state of charge of the batteries and the toxicity of the cadmium, which creates an environmental concern during production and disposal. Industrial nickel-cadmium batteries used in PV systems are normally of the open type designed for standby use at low discharge rates. Industrial open type nickel-cadmium batteries are typically 3-4 times more expensive per kWh of energy stored than industrial open types of lead-acid batteries.

Nickel-Metal Hydride: The NiMH is an extension of NiCd technology, and offers an improvement in energy density over that in NiCd. The major construction difference is that the anode is made of a metal hydride. This eliminates the environmental concerns of cadmium. Another performance improvement is that it has negligible memory effect. The NiMH, however, is less capable of delivering high peak power, has high self-discharge rate, and is susceptible to damage due to overcharging. Compared to NiCd, NiMH is expensive at present.

3.2 Lithium Batteries

The lithium technologies appear quite attractive due to energy densities up to 150 Wh/kg and long charge retention and shelf life. They can be charged with a constant voltage or constant current source in which the maximum charge current should not exceed the 10h rate and the termination voltage should not exceed 2.1-2.2 V per cell. If the temperature is below 0°C, charging should be carried out at the 20 h rate and should not be carried out at temperatures below - 10°C.*Patel, M. R.,(1999).*

They have low cycle life, relatively poor high rate performance, relatively poor low-temperature performance, capacity fading and potential safety problems. It should be remembered that metallic lithium is highly reactive and presents danger if it contacts water or humans. *Messenger, R. A., & Ventre J. (2005).*

Lithium-Ion: Lithium-ion technology is a new development, which offers three times the energy density over that of lead-acid. The lithium-ion has higher cell voltage of 3.5 versus 2.0 for lead acid and 1.2 for other electrochemistry. In operation, the lithium-ion electrochemistry is vulnerable to damage from overcharging or other shortcomings in the battery management. Therefore, it requires more elaborate charging circuitry with adequate protection against overcharging.

3.3 Lead-Acid Batteries

Today the most popular battery material is lead-acid. Depending on aided material its characteristic changes. This type of batteries consist of charged lead dioxide (PbO_2) positive plates, negative lead active material spongy plates and an electrolyte of sulphuric acid solution in water. During discharge the lead dioxide of the positive plate and the spongy lead of the negative plate are both converted to lead sulphate. During the charge and discharge, the sulphuric acid concentration (density) changes. So, adequate acid must be supplied to fully charge battery. *Markvart, T.,& Castafier, L.(2003).*

The cycle life of lead-acid batteries is related to thickness of plates. For example, while an automotive battery plate's thickness is about 1.016 mm, the forklift batteries almost 7 times (6.502 mm) as thick as auto batteries. In the same way, golf car plates' thickness are from 1.778 to 2.794 mm and AGM's are 2.921mm.

Today, some important problems of lead acid batteries are self discharging and water losing so a few industrial batteries has special caps that convert the Hydrogen and Oxygen back into water, reducing water loss by up to 95%. Lead-Antimony batteries have a much higher self-discharge rate (2-10% per week) than Lead or Lead-Calcium (1-5% per month), but the Antimony improves the mechanical strength of the plates, which is an important factor in electric vehicles. The Antimony increases plate life at the expense of higher self discharge. If left unused for long periods, these should be trickle charging to avoid damage from sulfating. (*Deep Cycle Battery FAQ.htm)*

3.3.1 *Construction* of *Lead-Acid Batteries*

3.3.1.1 Plate Type

Lead-acid batteries for PV systems are manufactured by using *pasted flat plates* or *tubular plates*.

Pasted flat plates: The most common form of lead-acid battery plate is the flat plate or grid. It can be mass produced by casting or it can be wrought. The active material is applied to the grids by pasting and drying.

Tubular plates: These are used in the positive plates of some larger industrial lead-acid batteries. Cycle life is longer because the active material is more firmly retained in woven tubes. So-called positive plate batteries actually have a tubular positive plate and flat negative plate.

3.3.1.2 Grid Alloy

Pure lead is too weak to use as a conventional grid material and for longer battery life, alloy additives is important. Alloy additives (antimony or calcium) are mainly used to strengthen the grid, but these primary additives can have bad effects on cycling, corrosion or water consumption, so secondary additives are also used.

High antimony alloys give high water consumption as the battery ages but give good cycle life. Their use is mostly restricted to traction batteries at present.
Low antimony alloys (1-3%) plus other elements such as selenium or arsenic are widely used in open lead-batteries, but cannot be used in ‘sealed’ batteries because a small amount of hydrogen gas is always produced.

Calcium alloys (0.06-0.9%) are used for sealed batteries but pure lead calcium alloys give poor cycle life and poor recovery from a deep discharge. The addition of tin to the alloy corrects this. Other alloys are used by some manufacturers but have

similar properties to low antimony or lead-calcium-tin alloys. It is important to check whether the grid alloys are suitable for a battery selected for PV use.

3.3.1.3 Grid Thickness

Especially for the positive grid where the corrosion mostly happens, the thicker the grid, the longer the battery life in most cases. However, the thicker the grid, the more expensive the battery is likely to be. For tubular plates, the same applies to the spine thickness.

3.3.2 Types of Lead-Acid Batteries

Many different types of lead-acid batteries are manufactured for different uses. The use of modified lead-acid solar batteries is increasing day by day. We can basically classify lead-acid batteries with respect to production types in two ways:

- Open or ‘sealed’ construction
- Mass-produced or ‘industrial’ types

There is a wide range of lead-acid battery types to choose from when designing a PV system, and there is always a trade-off between battery cost and expected lifetime. In order to understand the differences between the various types of lead-acid battery available, it is necessary to understand a little about how they differ in construction.

3.3.2.1 Sealed lead-Acid Batteries

There is a fundamental difference between open (vented) or ‘sealed’ (valve-regulated) lead-acid batteries. In open batteries, overcharge results in the conversion of water into hydrogen and oxygen gases, which are lost to the atmosphere. Water has to be added to these batteries from time to time to make up this loss. In valve-regulated batteries, overcharge results in oxygen gas production at the positive plate.

Because the space between the plates is not completely filled with acid, the oxygen gas can reach the negative plate where it is re-converted back to water. This recombination of oxygen gas can only proceed at a certain rate. If the charging current is too high, then oxygen gas pressure will build up inside the cell, and eventually the safety valve will release oxygen (and some acid spray) into the atmosphere. This will result in permanent loss of water. There are two types of 'sealed' (more correctly, valve-regulated) lead-acid battery, the so-called AGM and Gel types.

- **AGM *Type***: This type of battery uses an absorbent glass mat (AGM) between tightly-packed flat plates. All the acid is absorbed in the glass mat separator, but the pores of the glass mat are not completely filled. The empty (or part-empty) pores provide a pathway for oxygen gas formed at the positive plate during charging to move to the negative plate for recombination. AGM batteries were mainly developed for a good high current (short discharge time) performance. They contain very little acid (the fiberglass mat is only 95% saturated with sulfuric acid and there is no excess liquid), which means that they are very susceptible to water losses which especially occur at high temperatures. In contrast, they have a good resistance to being frozen solid, since there is space for expansion within the AGM and there is no liquid to freeze and expand, they are practically immune from freezing damage. Nearly all AGM batteries are sealed valve regulated (commonly referred to as "VRLA" - Valve Regulated Lead-Acid).

  The newer AGM (absorbed glass mat) batteries have all the advantages (and then some) of gelled, with none of the disadvantages and its self-discharges at about 1-2% per month, while an old one may be as much as 2% per week. This means that they can sit in storage for much longer periods without charging than standard batteries. The charging voltages are the same as for any standard battery - no need for any special adjustments or problems with incompatible chargers or charge controls. The internal resistance is extremely low, there is almost no heating of the battery even under heavy

charge and discharge currents. In the recombinant batteries AGM, the Oxygen and Hydrogen recombine inside the battery and the recombination is typically 99 % efficient, so almost no water is lost. AGM's will cost 2 to 3 times as much as flooded batteries of the same capacity. AGM batteries main advantages are no maintenance, completely sealed against fumes, Hydrogen, or leakage, non-spilling even if they are broken, and can survive most freezes.

- **Gel *Type:*** In lead-acid gel batteries, the sulphuric acid is mixed with finely-divided silica which forms a thick paste or gel. The freshly mixed gel is poured into the cell container before it sets. As the gel dries, microscopic crack forms which allow the passage of gas between the positive and negative plates are required for the recombination process. This formation of cracks may occur during the early part of a gel battery's service life, so both hydrogen and oxygen can be given off from a new battery through the safety valve. Attention should be paid to the manufacturer's instructions concerning this, especially regarding ventilation requirements. Unlike AGM batteries, gel batteries can be made with either flat or tubular positive plates and when the battery's cases are broken, acid spilling is impossible. The gel provides a better means of heat conduction from the plates to the cell walls than in AGM batteries, so heat produced on overcharge is lost more efficiently. According to the references *Deep Cycle Battery FAQ.htm, Messenger, R. A., & Ventre J. (2005*).

  The gel batteries have several disadvantages. Some of them are explained below; the sustained high current capability (to prevent excess gas from damaging the cell, both charge and discharge are made at slower rate C/20) is not as good for gel batteries as for AGM batteries. They can not be fast charged on a conventional automotive charger or they may be permanently damaged, but these are not normally a problem for PV use except in any hybrid system an auxiliary generator or inverter bulk charger is used, current must be limited to the manufacturer's specifications. Some other disadvantages of gel cells are that they must be charged at a lower voltage

(2/10 th's less) than flooded or AGM batteries. If overcharged, voids can develop in the gel which will never heal, causing a loss in battery capacity. In hot climates, water loss can be enough over 2-4 years to cause premature battery death. At high operating temperatures, they will suffer to some extent from water loss, but since there is more acid that in an equivalent AGM battery, the lifetime reduction will not be so severe.

3.3.2.2 Mass-produced and industrial Batteries

The mass-produced lead-acid batteries are basically of the type used in cars for starting, lighting and ignition (SLI) use. They have relatively thin flat plates that are optimized for producing the high currents needed to start a vehicle engine. Conversely, the thin plates do not lead to a long lifetime in any other application which involves either cycling or operation at elevated temperatures. Most SLI batteries are of the open type. For trucks and boats, batteries with thicker plates are produced, and with some modification these may make a reasonable PV battery for light duty (infrequent or shallow cycling, no high temperature operation). Sealed types with moderately thick flat plates are made for uses such as golf carts, carriages and general leisure uses. Although not strictly speaking mass-produced on the scale that SLI batteries are produced, they are capable of being made in reasonably large volumes and at relatively low cost. Industrial batteries are made for two general applications: float (or standby) duty and deep cycling (especially traction batteries for fork lift trucks, etc). In Europe especially, the tubular plate construction is often used for both types. The tubular plate standby battery type, whether open or gelled, is often the battery of choice for larger PV systems where the highest possible lead-acid battery lifetime is required. The tubular plate battery is also available in deep cycling or ‘solar’ versions from some manufacturers. Unfortunately the techniques used to increase the cycle life nearly always reduce the standby life at the same time, and this generally means that they give a lower PV service lifetime unless the cycling requirement is unusually deep. Industrial lead-acid batteries with very thick flat plates are also made, especially for standby use. They are available as open, gelled or AGM types. The thickness of their flat plates determines their maximum lifetime on

standby duty, and it is common to see such industrial batteries described by the manufacturer as 5 year design life, 10 year design life or even 20 year design life. These of course refer to the design life under optimum operating conditions, not those in PV systems. Higher capacity industrial lead-acid batteries are mostly available only as 2 V single cells. These are assembled into batteries of the required voltage. Lower capacity industrial lead-acid batteries are normally available as 12 or 6 V units, known as blocks or monoblocks.

- **Starter Batteries:** These batteries are used generally for cars starting, lighting and ignitions (SLI) systems. Starter batteries includes lead-acid batteries type and composed of relatively thin flat plates which are made as effective as possible for producing the high currents required for starting vehicle engine. The shallow discharge units typically have a small amount of calcium combined with the lead to impart greater strength to the otherwise pure lead. The plates can then be made thinner with greater area to produce higher starting currents. These units should not be discharged to less than 75% of their capacity. However, their thin plates do not lead to long life time at applications with deep cycling and high temperature. Its available capacity is not extracted more than 20-25% at any time. Automotive batteries will generally fail after 30-150 deep cycles if deep cycled, while they may last for thousands of cycles in normal starting use (2-5% discharge).(*Deep Cycle Battery FAQ.htm*) Furthermore with some modification they are used in PV systems. Their prices are low cost and are mass-produced at required volume.

- **Stationary Batteries:** Sometimes called "fork lift", "traction" or "marine" batteries, are used where power is needed over a longer period of time, and are designed to be "deep cycled", or discharged down as low as 20% of full charge (or DOD 80%). These are often called traction batteries because of their widespread use in forklifts, golf carts, and floor sweepers. Deep discharge lead-acid batteries use antimony to strengthen the lead and can be cycled down to 20% of their initial capacity. The major difference between a true deep cycle battery and others is that the plates are Solid Lead plates - not

sponge. The plates are thicker with less area and are designed for sustained lower level currents. The popular golf cart battery is generally a "semi" deep cycle - better than any starting battery, better than most marine, but not as good as a true deep cycle solid Lead plate. Marine batteries are usually actually a "hybrid", and fall between the starting and deep-cycle batteries. In the hybrid, the plates may be composed of Lead sponge, but it is coarser and heavier than that of starting batteries. "Hybrid" types should not be discharged more than 50%. These batteries are designed for using in golf carts, marine applications, electric forklifts and PV system. Although the deep discharge batteries are designed for deep discharge applications, their lifetime in cycles depends on the depth of discharge during normal operation.

- **Traction Batteries:** Application in fork-lift trucks, traction engines, and underground mining vehicles and so on; designed for daily complete cycling with moderate currents and regular and controlled complete charging and cycle lifetimes of 1000 to 2000 cycles with 80% DOD can be achieved. The most common electrode technology in these applications is tubular-plate. Flooded batteries show longer lifetimes than VRLA and are widely used. *(Luque, A.& Hegedus, S. (2003).)*

3.3.3 Properties of the Lead-Acid Storage Battery

The temperature of operation, the rate of discharge and the rate of charge all affect the performance of the battery. Since the electrical path of the battery presents ohmic resistance, some of the electrical energy intended for charging, i.e., storage is converted to heat. When hydrogen is lost, it also represents an energy loss. Typically, the charging process is about 95% efficient. The discharge process also results in some losses due to internal resistance of the battery, so only about 95% of the stored energy can be recovered. The overall efficiency of charging and discharging a lead-acid battery is thus about 90%. Since battery losses to internal resistance are proportional to the square of the current, this means that high current charging or high current discharging will tend to result in higher internal losses and less overall

performance efficiency. This effect is offset somewhat by the increase in temperature of the battery during charging or discharging at high rates due to the higher I^2R losses. It turns out that a warmer battery can hold more charge. It also turns out that if a battery is too warm for too long, its life expectancy is shortened, so charging and discharging rates need to be carefully observed so they will not exceed rated values for a specific battery. The capacity of a battery is often referred to as C. Thus, if a load is connected to a battery such that the battery will discharge in *x* hours, the discharge rate is referred to as C/*x*. Figure 3.1 indicates the effect of discharging rates on the relative amount of charge that can be obtained from a lead-acid battery. The battery can be fully charged at higher charging rates, but it takes more energy at higher charging rates to obtain full charge.

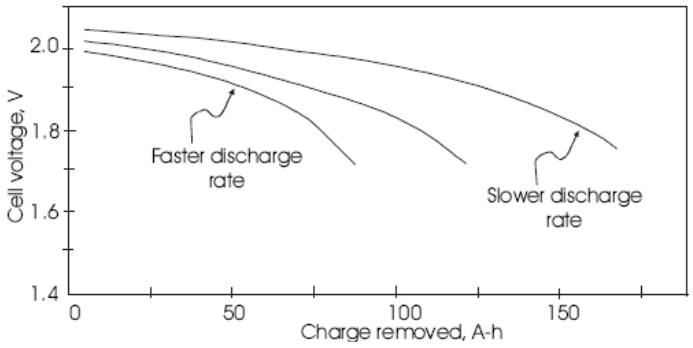

Figure 3.1 Effect of discharge rate on available energy from a lead-acid battery.

When the charging or discharging current must pass through the internal (Thevenin) resistance of the battery, a power loss equal to I^2R occurs. For constant current charging or discharging, the charge delivered to or removed from the battery is given by $Q = I \times t$. Since Q is proportional to energy storage, the energy stored is thus proportional to *I*, whereas the energy lost is proportional to I^2. Hence, at higher charging or discharging rates, a larger fraction of available charging energy is lost to resistive heating. This effect is compensated by the fact that warm batteries are capable of storing more charge than cold batteries, as shown in Figure 3.2. This figure shows the effect of discharge rates and temperature on the relative amount of charge that a battery can deliver. Again, slower discharge rates result in a higher overall amount of charge being delivered by the battery.

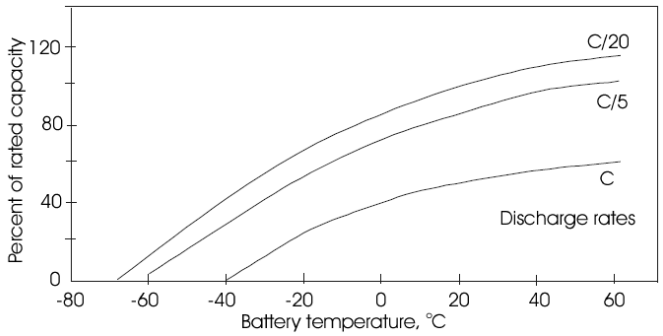

Figure 3.2 Effect of temperature and discharge rate on available energy from a lead-acid battery.

As it is known, thin plate starter batteries should not be discharged to less than 75% of their capacity. In contrast, stasyonel batteries can be cycled down to 20% of their initial capacity. Although the deep discharge batteries are designed for deep discharge applications, their lifetime in cycles depends on the depth of discharge during normal operation. Figure 3.3 shows how the depth of discharge affects the number of operating cycles of a deep discharge battery.

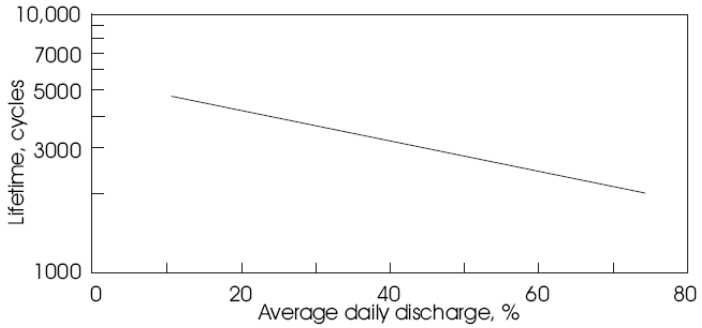

Figure 3.3 Lead-acid battery lifetimes in cycles vs. depth of discharge per cycle.

There is a trade-off between lead-antimony and lead-calcium batteries when venting is considered. Lead calcium battery loses minimal waters from the electrolyte since they are sealed off. Hence, they are maintenance free. As a drawback of these batteries is that if these batteries are either purposely or inadvertently discharged to less than 75% of their maximum charge rating, their expected lifetime may be significantly shortened. Lead-antimony electrodes, on the other hand, may be discharged to 20% of their maximum charge rating. This means that a 100 Ah lead-calcium battery has only 25 Ah available for use, while a 100 Ah

lead-antimony battery has 80 Ah available for use, or more than 3 times the availability of the lead-calcium unit. However, the lead-antimony unit produces significantly more hydrogen and oxygen gas from dissociation of water in the electrolyte, and thus water must be added to the battery relatively often to prevent the electrolyte level from falling below the top of the electrodes. In addition to being maintenance free, sealed deep-discharge units do not leak and have long life and low self-discharge. Charging requirements for sealed lead acid batteries differ somewhat from non-sealed units. While non-sealed units are designed for occasional overcharge, sealed units should not be overcharged.

IEEE1187-2002 provides information on the degree to which the life of lead-acid batteries is shortened if the batteries are operated at temperatures above 25^{o}C. For example, at a temperature of 35^{o}C, the battery lifetime will be shortened to 44% of its expected lifetime at 25^{o}C. This means that it is important to provide adequate ventilation for batteries, not only to vent any hydrogen or other gases, but also to maintain a battery operating temperature close to 25^{o}C. The serious PV system designer should be sure to have access to the *NEC* and IEEE 1187.*Messenger, R. A., & Ventre J. (2005).*

3.4 Battery Charging

In this study, lead-acid batteries are used as storage components as they are generally used. So charging and discharging methods, circuits and modeling of lead acid batteries are introduced and finally a battery charging circuit and modeling are constructed.

As mentioned before the battery's Thevenin equivalent circuit consists of internal resistance and battery-cells voltage. The battery cell voltage is simply the battery open circuit voltage and from this hint, the battery internal resistance can be found with the help of measuring the charging or discharging current and the terminal voltage. During charging, the charge voltage must be greater than battery voltage; as the process continues, V_{cel_Bat} itself increases so the V-I line slides to the right but

during discharging the output of battery voltage is less than $V_{cel\text{-}Bat}$, the slope of the line flips, and the V-I curve moves back to the left.

Thevenin equivalent circuit is; $$R_{int} = \frac{V_{cel\_Bat} - V_{Ter}}{I_{charging\ or\ discharging}}$$

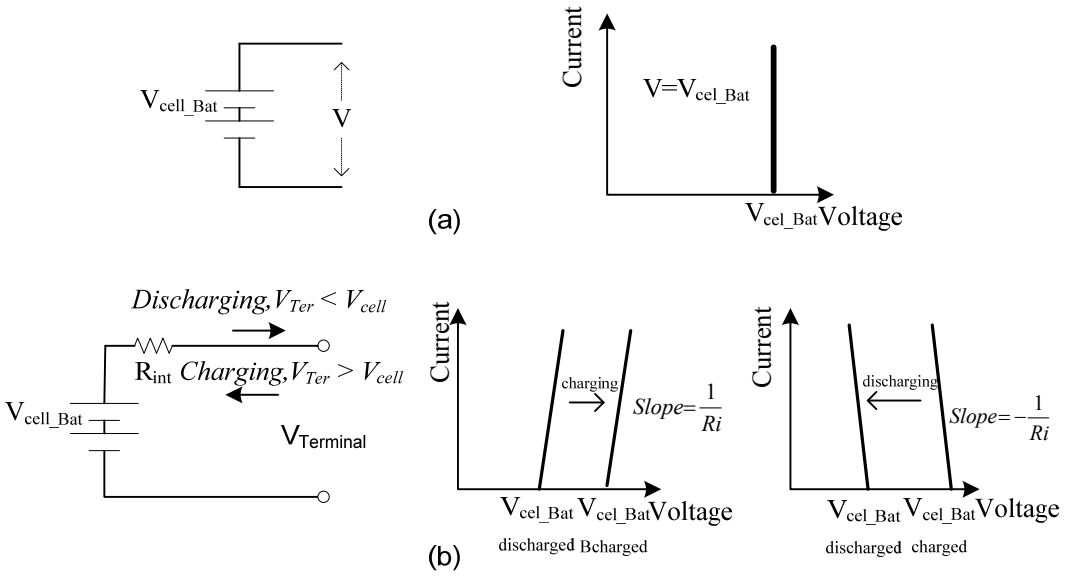

Figure 3.4 An ideal battery symbol and V-I characteristic curve (a), Thevenin İdeal equivalent circuit with internal resistance for a battery under charging and discharging conditions (b).

When the battery temperature decreases the open circuit voltage decreases and its resistance increases. Furthermore, the Thevenin equivalent circuit for an old battery is different from that of a new battery of the same type. Hence, optimal charge controller should consider all of batteries characteristics, and it should incorporate several important features. When the batteries are charged with a specific value, for example 12V, if the charger senses the terminal open voltage as batteries voltage, the charger oscillatory connect and disconnect the batteries terminal from the PV array. Internal resistance voltage drop is misleading for the charger. This causes overcharging of batteries. As a precaution, a circuitry is added to the controller, which senses the oscillation and decreases the charging current. With reducing turnoff set point of the controller and introducing (on-off charge, discharge point)

hysteresis into the circuit the overcharging or insufficient charging of the battery can be eliminated but these are not enough.

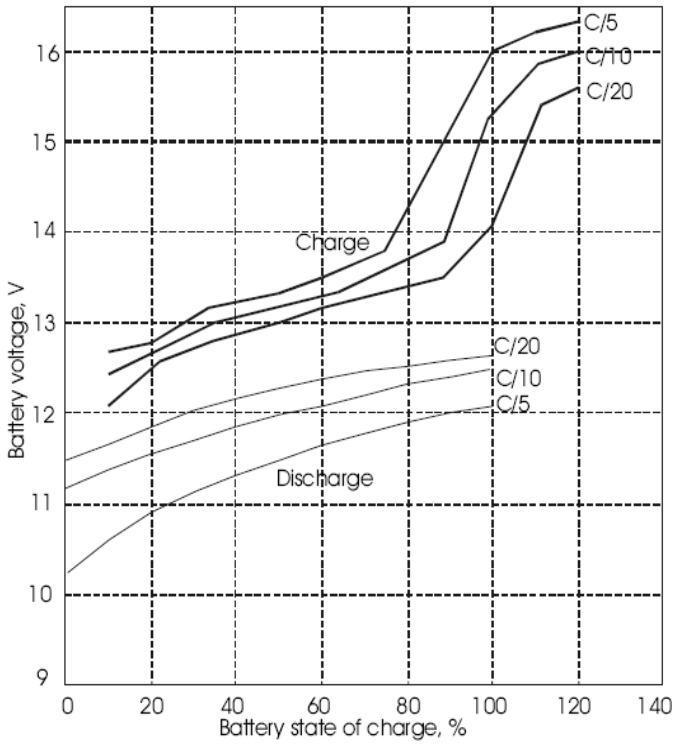

Figure 3.5 Terminal voltages as a function of charging or discharging rate and state of charge

Figure 3.5 shows how the terminal voltage of a battery depends on the charge or discharge rate and the state of charge for a typical battery. Note, for example, that if the battery is charged at a C/5 rate, full charge will be reached at a terminal voltage of 16 V, whereas if the battery is charged at C/20, then the battery will reach full charge at a terminal voltage of 14.1 V. If the charging current is then reduced to zero, the terminal voltage will drop to below 13 volts *(Messenger & Ventre, 2005)*.

Most flooded batteries should be charged at no more than the "C/8" rate for any sustained period. Gelled cells should be charged at no more than the C/20 rate, or 5% of their amp-hour capacity. Note that flooded batteries must bubble (gas) somewhat to insure a full charge and to mix the electrolyte.

3.4.1 Battery Charging Methods

Today many charge control methods are used in PV systems, the following method has been used currently in the modern charge controllers and to understand the other charging methods, this method is explained briefly. The controller initially starts to charge at a relatively high rate, such as C/5 as mentioned before. When the terminal voltage reaches about 15V (2.5V per cell), indicating approximately 85% of full charge, the charging rate is then decreased; taking temperature into account until the battery ultimately reaches 100% charge at a very low charging rate and a correspondingly lower voltage.

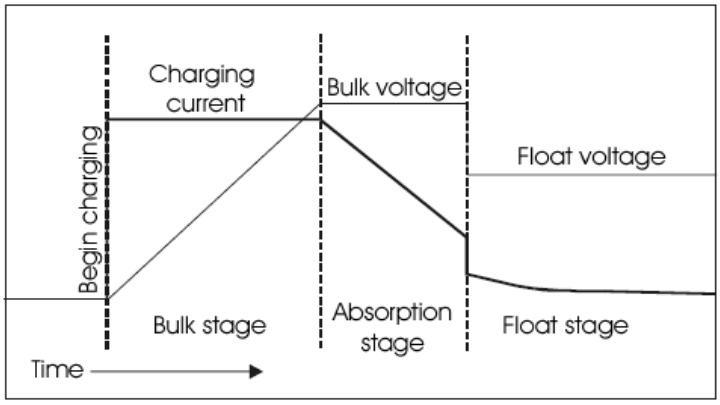

Figure 3.6 Three-stage battery charge control.

In the above Figure.3.6 initially, the charge controller acts as a current source. If the charging mechanism is a PV array, then presumably full array current will be used for charging. This is the bulk stage. When the charging voltage reaches a preset level, the *bulk* voltage, and the charging mode is switched to constant voltage, during which the charging current decreases nearly linearly. This is called the *absorption* stage. The absorption mode is continued for a time preprogrammed into the controller, after which the charging voltage is decreased to the *float* stage voltage. The float voltage is then maintained by the charge controller. The float voltage must be set to a level that will not result in damage to the battery. In fact, since battery temperature affects battery terminal voltage and state of charge, modern charge controllers incorporate battery temperature sensor probes that provide temperature

information to the controller that results in automatic adjustment of charging set points for the charging modes.

A further mode that is available in modern chargers is the equalization mode which is explained detailed in Section *3.4.1.10.* The equalization mode involves application of a voltage higher than the bulk voltage for a relatively short time after the batteries are fully charged. This interval of overcharging causes gassing, which mixes the electrolyte as a result of the turbulence caused by the escaping gases. This mixing helps prevent sulfate buildup on the plates and brings all individual cells to a full state of charge. Only unsealed or vented batteries need equalization. For specific equalization recommendations, manufacturers' literature on the battery should be consulted. Some charge controllers allow for automatic equalization every month or so, but often it is also possible to set the controllers for manual equalization. *(Messenger & Ventre, 2005).*

The following battery-charging methods have been used in PV system. These methods are explained briefly:

3.4.1.1 Direct Connection

In this method; the batteries are connected directly to the PV system. The batteries are charged at the connection point of batteries' load line and PV's V-I curve and the charging current can be restricted by PV max current. *Yamazaki, T., & Muramoto, K.(1998).*

3.4.1.2 On-Off Connection from PV

In this method; firstly a preset overcharge set point is determined. Then, when the battery voltage reaches this point, the batteries are disconnected from the PV arrays. As it seen in direct connection methods, batteries are supplied with the maximum available PV current, which depends on the battery charge state.

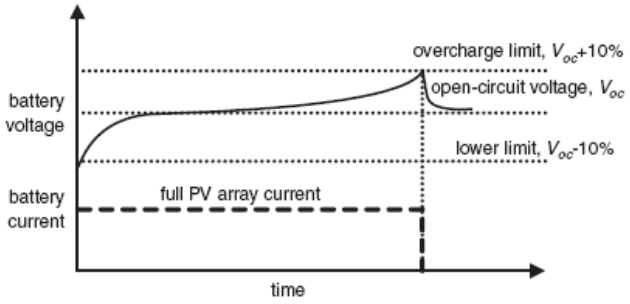

Figure 3.7 On-Off connection of PV system charging shape.

3.4.1.3 Continuously On-Off Connection from PV

This method can be examined in two sections and is based on continuously applying on-off control.

In the first charging method; the on/off current control process, shown in Figure 3.8, is initiated after the battery voltage rises above the end point charge voltage and aims to regulate the battery voltage to a lower floating voltage level.

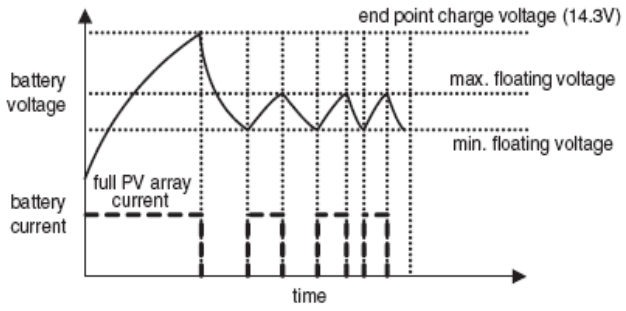

Figure 3.8 Continuously On-Off battery charge regulation control shape at a floating voltage

In the second charging method, a battery charger limits the battery current using on/off control to regulate the battery voltage to an upper set point after the battery voltage rises above a lower set point as shown in Figure 3.9.

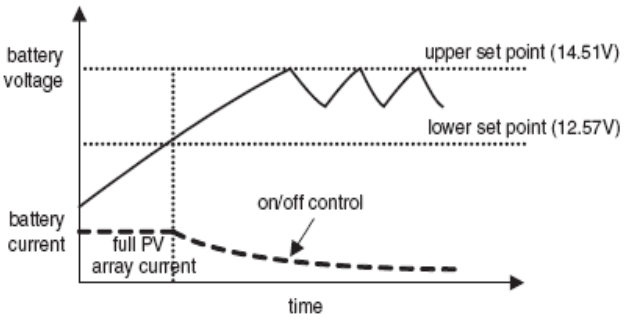

Figure 3.9 Continuously On-Off battery charge regulation control shape at an upper set point

3.4.1.4 With Regulation Set Point

In this method; the batteries voltage is increased to the voltage regulation set point and than batteries voltage is set to regulation at this point. *Harrington, S., & Dunlop, J.(1992).*

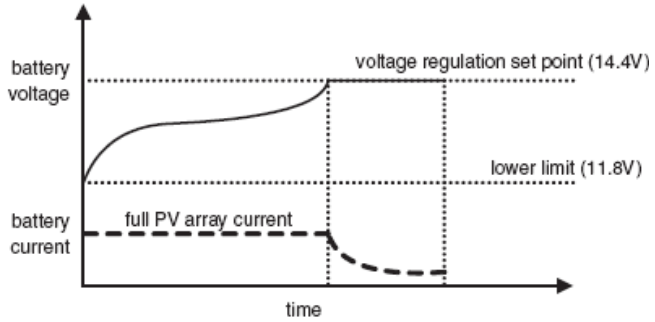

Figure 3.10 Charging batteries with voltage regulation set point

3.4.1.5 Floating Point

This method is similar to aforementioned methods but the battery voltage is set to the floating voltage level and regulated at this lower floating voltage. *Ross, J., Markvart, T., & He, W.(2000).*

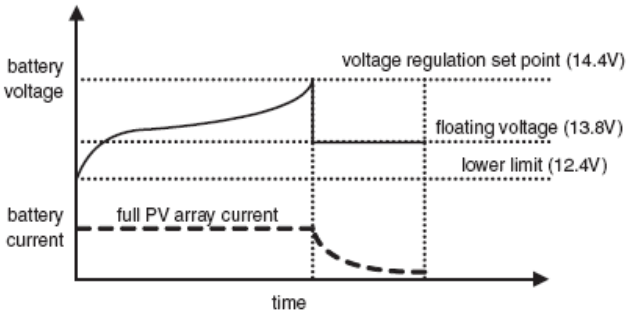

Figure 3.11 Charging batteries with voltage regulation at a lower floating voltage

The disadvantage of these methods is that the overcharge limit or the voltage regulation set point do not always correspond to the battery 100% state of charge condition since, as explained below, the voltage at which battery overcharging begins depends on the charge rate, which varies with respect to atmospheric conditions. Thus, the battery remains in a floating charging state for a longer time until it is fully recharged. Additionally, the on/off control algorithms is that, during the off time, which increases with respect to the battery state of charge, no energy is transferred to the battery, resulting in a prolonged time required to finish the charging process and voltage regulation is not effective in large battery strings, as it results in a non-uniform charging of the individual cells, thus degrading the battery service time performance. *Koutroulis, E., & Kalaitzakis, K. (2004).*

3.4.1.6 Constant-Potential (CP) Charging

This is the preferred method for charging calcium-lead alloy grid low-maintenance batteries. By selecting an appropriate constant charging voltage and initial charging current, the battery can be safely recharged regardless of the depth of discharge in previous discharge cycles. The recommended initial charging currents for calcium-lead alloy low-maintenance batteries can be found formula of;

$$Max\ Initial\ Current\ (A) \cong \frac{Nominal\ Capacity\ (Ah)}{4}$$

When carrying out constant-potential charges-discharges in cyclic use, the battery should be charged at a maximum of 2.5 V/cell. For example in the beginning of charging an approximately 10A h battery initially is charged with 2.2-3 A, as the cell approaches full charge after 4-5 h, the charging current reduces to 0.1 A.

3.4.1.7 Shallow Cycle CP Charging Of Lead-Acid Batteries

A battery is said to be in this category when 5-50% of its rated capacity has been removed. Under this condition the constant potential and limiting current should be decreased from the values required for deep service. The charging conditions are:

1. Constant potential: 2.40-2.56 V/cell.
2. Limiting current: 10-15% of rated capacity.
3. Charge time: 10-18h; should capacity appear to be decreasing, charge time should be increased periodically to 28-30 h.

Taper charging with constant potential, the simplest method of charging, is satisfactory for charging batteries in cyclic service. This method requires control of overcharging and of battery heating, both of which adversely affect battery life. In general, battery life is shorter than is obtained in the other charging methods discussed. *(Crompton C.R, 2000)*

3.4.1.8 Deep Cycle CP Charging of Lead-Acid Batteries

A battery is said to be in this category when 50-100% of its rated capacity has been removed to the end voltage specified by the manufacturer. Under this condition the constant potential and limiting current should be increased. The charging conditions are:

1. Constant potential: 2.45-2.50 V/cell.
2. Limiting current: 20-50% of rated capacity.
3. Recharge time: limited to 12-20 h; should capacity appear to be decreasing, charge time should be increased periodically to 24-30 h.

3.4.1.9 Float CP Charging of Lead-Acid Batteries

A battery on float service is the one subjected to continuous charge and is called on to work in case of emergency. Under these conditions the battery is charged at a constant potential sufficient to maintain it at full charge. Charging conditions are:

1. Constant potential: 2.28-2.30V/cell.
2. Limiting current: 1-20% of rated capacity.
3. Charge time: continuous.

All lead-acid batteries will charge most efficiently in the range of 15-30°C. When float charging is carried out under conditions where the battery temperature does not fall outside the limit 0-40°C there is no requirement for temperature compensation to be built into the charger to enhance charge efficiency. When batteries are likely to reach temperatures outside the 0-40°C range a temperature compensator built into the charger, operating on 4mV/^{o}C per cell based on 25°C is desirable. *(Crompton C.R, 2000)*

3.4.1.10 Two-Step Cyclic Voltage-Float Voltage CP Charging

There are applications that require a lead-acid battery in standby service to be recharged rapidly after a discharge. Under this condition a two-step charger would be most efficient; that is, the one having a capability to switch from a cyclic voltage to a float voltage. In these circumstances the following conditions are recommended:

1. Initial constant potential: 2.45-2.50V/cell.
2. Float constant potential: 2.28-2.30 V/cell.
3. Limiting current: 20-40% of rated capacity.
4. Initial charge time: time required to reach
5. Float charge time: continuous.

Partially recombining sealed lead-acid batteries have the ability to accept a high-rate charge efficiently without a serious sacrifice in life. In applications where it is necessary to recharge in a limited time, the battery can be restored to 90-95% of full capacity within a 1-3h period. A charger with the following characteristics is required:

1. Constant potential: 2.50-2.55 V/cell.
2. Limiting current: 100% of rated capacity.
3. Charging time: 1-3 h.

If charging at the high rate is allowed to continue excessively beyond a 3 h period, greater than normal amounts of gassing occurs. It is not recommended that

high-rate charging be performed in an airtight enclosure. It is recommended that battery compartments have adequate ventilation to prevent accumulation of gases, which could reach dangerous proportions in the event of a charger or battery malfunction.

In Koutroulis & Kalaitzakis (2004), cell overcharging starts at about 2.4V/cell, irrespective of the charge rate, and the 100% state of charge condition coincides only with the overcharging at a C/100 charge rate, the battery current is continuously monitored and a limit is set to the maximum permissible charging current, indicated by the bold line in Figure. 3.12.

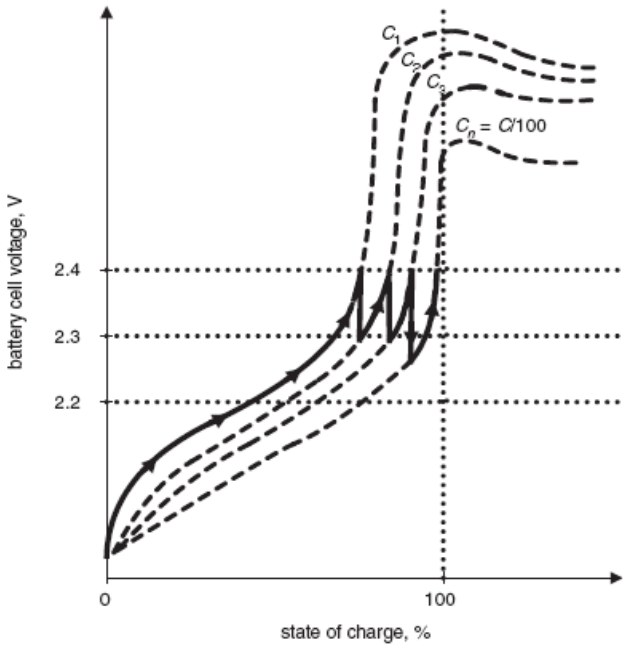

Figure 3.12 Battery-charging regulation concept from C_1 to C_{100} is the charge rates.

The actual charging current is allowed to be equal to or less than this maximum current. The battery voltage is also measured and every time it rises above 2.4 V/cell, denoting an overcharging condition, the maximum permissible battery current is decreased. This process is repeated until the maximum battery current is reduced to C/100. Then a battery voltage increment above 2.4V/cell indicates a 100% state of charge. In this case, the battery current is kept to a low value to compensate for the control unit power consumption and the battery self discharge. The initial value of

the maximum battery charging current is restored when a discharging condition is detected.

3.4.2 Battery Charging Control Circuits

The ideal charging cycle for lead-acid batteries that is demonstrated in Figure 3.6 can not be achieved easily with a PV system since PV system power is constantly changing. There are two basic circuits for controlling or regulating the charging of a battery from a PV module which the voltage or current may be controlled.

- Shunt controlled regulator
- Series controlled regulator.

Shunt controlled regulator; This circuits regulates the charging of batteries by varring resistance which is parallel between the array and the batteries or by interrupting the PV array from batteries (short-circuiting the PV). The blocking diode must be used in series between the battery and the switching element to avoid being discharged batteries either through PV or through the shunt regulator switch. Shunt regulator switch which dumps current from the PV array pull down both load and PV array voltage. When a transistor or MOSFET are used as variable resistance elements, the large heat sinks are required for dissipating a large amount of power.

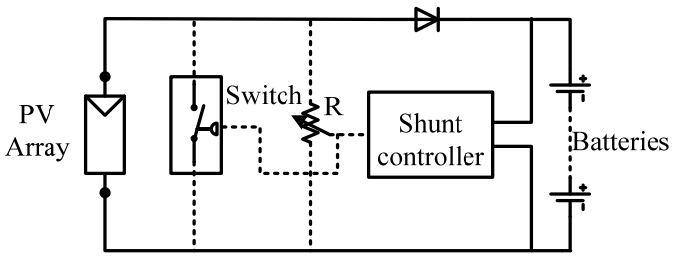

Figure 3.13 Shunt switching or variable resistance regulators.

So it is not generally used. The much more popular approach is to use the transistors as switches which turn on and off in such a way as to reduce the mean current flowing to the battery. Two circuits are illustrated in one figure above;

Series controlled regulator; Series regulators use some type of controlled elements (resistance or switch) in series between the array and the batteries as illustrated the figure below.

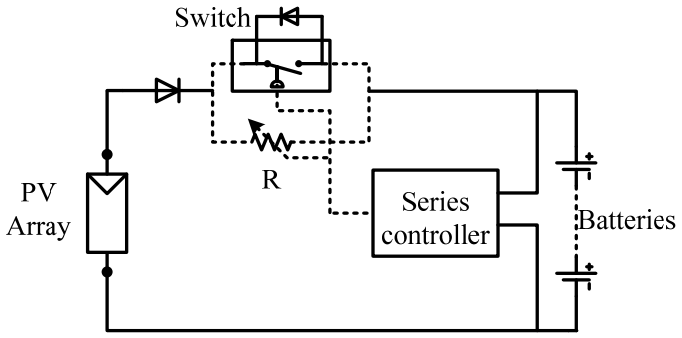

Figure 3.14 Shunt switching or variable resistance regulators.

The aim is to reduce the load current but to allow the array voltage to rise towards its open circuit value. If the switch element has a blocking diode internally, a power blocking diode must be used to avoid the battery being discharged through the array. In the series switching regulator the switch makes and breaks the current to the battery. The mean switch current depends on the fraction of the time for which the switch is on. If the switching is rapid, the voltage across the battery will be almost constant as the battery voltage responds quite slowly to changes in current.

Aforementioned two major charging system circuits' structures are explained. The new generation charging systems (buck, boost, cuk etc.) are related to the major two systems.

3.4.3 Determination of Battery Charging State

Battery state of charge is determined by either reading terminal voltage or measuring the specific gravity or density of the electrolyte. The gravity is read with a hydrometer but hydrometer is not used with sealed or gel batteries.

Measuring battery voltage is used to indicate battery state of charge. In contras to hydrometer, the voltage meter relatively inexpensive and easy to use. As mentioned before, the main problem with relying on voltage reading is the high degree of

battery voltage variation through the working day, because battery voltage reacts highly to charging and discharging. To solve this problem and to have reliable measurements, battery must be rested at least 2 hours. In PV systems usually both charging and discharging are done at the same time. The designer of chargers must look at the battery companies' catalogue.

3.4.4 Proposed Charging System

Up to now, various charging methods are explained, but they have some disadvantages. For example, in the above method (Koutroulis & Kalaitzakis (2004)) step down converter have been used; however the input capacitor, which must be used in DC/DC buck converter, dries in the course of time, so the charger can be corrupted. Furthermore, the charger doesn't take into consideration the battery' internal resistance whereas internal resistance is important for charger and load was not connected to the batteries. When the load is connected to batteries, the charger characteristic changes, so the controllers unfortunately take that situation into consideration and charging can not be performed properly. We know that the battery internal resistance changes from battery to battery. Moreover, it is changed with respect to battery ages. So it must be determined before charging batteries.

The proposed charger must consider the temperature of batteries to determine minimum and maximum battery charge voltage. In the below formula, the V_{def_bat} is predefined voltage level which its minimum level per cell is 1.96V (for 12 cell is 23.52 V) and maximum level per cell is 2.44 V (for 12 cell is 29.28 V). Where V_{bat} is battery voltage level, Ta is the ambient temperature, N_c is the number of cells of the battery stack and α is changed from -3 to -6 mV/^{o}C/cell and called temperature compensation coefficient.

$$V_{bat} = V_{def\_bat} + (T_a - 25)\, N_c\, \alpha$$

The following are general voltage ranges for twelve-cell lead-acid batteries and these values can be used for proposed study.(http://en.wikipedia.org/wiki/)

Open-circuit at full charge: 25.2 – 25.6 V (2.1-2.13)
Open-circuit at full discharge: 23.6 – 24.0 V (1.96-2)
Loaded at full discharge: 21V (1.75)
Continuous-preservation (float) charging: 27.6V (2.3) for gelled electrolyte; 27V (2.25) for AGM (Absorbed Glass Mat) and 26.8 V (2.24) for flooded
All voltages are at 20^{o}C, and must be adjusted for temperature changes. Float Voltage recommendations vary, according to the manufacturers' recommendation.
Precise (+/- 0.05V) float voltage is critical to longevity; too low (sulfation) is almost as bad as too high (corrosion & electrolyte loss)
Typical (daily) charging: 28.4-29V (2.36-2.41V) (depending on manufacturer's recommendation)
Equalization charging (for flooded lead acids): 30 - 32 V (2.5-2.67V)
Gassing threshold: 28.8 V (2.4V)
After full charge the terminal voltage will drop quickly to 26.4V (2.2V) and then slowly to 25.2V (2.1V).

In this study, two charging methods have been employed. While the only battery voltage has been considered in the first methods, the charging current and voltage have been taken into account in the second method. In both of them, two 12V 18A sealed lead-acid batteries are used (as series) and a rheostat is used as a load.

To charge the batteries with load together in the first method, the following control actions are applied.

- Sensing battery voltage; firstly, the batteries voltage (V_{bat_yuksuz}) is measured with the help of microcontroller’s ADC (if there is no connected load, the PWM signal is stopped in order to eliminate the excessive voltage rise and return to the main program.)

  Secondly, the test load (8.8Ω, 9W) is connected and batteries voltage (V_{bat_yuklu}) is measured again.

- Battery internal resistance (V_{Rin}) is calculated and minimum battery charging voltage (boost output voltage,$V_{boost\_out\_min}$) is determined.
  $V_{Rin}=(V_{bat\_yuksuz} - V_{bat\_yuklu})$

- The maximum PV Power (maxguc_hesa), maximum PV voltage ($v_{oc\_hesap\_max}$) and maximum PV current ($i_{sc\_hesap\_max}$) are calculated in accordance with some methods (open circuit, short circuit and linear characteristic of semiconductor switch.)

- A this point, the minimum boost voltage ($V_{boost\_out\_min} = V_{Rin} + V_{bat\_yuksuz}$) and allowable maximum voltage $V_{boost\_out\_max}$ can be calculated;

$$V_{boost\_out\_max} = V_{boost\_out\_max} + (T_a - 25)\, N_c\, \alpha$$

- The output of DC/DC boost converter is changing from $V_{boost\_out\_min}$ to $V_{boost\_out\_max}$. From $\frac{V_{boost\_out\_min\ or\ max}}{V_{oc\_hesap\_max}} = \frac{I_{sc\_hesap\_max}}{I_{boost\_out\_max\ or\ min}} = \frac{1}{1-(\frac{t_{on}}{T_s})}$

  (*Ts* is proportional 8 bit PWM word length and t_{on} is proportional duty cycle value *k* which is changing between 1 to 256) $k_{\_max}$ and $k_{\_min}$ maximum-minimum duty cycle value which are counterpart in orderly at the maximum and minimum boost output voltage.

$$k_{\_max} = 256\,\frac{(V_{boost\_out\_max} - v_{oc\_hesap\_max})}{V_{boost\_out\_max}}, \quad k_{\_min} = 256\,\frac{(V_{boost\_out\_min} - v_{oc\_hesap\_max})}{V_{boost\_out\_min}}$$

- To sensing the present battery voltage $V_{battery}$, PWM is adjusted according to the $k_{\_min}$ value. The new duty cycle value *k* is calculated by the following formula;

$$k = 256\,\frac{(V_{battery} - v_{oc\_hesap\_max})}{V_{battery}}$$

If founded new *k* value is between the $k_{\_max}$ and $k_{\_min}$, the PWM is changed according to this new *k*, else the PWM is adjusted in accord with to the

$k_{\_min}$ for floating charge.

The flowchart of first charging method is given below;

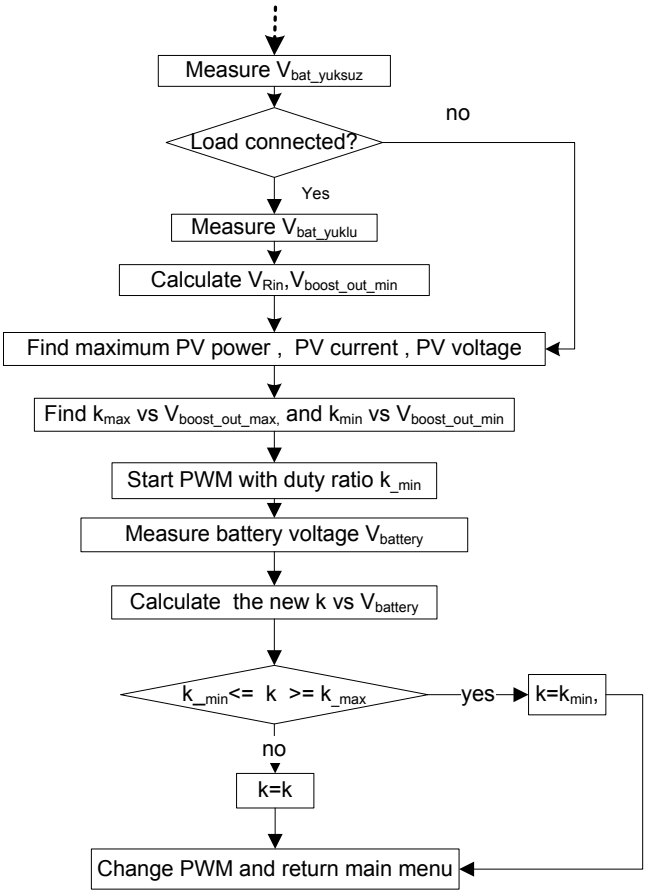

Figure 3.15 The flowchart of first charging methods (according to voltage values)

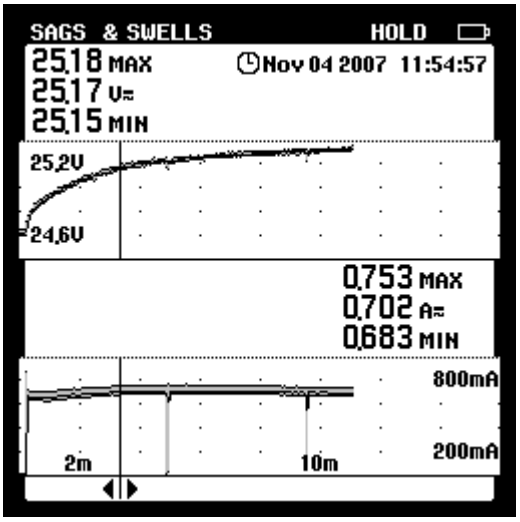

Figure 3.16 Changing battery voltage according to above method.

To charge the same batteries with load together in the second method, the following control actions are applied.

- Sensing battery voltage; firstly, the batteries voltage (V_{bat_yuksuz}) is measured with the help of microcontroller's ADC (if there is no connected load, the PWM signal is stopped in order to eliminate the excessive voltage rise and return to the main program.)

  Secondly, the test load (8.8Ω, 9W) is connected and batteries voltage (V_{bat_yuklu}) is measured again.

- Battery internal resistance (V_{Rin}) is calculated and minimum battery charging voltage (boost output voltage,$V_{boost\_out\_min}$) is determined.

$$V_{Rin}=(V_{bat\_yuksuz} - V_{bat\_yuklu})$$

- The maximum PV Power (maxguc_hesa), maximum PV voltage ($v_{oc\_hesap\_max}$) and maximum PV current ($i_{sc\_hesap\_max}$) are calculated in accordance with some methods (open circuit, short circuit and linear characteristic of semiconductor switch.)

- A this point, the minimum boost voltage ($V_{boost\_out\_min} = V_{Rin} + V_{bat\_yuksuz}$) and allowable maximum voltage $V_{boost\_out\_max}$ can be calculated;

$$V_{boost\_outmax}=V_{boost\_outmax}+(T_a \quad 25)\, N_c\, \alpha$$

- The output of DC/DC boost converter is changing from $V_{boost\_out\_min}$ to $V_{boost\_out\_max}$.

From $$\frac{V_{boost\_out\_min\ or\ max}}{V_{oc\_hesap\_max}} = \frac{I_{sc\_hesap\_max}}{I_{boost\_out\_max\ or\ min}} = \frac{1}{1 \quad (\frac{t_{on}}{T_s})}$$

(*Ts* is proportional 8 bit PWM word length and t_{on} is proportional duty cycle value *k* which is changing between 1 to 256) $k_{\_max}$ and $k_{\_min}$ maximum-minimum duty cycle value which are counterpart in orderly at the maximum and minimum boost output voltage.

$$k_{\_max} = 256\,\frac{(V_{boost\_out\_max} - v_{oc\_hesap\_max})}{V_{boost\_out\_max}}, k_{\_min} = 256\,\frac{(V_{boost\_out\_min} - v_{oc\_hesap\_max})}{V_{boost\_out\_min}}$$

- According to $k_{\_min}$, the maximum boost converter current value ($i_{boost\_out\_max}$) can be calculated by the microcontroller.

- If the maximum boost converter output current is higher than the maximum battery charging current ($i_{bat\_cap\_current}$), k is $k_{\_max}$ and PWM is changed, turn off MPPT mode and float mode is applied. If not the output current of PV (i_{sc_olcu}) is measured.

- If currently measured PV current (i_{sc_olcu}) is higher than the calculated short circuit current ($i_{sc\_hesap\_max}$) which is firstly measured with short circuit method and than calculated, k is increased by one. If less than, k is decreased by one, if both of them are equal, k is not changed.

- The battery voltage (V_{bat_yuklu}) is measured and if battery voltage (V_{bat_yuklu}) is higher than the maximum boost output voltage ($V_{boost\_out\_max}$), k is decreased by one if not k is not changed.

- PWM duty cycle is changed with the new k and the program return the main program from battery subroutine.

This charging method's flowchart is given figure 3.17 and the main scheme of system is given Figure 3.18.

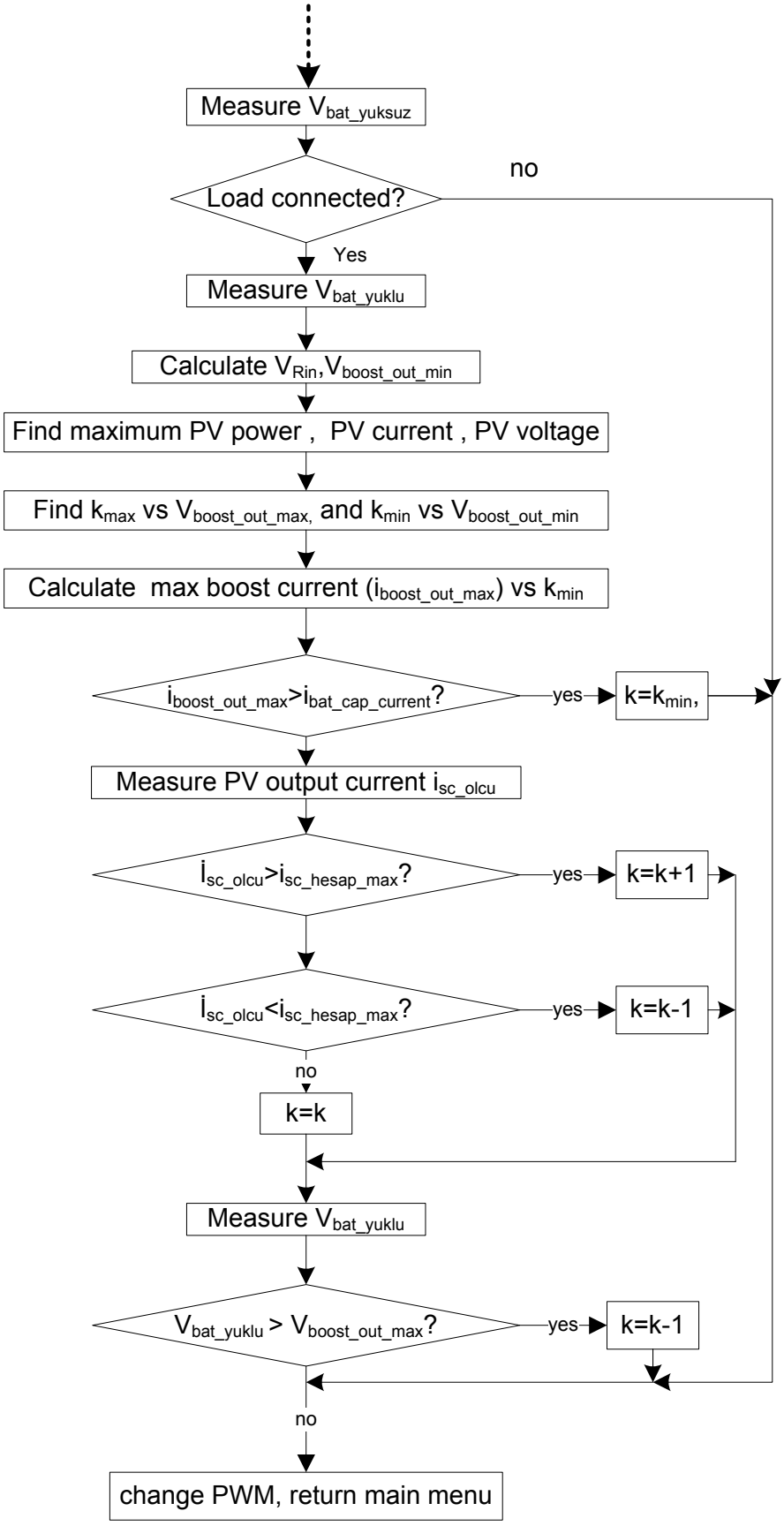

Figure 3.17 The flowchart of second charging methods (according to voltage and current values)

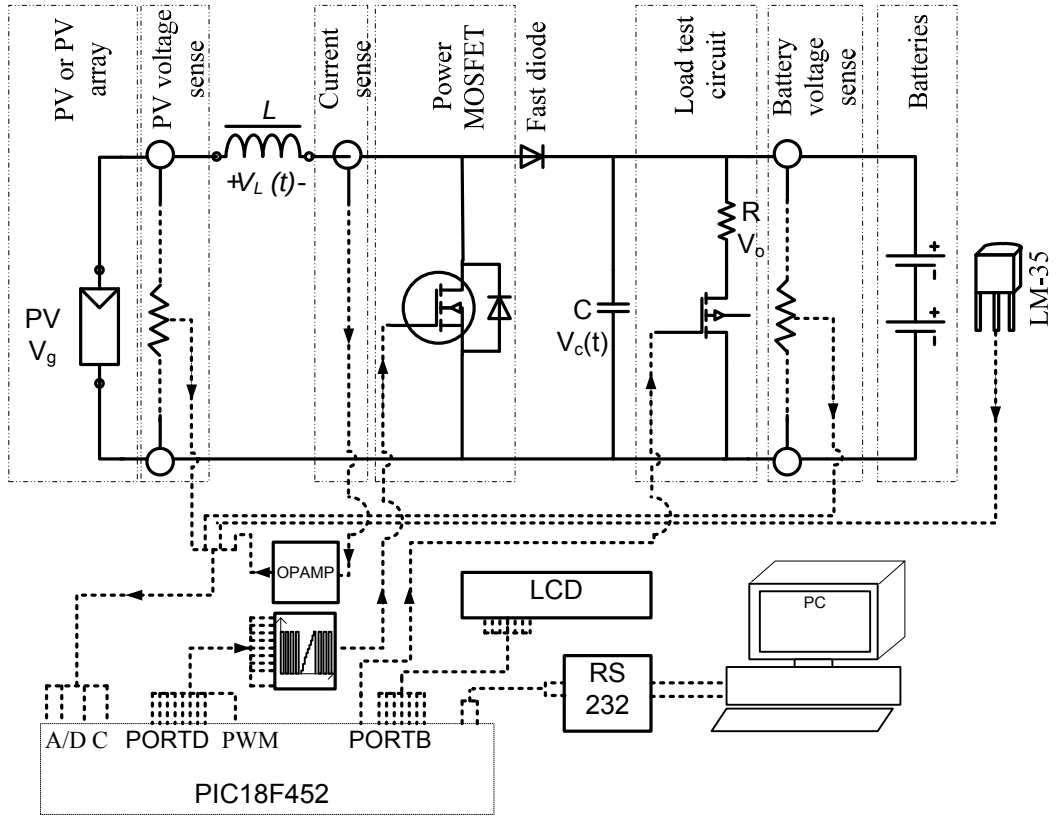

Figure 3.18 The proposed PV control and charging system

3.5 Conclusion

In this chapter, batteries are classified and lead acid batteries are analyzed in detail due to they are cheap and widespread. When the batteries are charged, the control system considers internal resistance of batteries. Batteries can be charged fully by this way. Generally the charger controller can not recognize the load which is connected parallel to batteries. In the proposed study, whether or not a load is connected to the batteries can be tested using a small test load and test circuit. Also, two different charge control methods are applied in the proposed study. The review show that, the charge characteristics of lead acid batteries change according to type of lead acid batteries. Charger is operated to transfer maximum power of PV panel which is determined by control circuits to the batteries.

In the study, three experiences are observed:

- When the batteries are empty, they can be charged by maximum power of PV panels. Also their voltage levels are near to 24V. The voltage levels of batteries are not changed rapidly and the battery charge current can be increased to the maximum current capacity of PV panel in this interval. This interval is called constant current interval.

- After the batteries are charged to the %50-75, the batteries charge voltage increases to the above gassing voltage. To prevent gassing of batteries the output voltage of charger must be controlled. The constant voltage is applied to the batteries in this interval. In this situation, the maximum power of PV panel can be high but this power can not be transferred to the batteries. This interval is called constant voltage interval.

- When the batteries capacity reaches to the %80-90, the floating voltage is applied to the batteries.

The characteristics of lead acid batteries are nonlinear and change battery to battery. A lot of study and experiments should be done for increasing of battery capacity and battery cycle life.

CHAPTER FOUR
SOLAR TRACKER

Solar energy is an important renewable energy source today. Consuming fossil fuels pollute environment and nature. So the need for solar energy and its efficient utilization is increasing. There are various maximum power obtaining techniques from the sun. One method is to track the sun. Compared to photovoltaic panels, trackers are relatively inexpensive, thus making them especially effective for photovoltaic systems using high-efficiency panels. The studies indicated that tracking of the sun is an energy production method used increasingly from 37% to 40% annually (Messenger, R. A., & Ventre, J. 2004). It was found that in (R.C. Neville, 1978) the energy available to the ideal tracker is higher by 5–10% and 50% than the east–west tracker and the fixed surface, respectively. Trackers maximize energy production by keeping the PV modules perpendicular to the incoming sunlight. Tracking of the sun is very crucial for concentrators PV modules, lens toward the sun, concentrating solar reflector and Parabolic Trough Collectors. They are used to obtain electrical energy from PV and vapor with heating water in order to heat and cool indoors *(http://www.solitem.com.tr/tur_inx_2.htm).* Modules or Parabolic Collector surfaces are exactly faced perpendicular the sun with the angle less than 0.1^{o}. A good tracker site is the one that starts to receive the sun very early in the morning and continue to receive sunlight until the sunset in the evening.

The sun is tracked by actuators that are operated continuously or stepwise. Baltas et al. made a comparative study between continuous and stepwise tracking. They showed that unlike concentrating systems, flat plate photovoltaic (FPPV) arrays yielded almost the same energy, when tracking in a stepwise fashion. Tracking motors could be idle for one or two hours, yet obtain more than 98% of the energy obtained from a continuous tracking array.

While the normal PV module (polycrystalline, mono-crystalline) efficiency is 14-16%, the concentrator PV modules efficiency reaches up to the value of 35 % *Fraunhofer Institute for Solar Energy System ISE (2005).* In harvesting solar energy

best, the control and tracking system should be simple, cheap, reliable and high efficient. A high efficient system can be achieved with low energy consumption and exact tracking of the sun.

In this proposed study, firstly tracking systems are classified, analyzed and compared with each other. Finally a microcontroller based open-closed loop two-axis solar position control system is designed, produced and analyzed.

4.1 Classifications

Tracking systems are generally classified into two forms in the literature. The first one is based on motion axis count and consists of;

- single-axis tracking system
- two-axis tracking system

The other classification system is based on control technique and consists of;

- open loop tracking system
- closed loop tracking system

The new classification proposed in this thesis is the combination of the above two systems which consists of;

- Single-axis open loop tracking
- Single-axis closed loop tracking
- Two-axis open loop tracking
- Two-axis closed loop tracking

4.1.1 Current Classification of Solar Trackers

4.1.1.1 With respect to Number of Moving Axis

Single-axis tracking system: In this tracking system, the tracker mechanism tracks only one axis (east-to-west), the other axis is fixed but it is manually adjustable (up-down according to the tilt angle). The boosted power is higher than to %30 comparing to any static mounted panels. The tilt angle of trackers can be set to the local latitude (called polar tracker) (Masters, Gilbert M. 2004). Although single axis tracking systems are considerably cheaper and easier to construct, their efficiency is lower than that of two-axis sun tracking systems. Furthermore, some solar systems work only with two-axis tracking such as point focus concentrators. (Salah Abdallah, & Salem Nijmeh, 2003).

Two-Axis Tracking System*:* In this tracking system, trackers can track the sun using both axes (from east-to-west during the day, from north to south depending on the season of the year) according to the azimuth and altitude angles in the way that the PV arrays or parabolic collectors are always pointing directly at the sun. The dual-axis tracking is achieved using two linear actuator motors, which aim at the sun within one degree of accuracy. During the day, it tracks the sun east to west and north to south. At night it turns east to position itself for the next morning sun. Old trackers did this after the sunset using a small battery. The new designs eliminate the battery requirement by doing it in the weak light of the dusk and/or dawn. (Mukund R. Patel. 1999). The increase in power production due to tracking, ranges from 50% in the summer to 20% in the winter.

4.1.1.2 With Respect To Controlling Type

a) Open-Loop Tracking Control:

- **Exactly Open-Loop Control**: In this method, the control devices need to know latitude, longitude, exact time and date of local point. Control unit compute the position of the sun at any time in anywhere. In this system the sun position is exactly tracked but in any cloudy day, when sun's irradiances are reflected by the cloud, the tracker rotates unnecessary. This causes extra energy consumption. To cope with this problem in the proposed system, any

MPPT techniques are added to the control system. This method is explained in detail and carried out in the proposed system.

- **Half Open-Loop Control**: The Earth rotates around both the sun and itself. One day is 24 hours and takes 360 degrees so the earth rotates 1 degree every 4 minutes. Half open loop control comes from this idea. This kind of trackers keeps the track of the sun from the morning to the evening together with known angle degrees. Its position is initially set to the sun and it rotates with the sun with the help of a controlled motor. After the tracker is synchronized to the sun, the tracker starts to rotate from left to right. This kind of trackers has a positioner, timer, sun tracker motor, limit switch, software limit and background for the automatic rotation of PV. For example motor rotation up to 100°, which means 8 hours of tracking the sun at the right angle. In the morning it starts to rotate 1 degree per every four minutes to the evening. When the time is 16:30 in the afternoon, it stops rotating. Then it returns to the morning position for next day in the midnight. This kind of system needs battery for motion and rotates as a polar tracker. In the proposed system, when we select this special feature, the control system can carry out this mode with machine learning techniques.

b) Closed-Loop Tracking Control

A typical closed loop system uses various sensors. They can find sun position with respect to the data that come from the sensors. There are many sensors that are capable of supplying such data for close loop control. The aim of the control strategy is to find the sun position by taking data from the sensors, analyzing the data and using it as the input to the control system. For this purpose; pyramid sensor, four or two sensor techniques are used. When the LDR can be used as a simple sensor, any little PV cells combination are used too. But in this method if there are any projectors or mirrors that reflect its light to the sensors, the tracker deviates from the right position. The actuators work continuously to track the sun and in a cloudy day, they

work randomly. In the hardware tracker system, the above problem can not be solved. However, the problem can be resolved with the help of software approach.

4.1.2 New Classification

4.1.2.1 Single-Axis Open-Loop Tracking

Single-axis and open loop tracking systems were explained separately in the previous sections. In this section, single-axis open loop tracking is explained. This kind of tracker includes one direction positioner and its control commands come from an open loop control device. Due to the fact that the other axis is controlled manually and the control system does not have any feedback, in spite of being cheap, the overall system efficiency is considerably low.

4.1.2.2 Single-Axis Closed-Loop Tracking

Single-Axis Closed Loop Tracking differs from *Single-Axis Open Loop Tracking* system discussed above (4.1.2.1) in the way that it consumes less energy for tracking in cloudy days. There are two tracker types in this system.

- Active Tracker: Active trackers use motors, sensors and gear trains to direct the tracker as commanded by a controller using the solar direction. The motor is used to move from east to west to find sun position. Nevertheless, the system has the drawback of having only one axis tracking feature.

  TRAXLE™ tracker can be examined in this class. The tracker is based on a new arrangement of two antiparallel solar cells, which provides both sense and energy to a reversible DC motor. Figure 4.1 shows the principle of the tracker. When solar collectors are oriented eastwards and the sun moves from east to west (Figure 4.1b), the angle β between solar radiation and sensing/driving cells increases until the power of the driving DC motor is high enough to move solar collectors. Then the collectors start to move and the angle β starts to

decrease until the power of DC motor is lower than what is necessary to move solar collectors. Poulek V., Libra M. (2007)

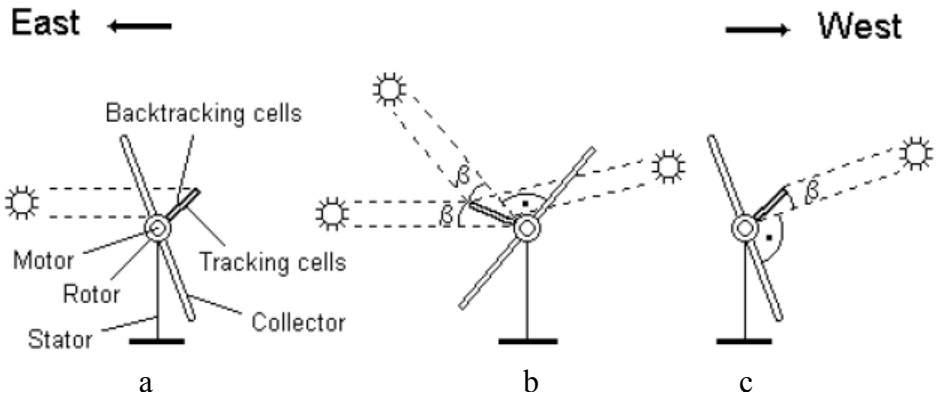

Figure 4.1 The working principle of the new solar tracker

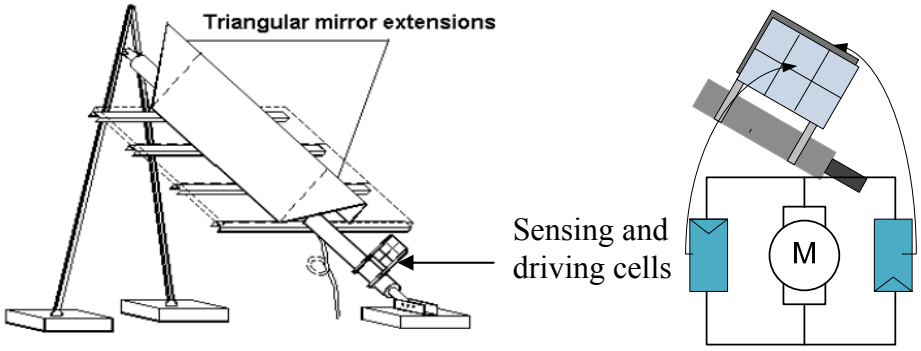

Figure 4.2 Sensing and driving cells and their location

The area of the auxiliary solar panel with sensing/driving cells is about 1% of the area of the moved solar collectors. The apparatus enables backtracking within 5 minutes. It is a significant advantage in comparison with popular passive trackers where backtracking times are often longer than one hour. The tracker works also at low temperatures below –40°C with average tracking accuracy $\pm 5^{O}$.

Another advantage of electrically operated trackers is that they ignore temperature since they are powered by electricity not the sun's heat. This makes this type of tracker more accurate in climates with cold winters. (Perez R., 2004)

Being electrically operated, however, can also be considered as a disadvantage since the tracker becomes sensitive to the damage from lighting. One more disadvantage of electrically operated trackers is the fact that they are expensive. Another minor disadvantage is that these trackers use some electricity to operate. (Perez R., 2004)

- Passive Tracker (Based On fluid, Shape Memory Etc.): Passive trackers use a low boiling point compressed gas fluid that is driven to one side or the other (by solar heat creating gas pressure) to cause the tracker to move in response to an imbalance. As this results in a non-precision orientation it is unsuitable for certain types of concentrating photovoltaic collectors but works fine for common PV panel types. These will have viscous dampers to prevent excessive motion in response to wind gusts. Shader/reflectors are used to reflect early morning sunlight to "wake up" the panel and tilt it toward the sun, which can take nearly an hour but more than 1 hour in cold climate (-40 ^{o}C). The time to do this can be greatly reduced by adding a self-releasing tie down that positions the panel slightly past the zenith (so that the fluid does not have to overcome gravity) and using the tie down in the evening. (A slack-pulling spring will prevent release in windy overnight conditions.)

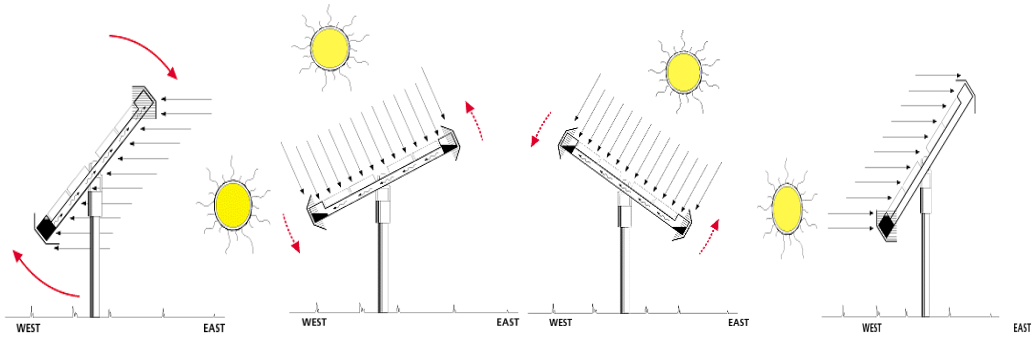

Figure 4.3 Fluid based Passive tracker's tracking of the sun

The Track Rack begins the day facing west. As the sun rises in the east, it heats the unshaded west-side canister, forcing liquid into the shaded east-side canister. As liquid moves through a copper tube to the east-side canister, the tracker rotates so that it faces east. The heating of the liquid is controlled by the

aluminum shadow plates. When one canister is exposed to the sun more than the other, its vapor pressure increases, forcing liquid to the cooler, shaded side. The shifting weight of the liquid causes the rack to rotate until the canisters are equally shaded. As the sun moves, the rack follows at approximately 15 degrees per hour, continually seeking equilibrium as liquid moves from one side of the tracker to the other side. The rack completes its daily cycle facing west. It remains in this position overnight until it is "awakened" by the rising sun in the following morning. *(http://www.zomeworks.com/solar/trackrack/trackwork.html)*

The trackers which used the sun's heat to move the modules around a single east/west axis have had problems in cold windy climates where the tracker cannot build up enough thermal energy to operate and they do not track the daily and seasonal north-south motion of the sun. Thermal trackers are usually within 10° of perpendicular on their single east/west axis, and wherever the user set them on the north/south axis. Heat-powered trackers wait until they warm up in the morning and then swing to the east. Heat-powered trackers also have problems in cold and windy climates. The tracker simply can not build up enough heat to operate. (Perez R. 1991)

The big advantage of the thermal tracker is simplicity and thereby reliability. There are no electrical parts to fail. The fluid is inside a sealed system, requiring no maintenance or energy to operate other than solar heat. A second advantage of thermal trackers is cost; they are generally less expensive than electrically operated trackers. In contrast to advantages, they are not so suitable for tracking because; when the weather temperatures is subzero these trackers can not track the sun and in the morning their turning time to sun are about 2 hours (according to our observation at February 19 and May 2, 2008 in Denizli)

4.1.2.3 Two-Axis Open-Loop Tracking

This trackers track both the east to west axis and the north to south axis. Tracker keeps the modules perpendicular to the incoming Sunlight. The open loop trackers don not sense the sun's position, so control unit compute this position and convert it to a certain number of counts. Control systems use formulas for finding position of sun. The date, latitude, longitude and time data are stored in the controller memory (DSP, Computer, PLC etc.) for computing position. The controller can find solar tilt and azimuth angle for any time of day. After finding angles, the tracker tracks the sun and finds new angle values in a determined period. Two actuators drive the tracker according to computed tilt and azimuth angles.

As explained before, the sun azimuth angle changes day by day. While the sun azimuth angle path is 120^o in the winter, it is 240^o in the summer. This is illustrated in Figure 4.4. So the controller must take into consideration this variation range.

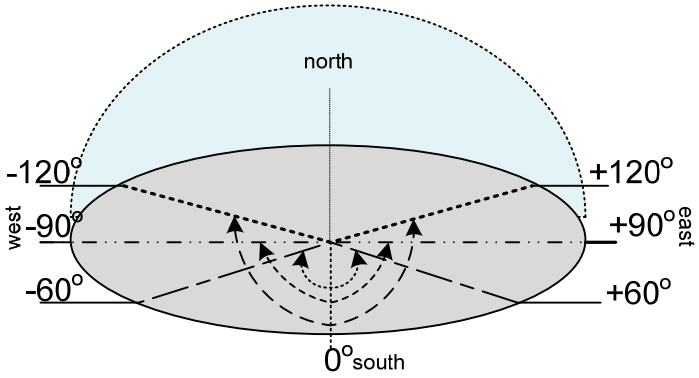

Figure 4.4 Sun azimuth angle positions according to seasons

The azimuth angle is higher than 180^o in the summer as can be seen from the figure below (e.g. DENIZLI's azimuth angle is about 220^o). This means that the east-west actuator can be moved higher than 180^o. Generally speaking one and two-axis tracking systems can be rotated maximum 180^o or less. In the proposed study it is done is this way.

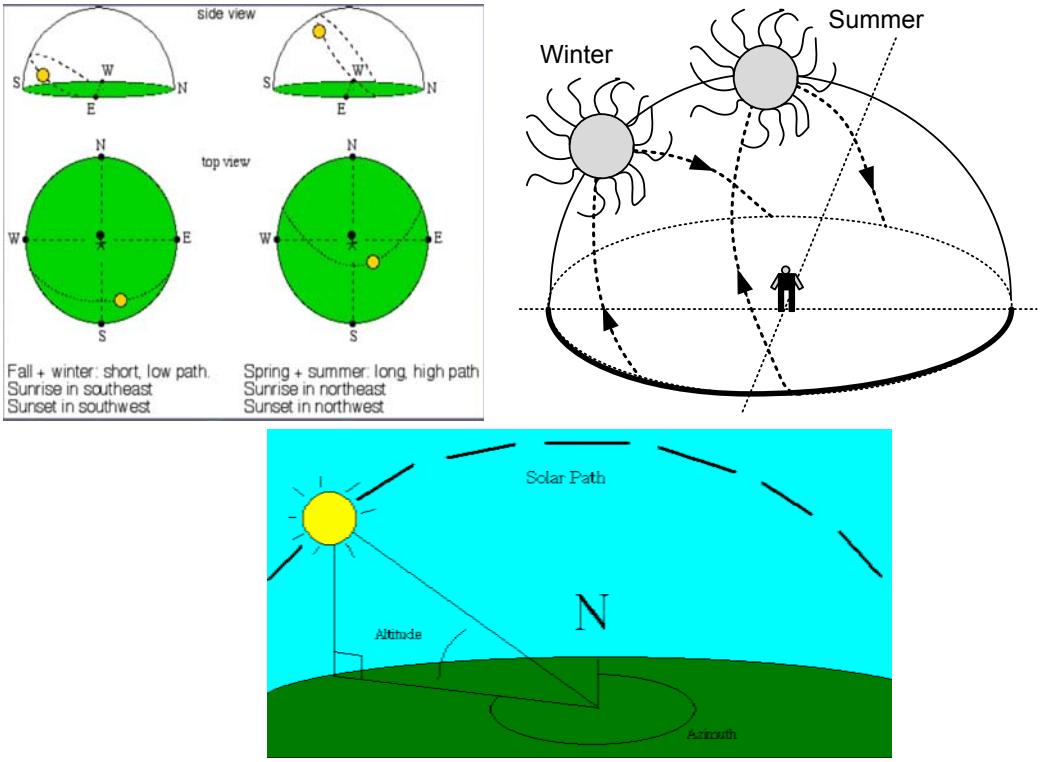

Figure 4.5 Solar geometry according to season and solar path angles http://www.astronomynotes.com/nakedeye/s5.

4.1.2.4 Two-Axis Closed Loop Tracking

As in the one-axis closed-loop tracker, the two-axis closed system use photosensors to discriminate the sun's position. The controller takes electrical signals from sensors and runs the motors to track the sun. Mini solar cells can be used as sensor. They can be constructed like a pyramid, back to back 180^{o} or 60^{o} etc. (Bilgin Z. 2006). A two-axis closed loop control tracker is illustrated in the figure below.

Figure 4.6 Two-axis closed loop tracker control box, sensor and mechanism. (www.dobontech.com).

4.2 Proposed Solar Tracking

For the better annual energy performance, the solar panels are tilted up at the angle equal to the local latitude angle. It is slightly increased ($+15^o$) in the winter and slightly decreased (-15^o) in the summer. Generally one-axis motion (east-west) is employed in the tracking system while two-axis tracking systems are used occasionally. Both systems do not rotate more than 90^o, 120^o or 180^o. New generation tracker systems can track the azimuth angle up to 270^o but they are not widespread and are controlled by more expensive and complex controllers such as DSP, PLC and PC etc. Besides they either use open loop control or closed loop control.

The aim of this study is tracking of the sun momentarily with respect to the altitude and azimuth angle and panel power using open loop and closed loop control techniques. Two DC motors are used as actuators, one for the joint rotating about the horizontal north–south axis to control the tilt angle and the other for the joint rotating about the vertical axis to control the azimuth angle.

4.2.1 Proposed Two- Axis Tracker System Mechanism

In this system, two motorized satellite dish antenna apparatus are used as actuators. These apparatus are modified in several ways. Their shafts are lathed, motor control circuits are changed and two left-right direction select control inputs are modified on the control board. One of motorized apparatus is fixed the other is mounted on fixed apparatus's shaft to move two axes. In addition, two linear potentiometers are mounted on the other side of shafts to take the position data in degrees. In the apparatus, the motors are connected to the reductors so that adequate torque is obtained to move the other parts of the system and solar panel which is mounted on the shaft.

Both apparatus are supplied with a 12V DC by main control board supplier while potentiometers are supplied with 5V DC. V_{cc} that is obtained from 7805 regulator

circuits over the apparatus control board. The analog position data are sent from potentiometer middle pin via two 0.5mm^2 cables to microcontroller's analog inputs. Two left-right or up-down control cables per every apparatus are connected from microcontroller' digital outputs to modified apparatus' inputs via 4 cables.

4.2.2 Calculating Sun Position Using Local Latitude, Longitude, Date and Time

In this section, it will be explained how to calculate the sun position at any time, at any location on any day of year. Firstly, we accept that (as ancient time) the earth is fixed and the sun spins around its north-south axis, after we must find the solar declination angle (δ). δ angle is between the plane of the equator and a line drawn from the center of the sun to the center of the earth. It varies between +23.45^o and -23.45^o.

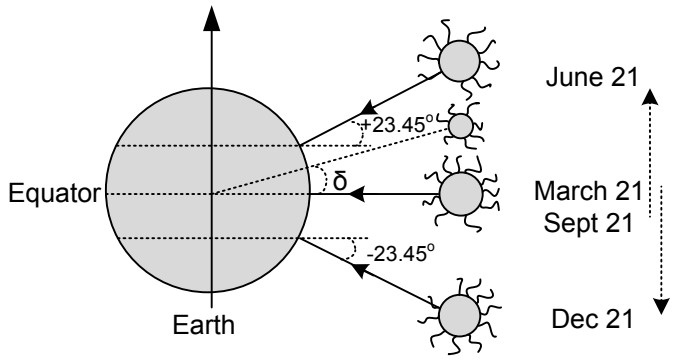

Figure 4.7 Sun position according to mount and declination angle δ

There are various formulas to find the declination angle but none of them can find exact values of declination, simply because δ varies slightly from year to year. One of them is

$$\delta = \delta_0 \, Sin[360\frac{(284+n)}{365}]$$

Where *n* is the day number counted from the beginning of the year and δ_o is 23.45^o. (A. Luque & S. Hegedus. 2003).

The other one that we use is;

$$\delta = 23.45\, Sin[\frac{360}{365}(n-81)]$$ Masters, Gilbert M. (2004).

To find local solar noon; $B = [\frac{360}{364}(n-81)]\ degrees$ and Equation of time (EOT) is calculated by the formula below;

$$EOT = 9.87\sin 2B - 7.53\cos B - 1.5\sin B$$

$$Solar\,time(ST) = Clock\,Time(CT) + \frac{4\ min}{degree}(Local\,Time\,Meridian \quad Local\,longitude)^{o} + EOT$$

CT=Solar noon.

For a fixed system, the optimum tilt angle is found from the formulas below:

$$Altitude \quad angle \quad = \beta_N = 90^{o} - L + \delta \quad , \; Panel\,Tilt\,angle = 90 - \beta_N$$

L is latitude of the site.

The above hints are useful for fixed panels, but they are not enough for the proposed study since solar position at any time of day must be calculated in the two-axis tracker system. As can be seen from the figure below solar location can be defined in terms of its altitude angle β and its azimuth angle φ_s.

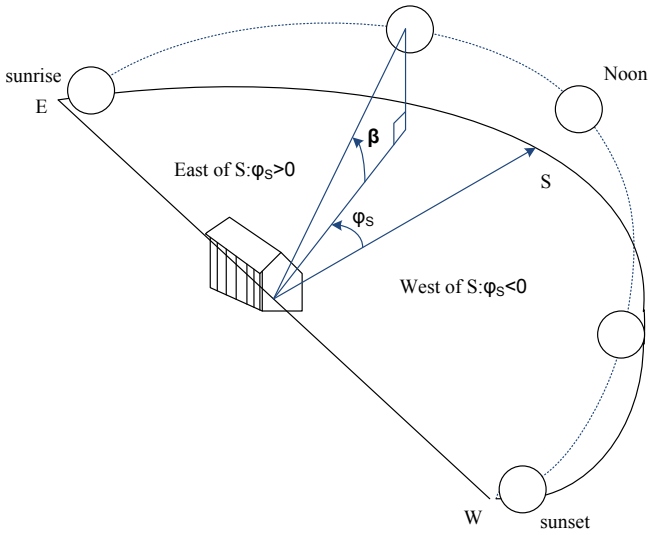

Figure 4.8 Determination of the sun position with respect to angle φ_s and altitude angle β

Azimuth angle φ_s is positive on east of south line and is negative on west of south line. Azimuth and altitude angle is found by means of the latitude, day number of the year and the time of the day. These angles can be found through the below formulas;

$$\sin\beta = \cos L \ \cos\delta \ \cos H \ + \sin L \ \sin\delta$$

$$\sin\varphi_S = \frac{\cos\delta \ \sin H}{\cos\beta}$$

H is called hour angle which is the number of degrees that the earth must rotate before the sun will be directly over your local meridian (line of longitude). The earth rotates 360^o at every 24 hours or rotates 15^o per hour, therefore the hour angle can be found as follows;

$$H = \pm(\frac{15^o}{hour}) \ x \ hour \ before \ or \ after \ solar \ noon \quad or \quad H = (ST - 12)x15^o$$

During the spring and the summer the azimuth angle is more than 90^o away from the south in the morning or afternoon (in Denizli most azimuth angle is approximately $\pm 105^o$). The controller must check that the azimuth angle is less or greater than 90^o away from south.

$$\text{For checking; if } \cos H \geq \frac{\tan\delta}{\tan L}, \quad \text{then } |\varphi_s| \leq 90^o; \quad \text{else } |\varphi_s| > 90^o$$

During the day the tracker moves from east to west therefore control unit must know the sunrise and the sunset time day by day. Because tracker must turn to east at every sunrise time and stop its motion at the sunset time.

To find these times the following formulas can be used. The sunset and sunrise moments, the azimuth angles are equal to zero, so we can write;

$$\sin\beta = \cos L \ \cos\delta \ \cos H \ + \sin L \ \sin\delta = 0$$

$$\cos H = -\frac{\sin L \ \sin\delta}{\cos L \ \cos\delta} = -\tan L \ \tan\delta$$

$$H_{hour\_angle} = \cos^{-1}(-\tan L \ \tan\delta)$$

The inverse cosine function has positive and negative values. The positive values are used for the sunrise and the negative value for the sunset. The sunrise and sunset times are obtained by converting the hour angle. As it is well known, the sun rotates 15^o/h, so;

$$Sunrise\ time = SolarNoon \quad \frac{H_{hour\_angle}}{15^o / h}, \quad Sunset = SolarNoon + \frac{H_{hour\_angle}}{15^o / h}$$

Using above formulas, the sun position at any time of any location, sunrise and sunset can be obtained by the controller.

4.2.3 Tracking the Sun with Proposed Tracker

The methods used above delivers different sets of sun position values. They also changes from year to year. In this study, the sun position is evaluated by using two external sun path chart programs which are released on the internet online (sun path chart program by *University of Oregon Solar Radiation Monitoring Laboratory (UO SRLM)* and *Solar Position Calculator by National Oceanic and Atmospheric Administration (NOAA)*) and our proposed method. The results on the charts from all three are compared. In Figure 4.9, the sun path diagram at December 3, 2007 Denizli/TURKEY according to *UO SRLM,* is illustrated;

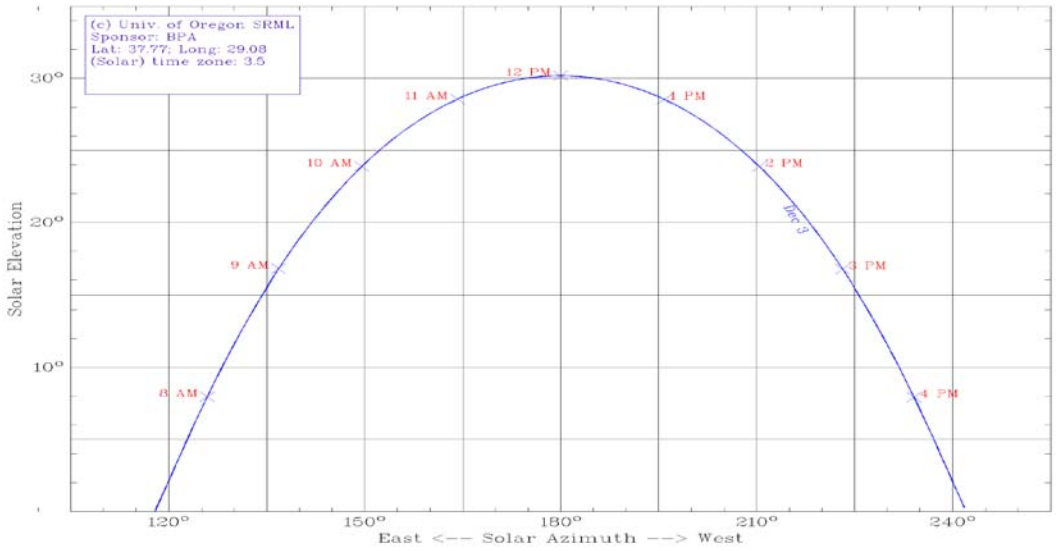

Figure 4.9 Sun position according to UO SRLM on December 3, 2007

The proposed open loop system finds the sun's position by computing the azimuth and altitude angles in the microcontroller and our sun position chart and NOAA sun position chart for December 3, 2007 are illustrated together on Figure 4.10.

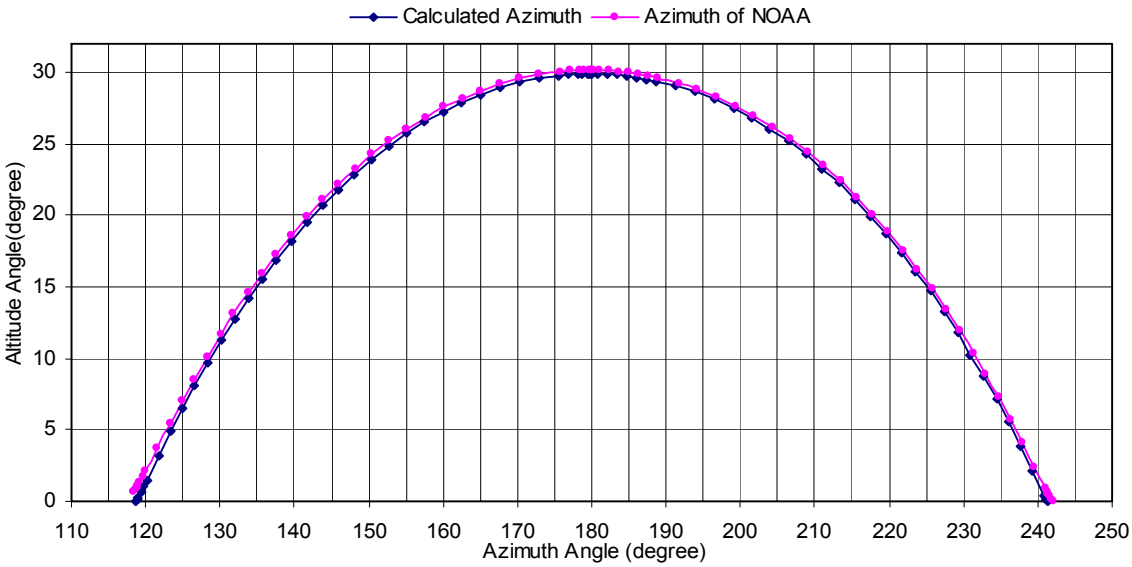

Figure 4.10 Sun position according to us and NOAA on December 3, 2007

In Figure 4.11, the sun positions (altitude angles) for December 3, 2007 in Denizli/TURKEY are illustrated versus to the day hours.

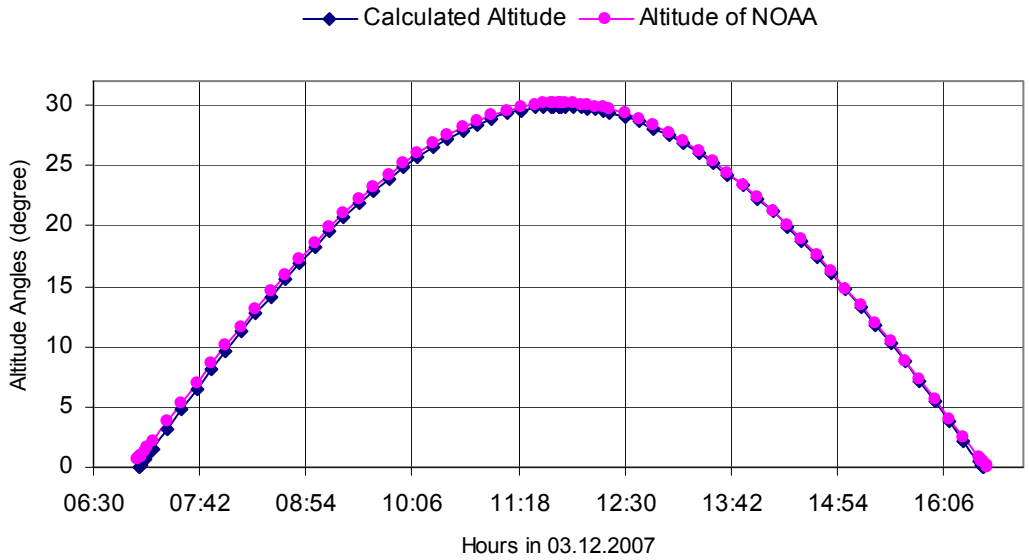

Figure 4.11 Sun position according to us and NOAA on December 3, 2007 versus hour

As can be seen from the figures above, the proposed control system finds sun position correctly at any time of day. Slight differences in solar positions angles in

the figures result from using different formulas. For example, different EOT formulas are used and different EOTs and NOAA are obtained as illustrated in Figure 4.12.

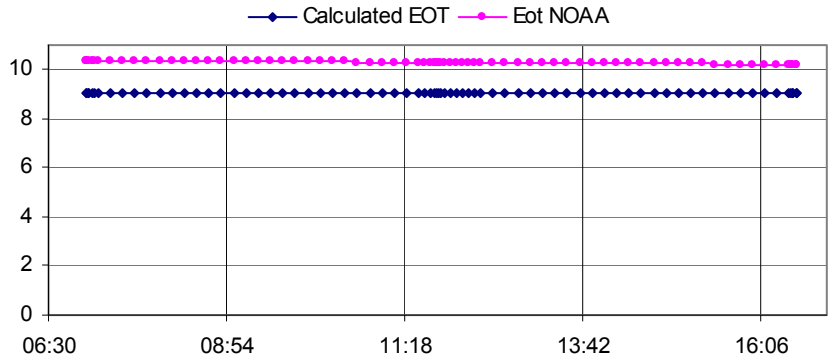

Figure 4.12 The differences of EOTs (Equation of Time)

Calculated sun position angles are tracked by the tracker system with open loop control method.

The detailed block diagram of the proposed system is shown Figure 4.13 below.

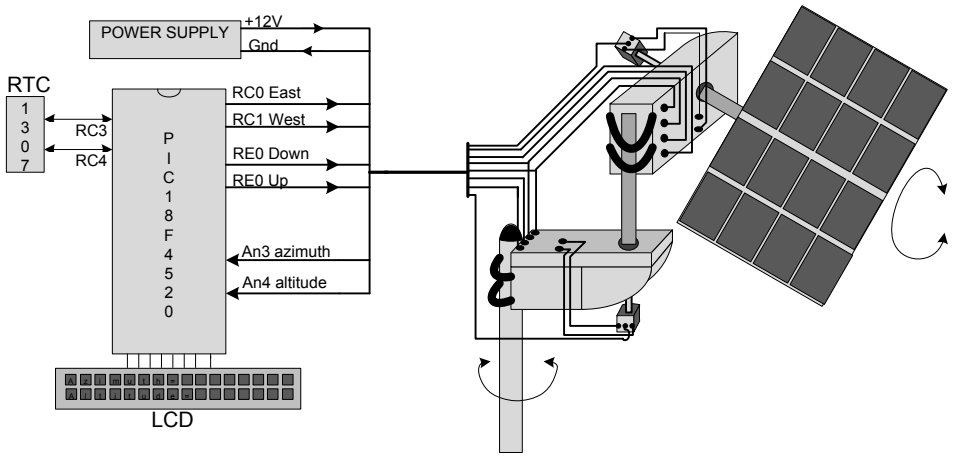

Figure 4.13 Open Loop Computing Tracker System block diagram

The designed control unit is common for sun tracking, MPP tracking and battery charging. But this application involves an external real-time clock, two position sensors (potentiometers) and motor driver circuits. While the latitude and longitude values are stored in microcontroller's ROM, the date and time data are read from Real-Time Clock (RTC) device for computing. The position knowledge of trackers are obtained from two linear potentiometers mounted on the shaft, namely the microcontroller reads the position angles on the two axes momentarily. Comparing

the current position angles on the two axes with altitude and azimuth angles, the microcontroller decides which motor is to run and what direction is to rotate. Firstly the altitude motor is started and when the computing altitude angle is equal to the current position angle the motor is stopped. Having found the altitude angle, the second motor is run and when the solar panel azimuth angle is equal to computing angle the second motor is stopped. For every four minutes, the control unit repeats these calculations and moves the motors accordingly. The control algorithm flowchart is shown in Figure 4. 14;

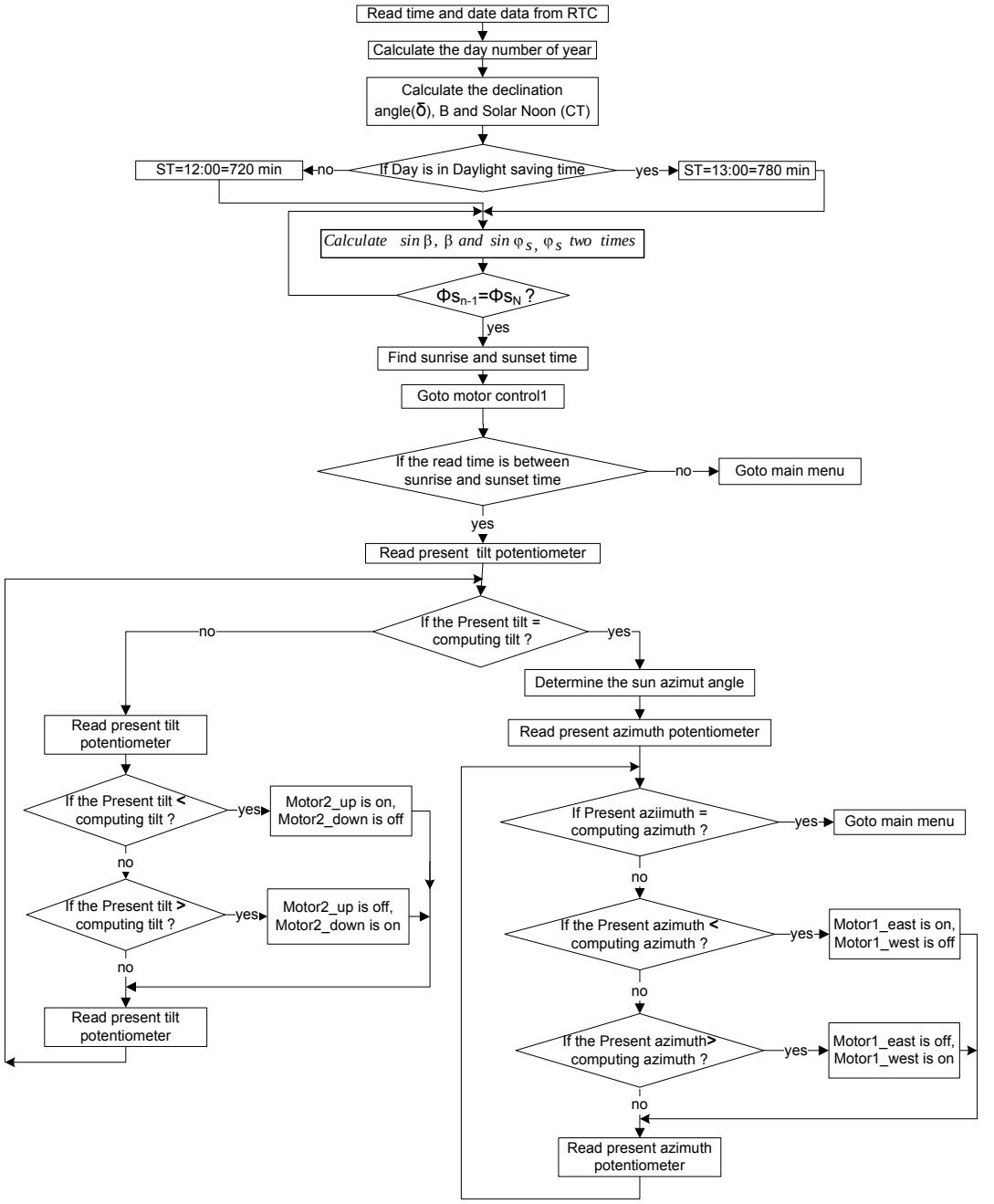

Figure 4.14 Open loop two axes tracker control algorithm flowchart

4.2.4 Tracking Sun with Proposed Tracker via Tracking of Voc

In this method, the tracker operates as a closed loop controlled tracker. It uses panels as sensors. Using I_{sc}, V_{oc} or any MPPT technique, sun's position can be found. For a cloudy day, the controller can find out sunny time and cloudy time and can interpret the approximate position of the sun. Under the certain panel power, voltage or current level, the tracker is not actuated. If the panel variables are very low, the controller can conclude that the time is night. How the realized tracker works is briefly explained below flowchart;

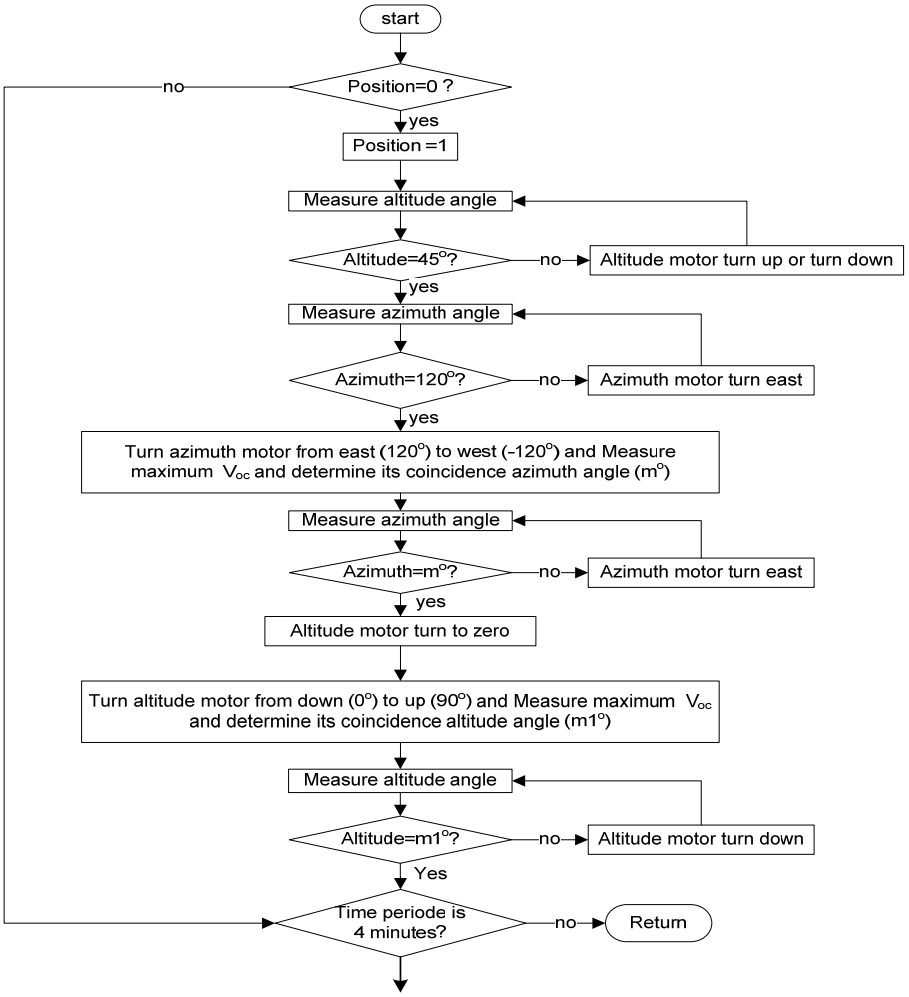

Figure 4.15 The first step algorithm of finding position of sun flowchart according to Voc

When the tracker is started, firstly it finds out the sun position according to open circuit voltage of panels (The controller must take into account the change of V_{oc} due to temperature effect). The altitude motor is rounded to 45^o and the azimuth motor is rounded to the east and the maximum voltage is searched from east to west by

rotating the azimuth motor. After finding the azimuth angle of maximum voltage, the azimuth motor rotates reverse at this angle point. After finding the azimuth angle, to find the altitude angle; the altitude motor returns to the 0^o. Similarly, to find the azimuth angle, the altitude motor rotates from 0^o to 90^o and the angle of maximum open circuit panel voltage is detected. The altitude motor returns to this maximum open voltage point angle.

The steps until now are done only once every time when tracker started. After the first start, the controller does not do these steps again. Microcontroller can understand this situation; checking position register's value which is 0 or 1.

After finding the sun position, the controller follows these steps: If the panel's open voltage V_{oc} (its nominal open circuit voltage is 21V) is lower than reference voltage (20V) and greater than minimum voltage (10V) the controller can realize that the sky is cloudy so it does not turn the motors and return to main program. If V_{oc} is lower than minimum voltage (10V) the controller decides that the time is night so return to the main program, not doing anything. If the V_{oc} is greater than the reference voltage (20V), the controller tests the sun position.

If the found azimuth angel point *m* is between 120^o and 0^o, and if 8 minutes period passes, the altitude angle point *m1* is increased (*m1=m1+1*) by one and according to the altitude angle of the tracker, the altitude motor is turned up. When the tracker altitude angle is reached to the *m1* angle, the motor is stopped and after that, the azimuth angle is controlled and referring to this angle the azimuth motor is run from west to east by one degree, and returns to main program.

If the found azimuth angel point *m* is between 0^o and -120^o, if the time is not night, and if 8 minutes period passes, the altitude angle point m1 is (*m1=m1-1*) decreased by one and according to the altitude angle of the tracker, the altitude motor is turned down. When the tracker altitude angle is reached to the *m1* angle, the motor is stopped and after that, the azimuth angle is controlled and referring to this angle the azimuth motor is run from west to east by one degree, and return to the

main program. If 8 minutes period does not pass, the azimuth angle is measured directly and with respect to *m*, the azimuth motor is run by one degree as before.

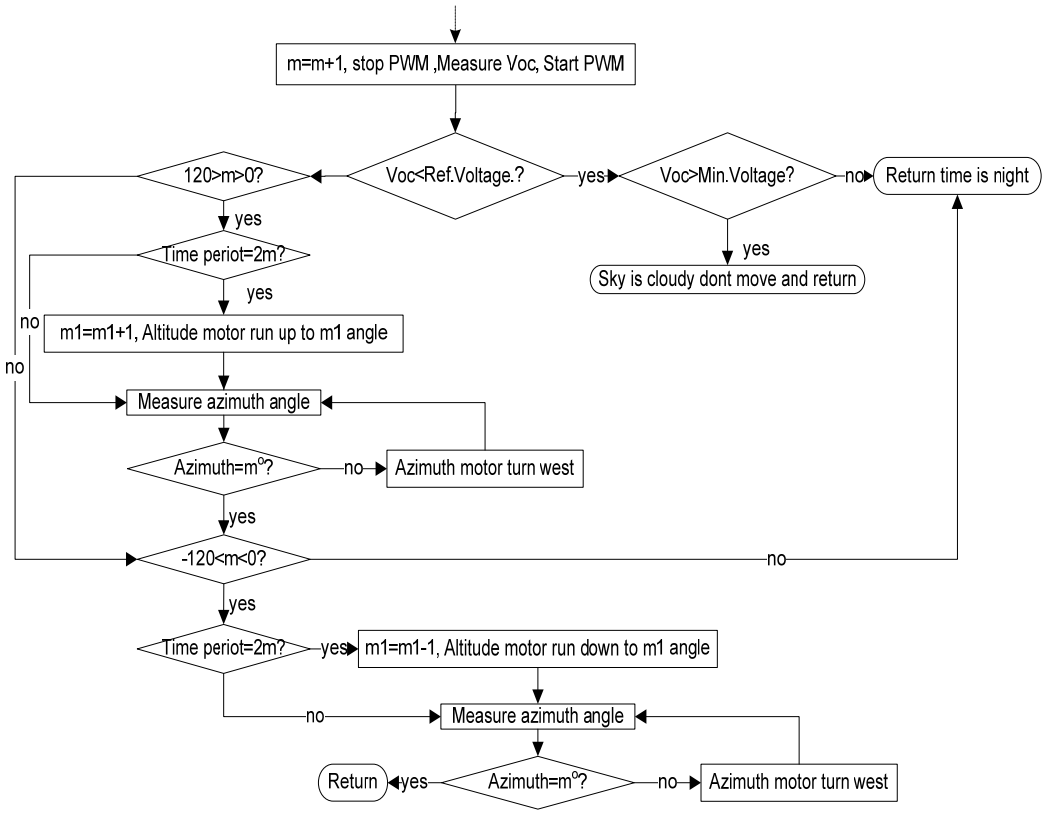

Figure 4.16 The second steps algorithm of finding position of sun flowchart according to Voc

Finding sun position via maximum Voc method is demonstrated in Figure 4.17. This process was performed at 14 February 2008, time is 14:30. According to this process the azimuth angle is 26.5 and altitude angle is 37.6. At the same time according to NOAA, the azimuth and altitude angle are 26.3, 37.4 consecutively.

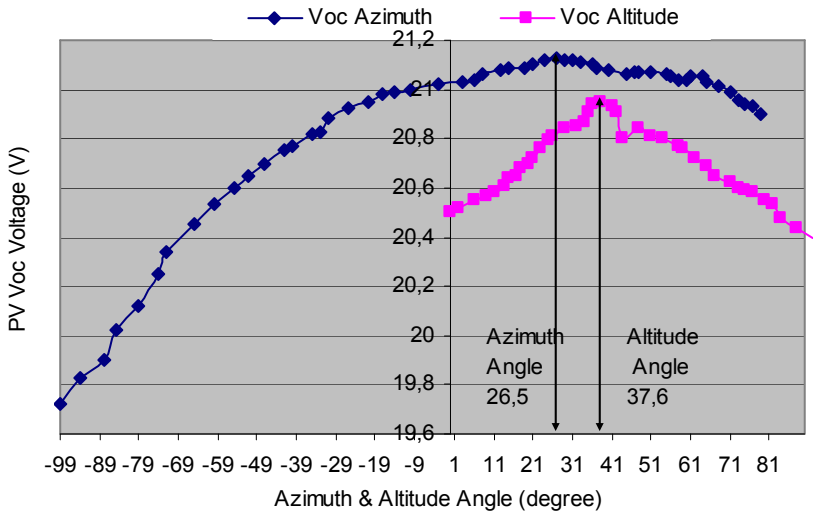

Figure 4.17 Finding sun position via maximum Voc

In the below figure, the sun azimuth and altitude angles, which are founded with the closed loop maximum Voc method, are demonstrated and they are compared with the open loop calculated method.

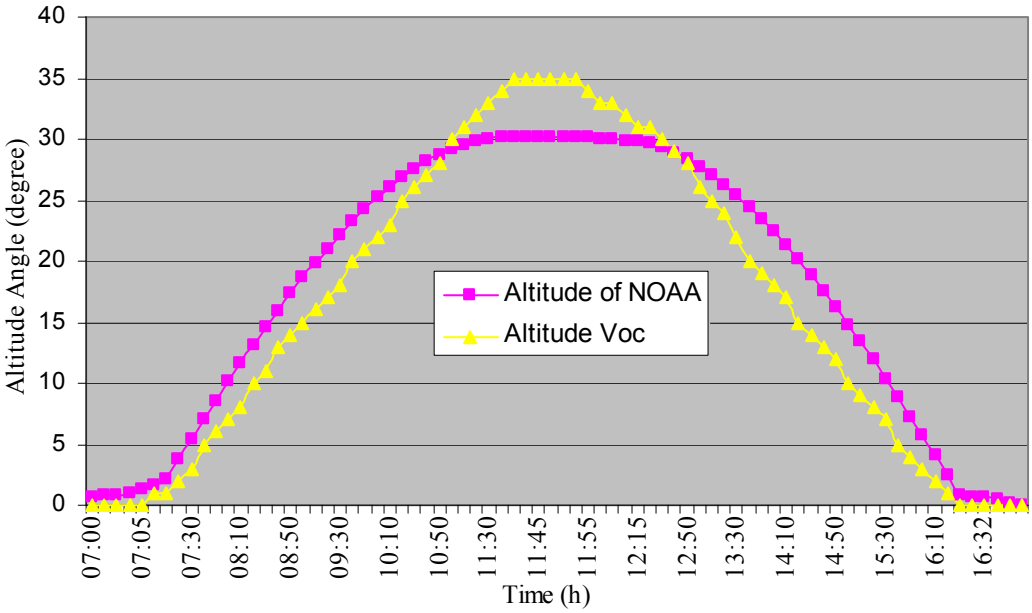

Figure 4.18 Finding altitude angle according to Voc method. February 14, 2008

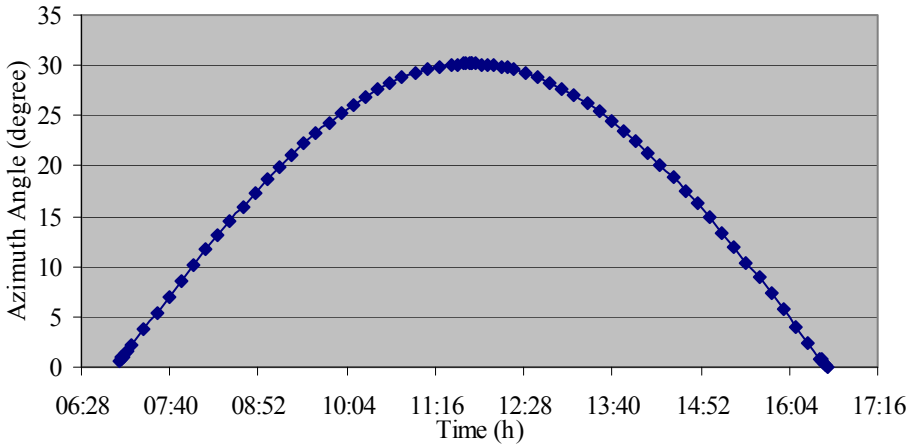

Figure 4.19 Finding azimuth angle according to Voc method February 14, 2008

4.3 Comparison of Performance of Performed Tracking System with a Fixed System

In order to show the increase in PV performance that will be obtained using the tracker, energy production values of the systems that are fixed and moving with two

axes positioned at the south-east angle latitude (37^o from Denizli) are measured at different times. In these measurements, two fixed panels which have 10W and 20W power and two moving panels with the same power levels are compared. During the analysis, two things are taken into consideration.

- Instead of using a method that employs a PV system connected to the battery or fixed load, measurements are made using the method whose details are explained in Chapter 2, which delivers direct maximum panel power. Other measurement methods have misleading results. (The power that a rechargeable battery draws from a fixed or moving panel is the same. This leads to wrong results in performance analysis.)

- All of these activities were performed on sunny days with little or no cloud cover. When a tracker can track the sun, tracker performance must be analyzed only on sunny days during a year. (This rule is taken into consideration in this study.)

Recall that in Chapter 2 a method is employed, which triggers a semiconductor switching component used in the Boost type convertors at the linear region to determine the maximum power point of PV panel. An additional measurement circuit was placed between panels and convertors (Figure 4.20). Using this circuit, existing control system determined the maximum power points of the fixed and moving panels with the measurements taken at one minute intervals. Then the results were transferred to the computer via the serial port.

Separate measurements were made using the panels with 10 and 20 W powers. Since the control circuit that finds the maximum power point is designed to work with high power levels, it has the tolerance ±1W. The tolerance is caused by the change in the OPAMP's characteristic at the output of the current transducer while it is read by ADC of the microcontroller. This problem could have been overcome by adding a voltage follower circuit to the system. However, no more changes were made in the circuit since the aim here was not to use the system as a datalogger.

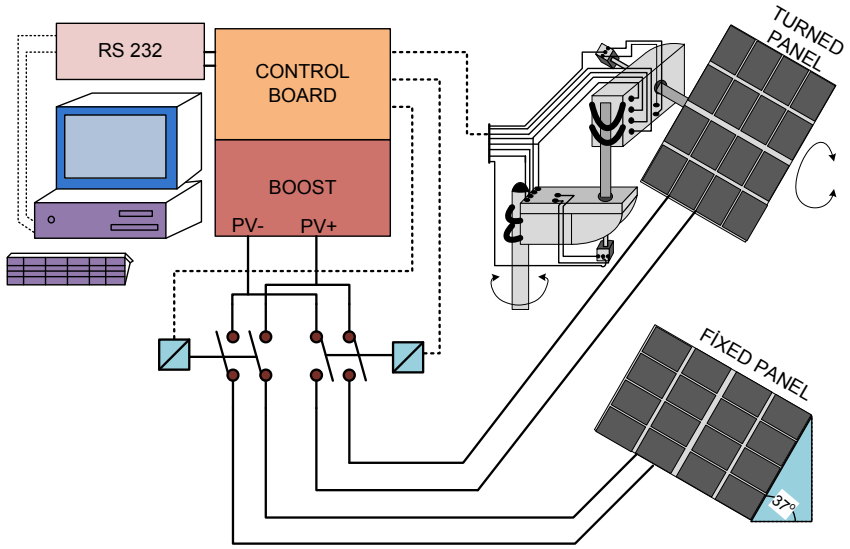

Figure 4.20 Schematic view of two-axis tracking and fixed systems

To verify the correctness of the values measured, a computer program in Visual C# that uses the equations for the sun beam values of fixed and moving systems in the Master Gilbert's book was developed. The comparison of the results obtained from the computer program and the results obtained from the system is as follows.

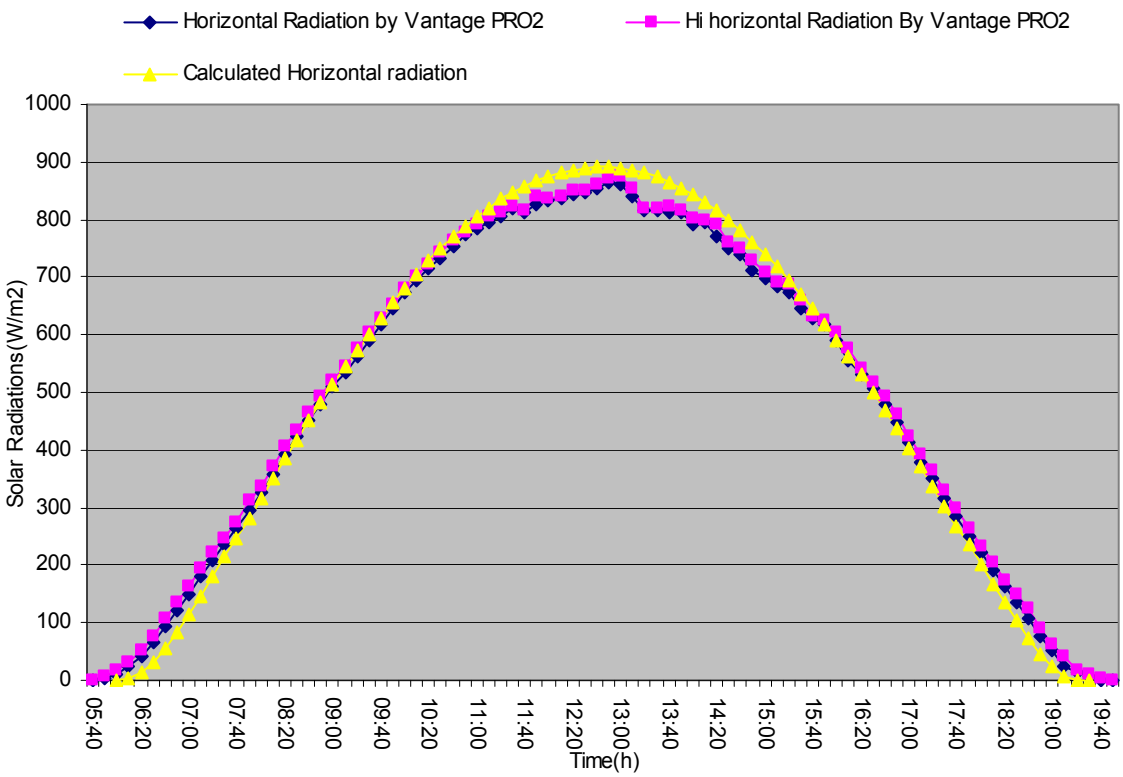

Figure 4.21 Comparison of the horizontal radiation and simulation values on May 2, 2008

The graphics in which the horizontal radiation values taken from Vantage PRO2 measurement device on 2 and 16 May and the ones taken from the simulation program are compared are given Figure 4.21-22-23. Note that in the simulation program the reflected and diffused radiation values were neglected.

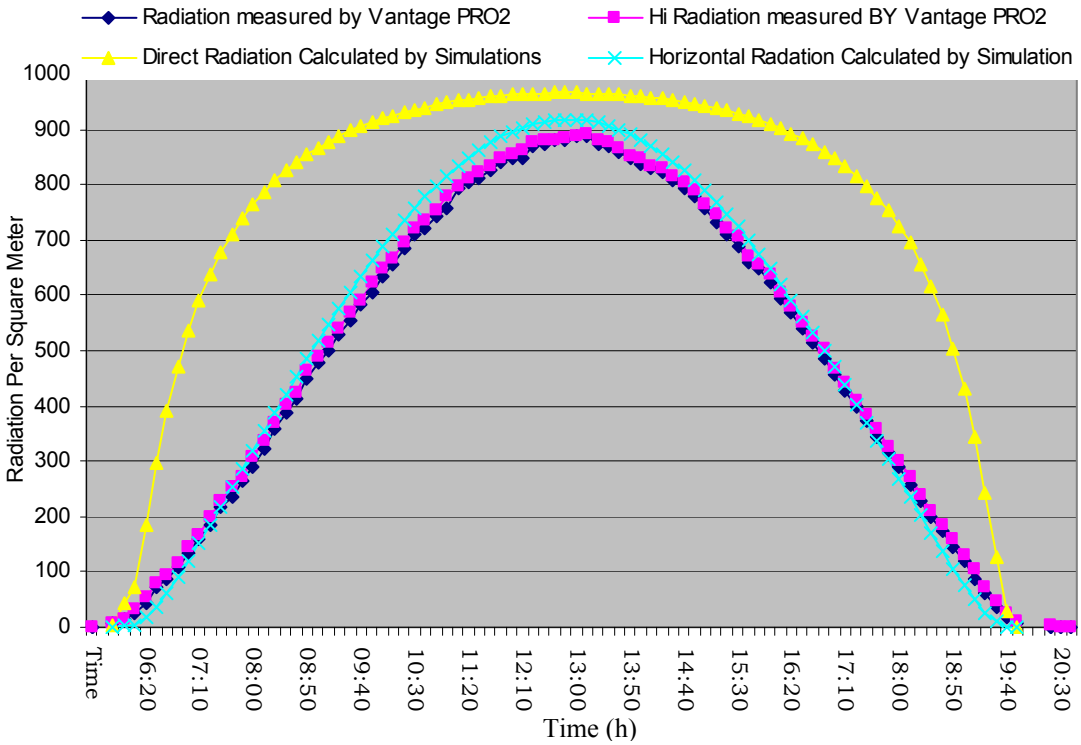

Figure 4.22 Comparison of the horizontal radiation and simulation values on May 16,2008

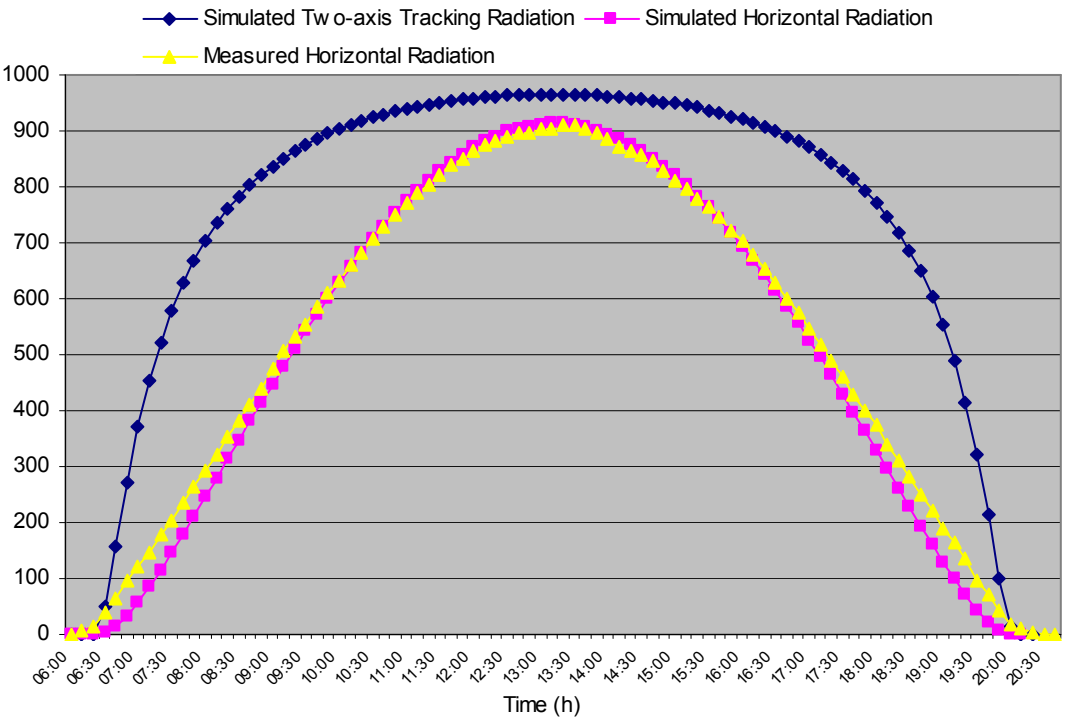

Figure 4.23 Comparison of the horizontal radiation and simulation values on May 13, 2008

The values measured by Vantage PRO2 device are in accordance with the values that come from the simulation program within a certain tolerance. Because of the fact that the simulation results are in harmony with the real values, it can be said that two-axis tracking system values can be obtained from the simulation program. The relationship between simulated and measured values of the two-axis tracking system will be explained in detail in the forthcoming sections.

In the figures below, simulation power values of a fixed panel whose efficiency is 14-16% and directed to the south at 37^{o} and a two-axis sun tracking panel are shown. The panels' power is 10 and 20 W. These simulation power values were compared with the power values of a fixed panel directed to the south at 37^{o} and a panel placed on the two-axis sun tracking panel.

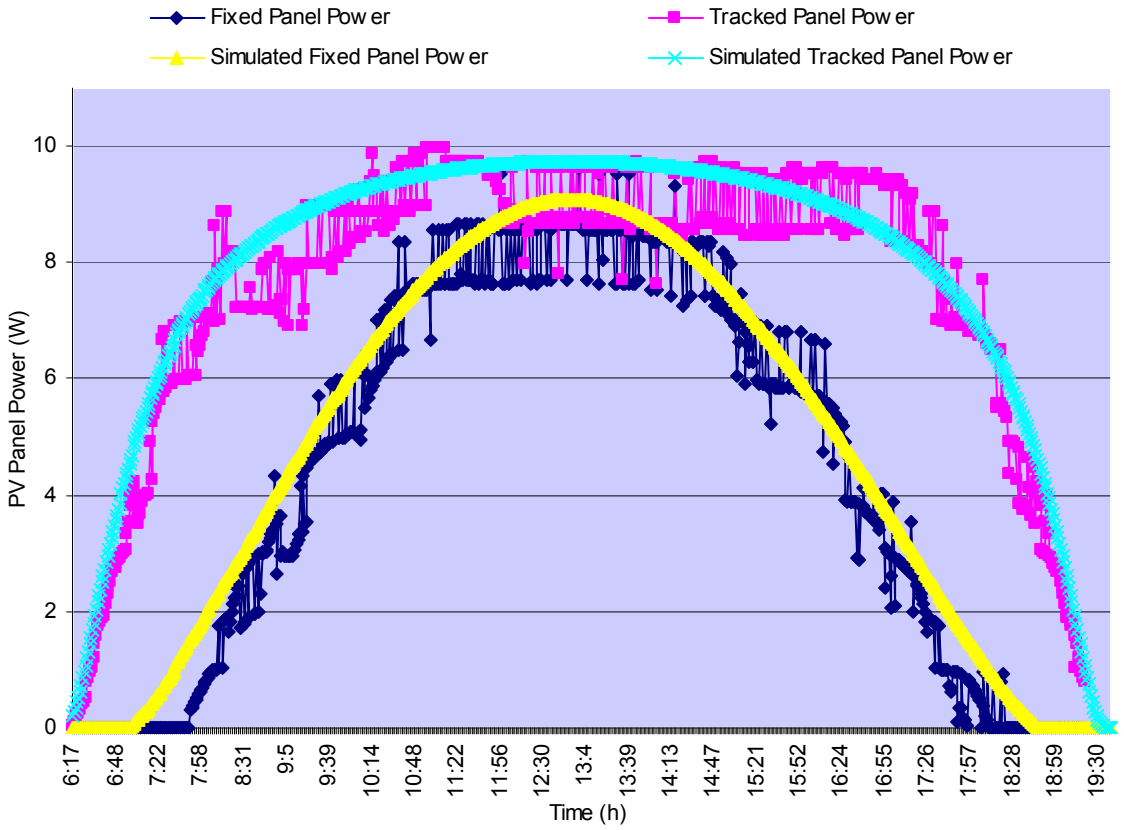

Figure 4.24 Comparison of the simulated and real power values for fixed and moving systems for 10 W panel directed to the south at 37^{o} on May 2, 2008

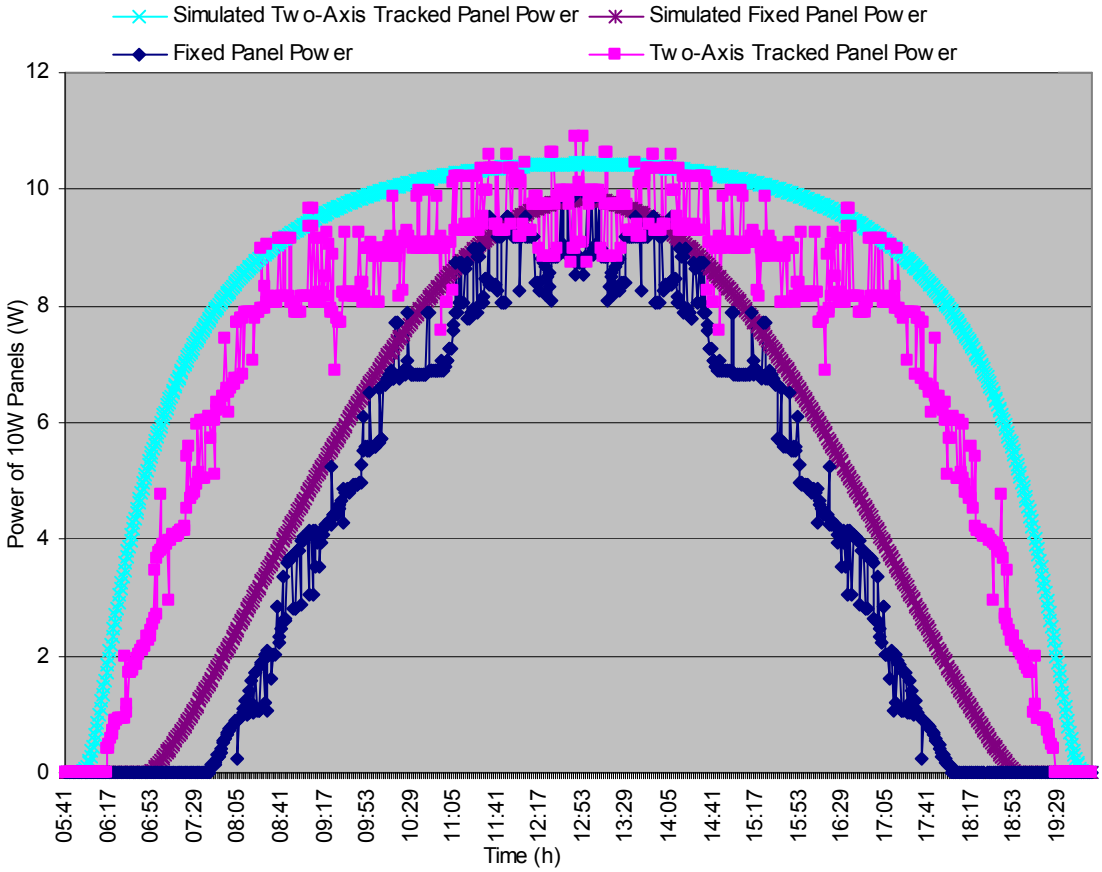

Figure 4.25 Comparison of the simulated and real power values for fixed and moving systems for 10 W panel directed to the south at 37° on May 20, 2008

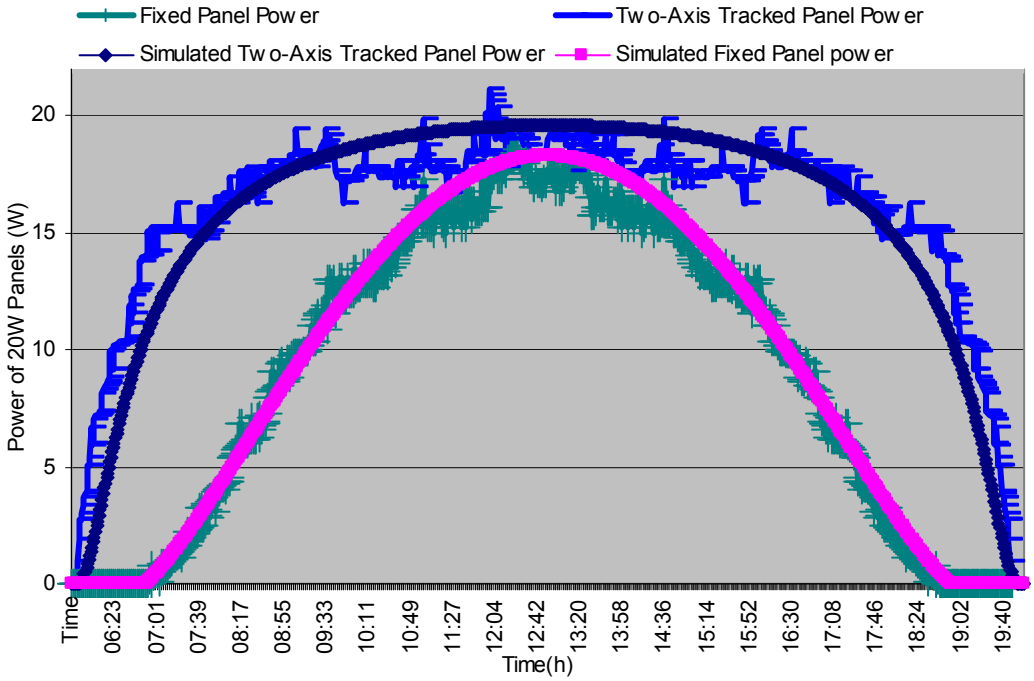

Figure 4.26 Comparison of the simulated and real power values for fixed and moving systems for 20 W panel directed to the south at 37° on May 27, 2008

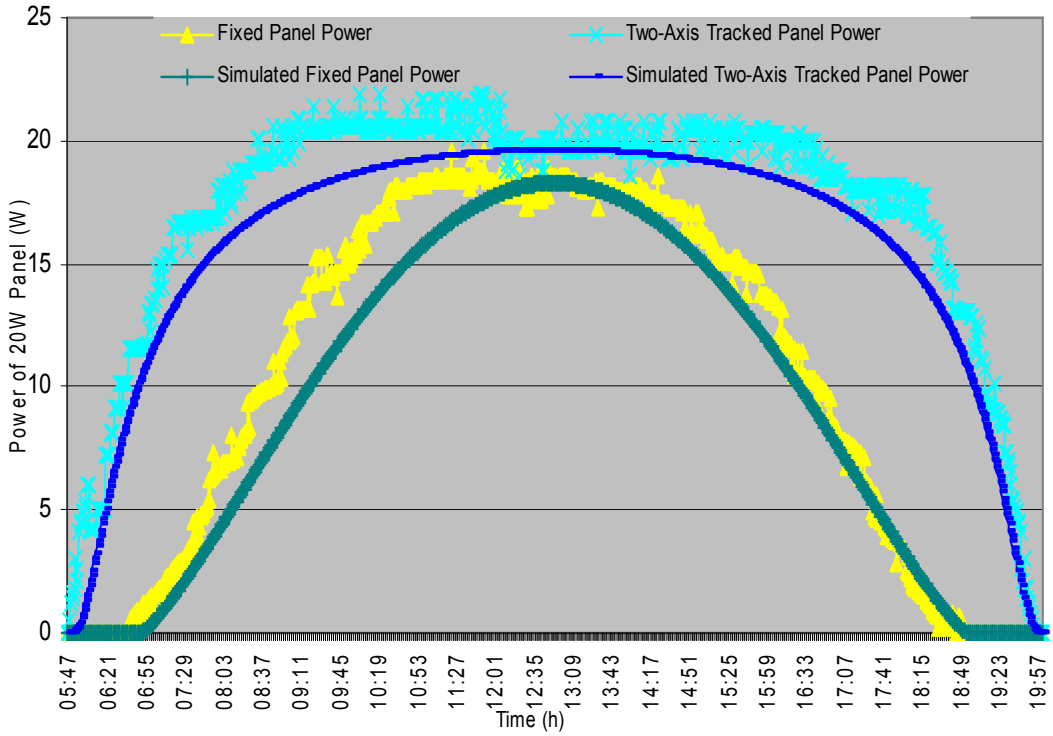

Figure 4.27 Comparison of the simulated and real power values for fixed and moving systems for 20 W panel directed to the south at 37° on May 28, 2008

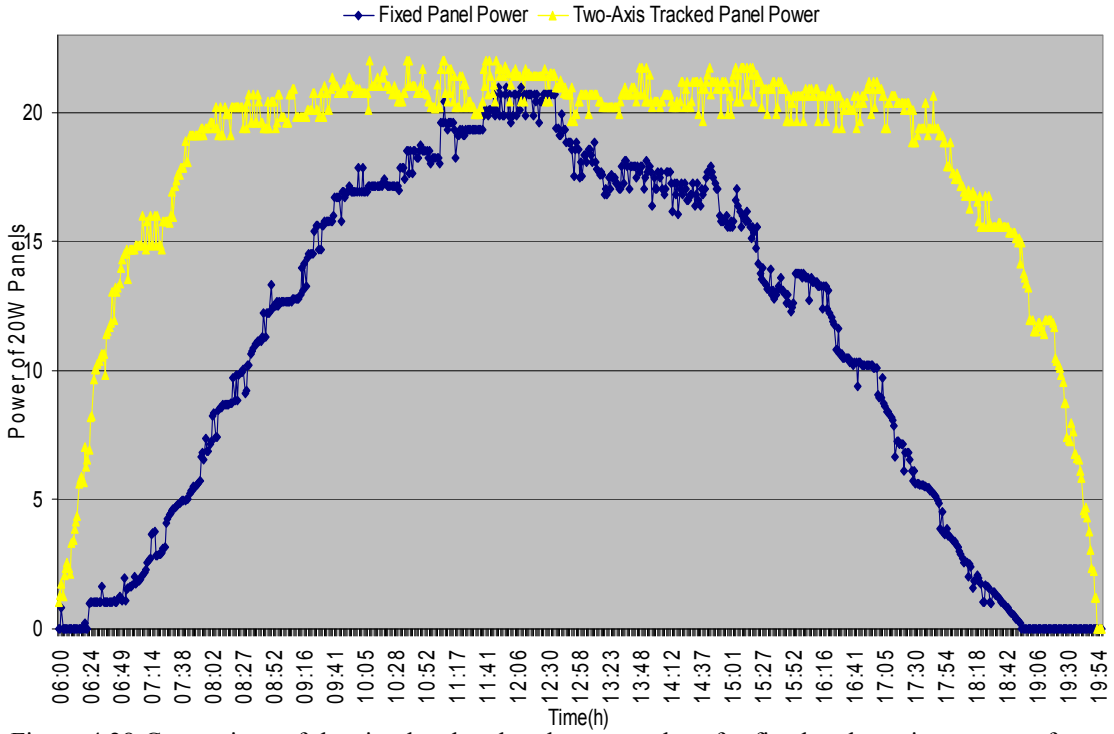

Figure 4.28 Comparison of the simulated and real power values for fixed and moving systems for 20 W panel directed to the south at 37° on May 30, 2008

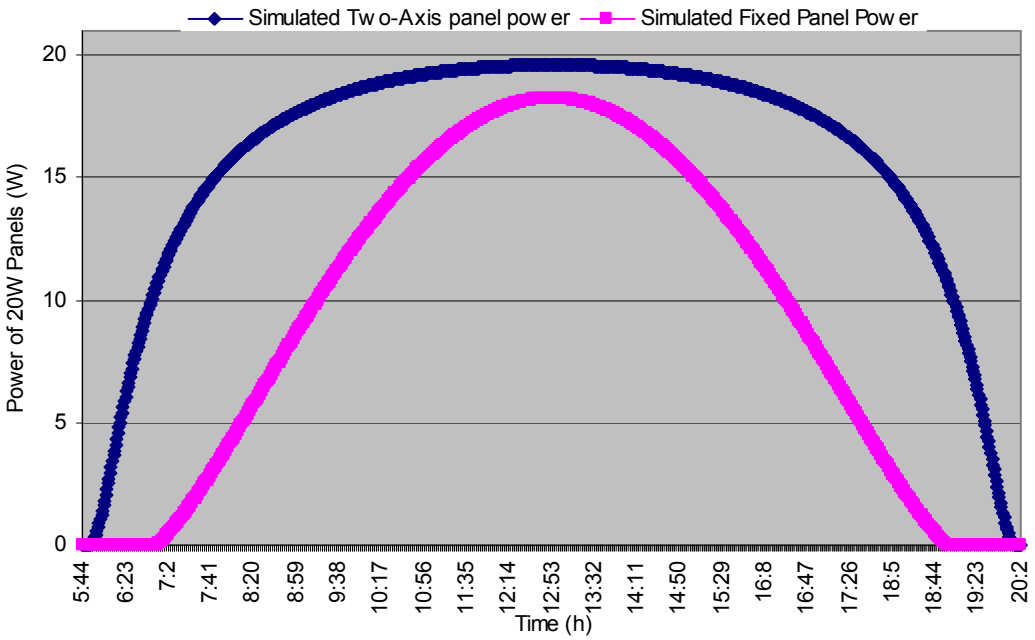

Figure 4.29 Comparison of the simulated and real power values for fixed and moving systems for 20 W panel directed to the south at 37^{o} on May 30, 2008

As seen from the figures above, daily radiation values measured by Vantage PRO2 device are in accordance with the values obtained from the simulation program. Besides, it is seen that the power curves of the fixed and moving systems obtained from the simulation program are in accordance with the results of the measurement system we setup. This leads to the fact that the 3 measurements and evaluation we made are correct. Therefore, it can be expressed that the performance of a fixed system can be compared with the performance of a moving system using the simulation program for the whole year. As an example, let us compare the simulated and measured values taken on May 30, 2008. Without taking reflected and diffused radiation values into account, it is found that radiation performance difference between a panel directed to the south at 37^{o} and a two-axis sun tracking panel is 68%. When reflected and diffused radiation values are taken into account, the difference is found to be 56%. In our work, the performance difference between fixed and moving panels is found to be 64% in May. We can say that our performance analysis has given the correct results considering various factors that depend on weather conditions. Based on this analysis, the results of the simulation analysis for the whole year are given in the following table.

Table 4.1 Solar Energy increasing rate of two-axis tracker with respect to a fixed system.

Month	Tracking System/Fixed system (%)
January	28.77
February	29,27
March	34,26
April	46,4
May	61,57
June	70,9
July	66,3
August	51,57
September	37,5
October	30,26
November	28,66
December	29,08
Annual Average	43,87

The work carried out up to this point has shown that PV trackers must definitely be used in PV systems regardless of whether or not they are expensive. Simply because, using tracker not only decreases the cost but also saves the area used. A system that is set up in the area of 1000 m^2, needs only 600 m^2 when a tracker is employed.

4.4 Conclusions

This study demonstrates that there is no single criterion for choosing open or closed loop control systems if the aim is to have an efficient tracking system. Open loop control tracking systems are more efficient for concentrator or parabolic systems. On the other hand, on a cloudy day, open loop control systems are not enough but only closed control systems are used as explained before the cost is increased and reliability is lower.

Two different tracker systems were designed and produced. They employ the sun tracking methods and control systems developed in this thesis. The first tracker used in the experiments is a small size two-axis tracker as shown in Figure 4.30.

Figure 4.30 A view from the work where two-axis tracking system are compared with a fixed system.

The other tracker is a two-axis tracker that has 1.75 KW power and is illustrated in figure 4.31a.b.c.d. It utilizes only one tenth of the energy (0.6 W/day) of an equivalent tracker available in the market. This tracker was applied to a PV system that supplies the energy of a farmhouse. It has been working efficiently since then. Both open and closed loop systems we developed while working on the prototype were applied to this system. The fact that the cost of our system is half of the cost of an equivalent system will play a key role in its widespread use as time passes.

a.)

b.)

c.)

d.)

Figure 4.31 a.b.c.d) 1.75 kWp two-axis tracking system.

CHAPTER FIVE
CONCLUSION

The study carried out in this thesis consists of three main parts in Chapter two, three, and four, respectively.

Chapter two is devoted to find a new MPPT technique based on semiconductor switch (MOSFET) in linear region on the boost converter. In the boost circuit, both newly discovered MPP finding method and previous MPP finding methods can be used easily. As an example in comparison, we used open circuit voltage method and short circuit current method. The chapter shows experimental results and comparison of old and new techniques. Furthermore, a new tracking method for MPP was developed. Any boost, buck or buck-boost converter must use semiconductor switch. Linear region characteristics of semiconductor switches were used as rheostat. That is, when you drive this component in linear region you can use it as a rheostat. For this purpose a boost converter and its semiconductor switch MOSFET were used in this thesis. This method is very useful for finding MPP. The method we developed to determine MPPs can be used not only on boost converter but also on buck or buck-boost converter. Its cost is very low and implementation power range is very wide. When the output characteristics of designed circuit are analyzed and compared with the others, the results draw attention. There is no need for extra elements (DSP, PLC etc.) except a microcontroller and hall effect current transducer whose costs are very low (both of them are 20$).

This prototype MPP tracking circuit does not only work with the new method, but also works with all the methods proposed previously. The invented MPPT technique was successfully applied to the boost converter. When the new method is compared with the other methods, the new method gives exact results in a short time. Contrary to the other methods, it can find real maximum power point by eliminating the other temporary maximum power points. Furthermore, information on the design of the boost converter and its elements used in the Chapter was given. Practical knowledge in this subject was explained in detail.

Chapter three presents a detailed explanation of battery characteristics and demonstrates an optimum charging algorithm for batteries supported by PV panel. The reason for discussing in depth batteries and their charging techniques is that theoretical and practical work is not sufficient in this subject in Turkey. Besides, considering in detail the diversity of battery charging techniques will play an important role in helping researcher who will work in this subject. One important point in this chapter is that all the charging methods given in detail were implemented successfully using the circuit we developed. In this chapter, batteries are classified and lead acid batteries are analyzed in detail since they are cheap and widespread.

Contrary to classical methods, in this study, the control system determines the internal resistance of batteries before batteries is charged. Than, it charges batteries properly by taking this resistance in to consideration. Batteries can be charged fully by this way (Since classical charge devices do not have this property, they cannot charge batteries fully). Generally the controller of the charger can not recognize the load connected parallel to batteries. In the proposed study, regardless of whether or not a load is connected to batteries, batteries can be tested using a small test load and control circuit finds out whether load connected to batteries. Also, two different charge control methods were applied. The characteristics of lead acid batteries are nonlinear and change from battery to battery. The experience and knowledge we have show that charge characteristics of lead acid batteries change with respect to the type of lead acid batteries. The charger is operated to transfer maximum power of PV panel determined by the control circuits to batteries. A lot of study and experiments should be done to increase battery capacity and battery cycle life. With the developed circuit, further work can easily be carried out.

Chapter four classifies tracking systems and demonstrates the a new two-axes tracking system controlled by Microcontroller. Tracking of the sun was done by both open-loop and closed-loop control methods. The azimuth and altitude functions of the sun were used in the open-loop control method. The open circuit voltages of PV panel changes were used in closed-loop control method. We concluded that the sun

should be track with a system that employs both open and closed-loop controls at the same time. Although open-loop control tracking systems are more efficient for concentrator or parabolic system, it will not be so in a cloudy day. If only closed-loop control system is used as explained before, the cost increases and reliability diminishes. The two-axes tracking systems are generally controlled by DSP, PLC, or PC. The cost of such control systems is so high. We developed two-axes tracking system controlled by a microcontroller. This system can track the sun with respect to open-loop or closed-loop control techniques. Using sun position formulas, it can find altitude and azimuth angles of the sun exactly for a given time. In addition, it has the ability to be improved further for future applications. The tracker we developed as a prototype was easily adapted to large-scale trackers. For this purpose, a PV system with 1.75kWp power was developed, which follows the sun in two axes. The mechanism and the control of the system were originally developed by the author and there is no system that resembles our system to the best knowledge of the author. One more point is that components used to build the tracker are cheap and can easily be obtained from the market.

The results of simulation and measurements we implemented make it clear how important is a tracker in a PV system. It was proved that a system with a tracker produces 40% more energy per year. Even in summer where energy production increase is more than 60%, it was concluded that trackers are crucially important for irrigation systems.

The developed tracking system can be used for PV panel systems or parabolic collectors, which tracks the sun with high sensitivity. Our work on developing a tracker that makes the water heating collectors track the sun using this method is ongoing.

To summarize, the system we developed is able to achieve sun tracking, maximum power point tracking and battery charging with optimum efficiency at the same time. All of these features are performed with a single electronic circuit which is very cheap.

The control system we developed has a flexible structure that can be used fr further work. Its software can also be developed further. For example, we implemented the comparison of a fix and moving system with a small circuit on this system. Even there is no need to adapt the control system to large systems, our work can easily be used as a sun tracking mechanism for pyrnometers.

The three works based on this thesis work we have already implemented and have been implementing shows clearly that the system we developed is flexible and suitable for widespread usage.

REFERENCES

Arias J.& Linera, F.F., Ramos J. M., M. Alberto & Cambronero J. (2004). A Modular PV Regulator Based on Microcontroller with Maximum Power Point Tracking. *IEEE.* 0-7803-8486-5/04/$20.00 IEEE

Alghuwainem, S. M. (1994). Matching of a dc motor to a photovoltaic generator using a step-up converter with a current-locked loop. *IEEE Trans. Energy Conversion, vol. 9,* pp. 192–198.

Andersen, M.& Alvsten, T.B. (1995). 200W Low cost module integrated utility interface for modular photovoltaic energy systems. *Proceedings of IECON '95 1* .pp. 572–577.

Abou El Ela, M.& Roger, J. (1984). Optimization of the function of a photovoltaic array using a feedback control system. *Solar Cells: Their Science, Technology, Applications and Economics 13 (2)* .pp. 185–195.

Alghuwainem, S.M. (1994). Matching of a dc motor to a photovoltaic generator using a step-up converter with a current-locked loop. *IEEE Trans. Energy Conversion 9* .pp. 192–198.

Abd El-Shafy, Faten, A.N. H.F. Abou El-Zahab, E.M. (2003). Evaluation of a proper controller performance for maximum-power point tracking of a stand-alone PV system. *Solar Energy Mater. Solar Cells 75* pp. 723–728.

Al-Atrash, Batarseh, H. Rustom, I. K. (2005). Statistical modeling of DSP-based hill-climbing MPPT algorithms in noisy environments Applied Power Electronics Conference and Exposition. *Twentieth Annual IEEE,* APEC 2005, vol. 3, pp. 1773–1777.

Abdallah, S. & Salem, N. (2003). Two axes sun tracking system with PLC control. *Energy Conversion and Management Volume 45, Issues 11-12*, pp 1931-1939, Elsevier Ltd.

Bilgin Z.(2006). *Design and Realizing Sun Tracking System*. .M.SC. Thesis Institute of Science and Technology Gazi University, ANKARA

Branbrilla,A. Gambarara, M. Garutti, A. Ronchi, F. (1999). New approach to photovoltaic arrays maximum power point tracking. *30th IEEE Power Electronics Conference*. pp. 632–637.

Bavaro, L.T.W. (1988). Power regulation utilizing only battery current monitoring. *Patent, US4,794,272.*

Cocconi, A. Rippel, W. (1990). Lectures from GM sun racer case history. The Sun racer power systems. Number M-101, *Society of Automotive Engineers,* Inc., Warderendale, PA. lecture 3-1:

Chetty, P.(1986). Maximum power transfer system for a solar cell array. *US4.* pp.604-567.

Crompton, C.R (2000). *Battery reference book.* (3rd Ed.). OXFORD: Newnes.

Charles, A.H. (1997). *Passive electronic component handbook* (First ed.). OH: McGraw- Hill.

Chris Cornwall, Aaron Horiuchi and Chris Lehman, 12/04/2007 from http://www.srrb.noaa.gov/highlights/sunrise/azel.html

Denizinger, W (1995. Electrical power subsystem of globalstar. *Proceedings of the European Space Conference.* pp. 171–174.

David, J.H. (1968). Power conditioning system. *US3,384,806.*

Erickson, R. W.(2000). *Fundamentals of Power Electronics. Second Edition. Secaucus*. NJ, USA. Kluwer Academic Publishers, p 19.

Enslin, J. H. R. (1995). Photovoltaic and wind energy system design and sizing. *Notes of 3rd Photovoltaic System Design Short Course,* Univ. Stellenbosch, Stellenbosch, South Africa

Enslin, J. H. R. (1991). Renewable energy as an economic energy source for remote areas. *Renewable Energy*, vol. 1, no. 2, pp. 243–248.

Enslin, J.H.R., Wolf, M.S., Snyman, D.B. & Swiegers, W. (1997). Integrated photovoltaic maximum power point tracking converter. *IEEE Trans. Ind. Electronics. vol. 44.* pp. 769-773.

Erickson, R.W., & Maksimovic, D. (1950). *Fundamentals of power electronics*. (2nd Edn.). pp. 39–55, New York, USA, John Wiley

Femia, N. Petrone, G. Spagnuolo, G. Vitelli, M. (2005). Optimization of perturb and observe maximum power point tracking method. *IEEE Trans. Power Electron*. pp 963–973.

Fraunhofer Institute for Solar Energy System ISE (2005). Annual Report. Page 52-53.

Harrington, S., & Dunlop, J.(1992).*Battery Charge Controller Characteristics in Photovoltaic Systems*. IEEE Aerosp. Electron. Syst. Mag., 15–21.

H.E.-S.A. Ibrahim, et al., (1999). Microcomputer controlled buck regulator for maximum power point tracker for DC pumping system operates from photovoltaic system. *Fuzzy Systems Conference Proceedings, FUZZIEEE'99. IEEE International 1 (22–25)* .pp. 406–411.

Hamdy, M.A. (1994). A new model for the current-voltage output characteristics of photovoltaic modules. *J. Power Sources 50 (1–2)*.pp. 11–20.

Harrington, S., & Dunlop, J.(1992).*Battery Charge Controller Characteristics in Photovoltaic Systems*. IEEE Aerosp. Electron. Syst. Mag., 15–21.

Hart. Daniel W. (1997). *Introduction to Power Electronics*NJ, USA, ,pp.196-200. Prentice Hall Inc. Upper Saddle River,

Hart, D.W. (1964). *Introduction to power electronics*. New York, USA, pp. 212–214. Prentice-Hall,

Hussein, K.H. Muta, I. Hoshino, T. Osakada, M. (1995). Maximum photovoltaic power tracking: an algorithm for rapidly changing atmospheric conditions. *IEE Proc. Generation Transmission Distrib.* pp 59–64.

Hohm, D.P. Ropp, M.E. (2003). Comparative study of maximum power point tracking algorithms. *Prog. Photovolt: Res. Appl*. pp 47–62.

Hua, Ch.& Shen, Ch. (1998). Comparative study of peak power tracking techniques for solar storage system. *IEEE Applied Power Electronics Conference and Exposition (APEC'98), vol. 2*. pp. 679–685.

Hua, Ch., Lin, J. & Shen, Ch. (1998). Implementation of a DSP-controlled PV system with peak power tracking. *IEEE Trans. Ind. Electron. 45 (1)*.pp. 99–107.

Hiyama, T. et al. (1995). Identification of optimal operation point of PV modules using neural network for real time maximum power tracking control. *IEEE Trans. Energy Conversion 10.* pp.360–367.

Hiyama, T. et al. (1995). Evaluation of neural network based real time maximum power tracking controller for PV system, *IEEE Trans. Energy Conversion 10.* pp. 543–548.

Hiyama T., et al. (1997). Neural network based estimation of maximum power generation. *IEEE Trans. Energy Conversion 12* pp.241–247.

Kim, Y. Jo, H. Kim, D. (1996). A new peak power tracker for cost-effective photovoltaic power systems. *IEEE Proc. Energy Conversion Eng. Conf. IECEC 96*. pp 1673–1678.

K.C. Tseng & T.J. Liang (2004). Novel high-efficiency step-up converte. Vol. 151, No. 2, pp182-190, *IEE Proc-Electr. Power Appl*

Koutroulis, E. & Kalaitzakis, K. (2004). *Novel battery charging regulation system for photovoltaic applications*. IEE Proc.-Electr. Power Appl., 151, 191-197.

Louis, A.U. (1972). System for detecting and utilizing the maximum available power from solar cells. *Patent US3, 696,286.*

Lafferty,D. (1993). Regulating control circuit for photovoltaic source employing switches, energy storage, and pulse width modulation controller, *Patent US5,270,636.*

Liu, X. Lopes, L.A. (2004). An improved perturbation and observation maximum power point tracking algorithm for PV arrays. *Power Electronics Specialists Conference*. PESC 04. 2004, IEEE35th Annual vol. 3, 2004, 2005–2010.

Lafferty, D. (1989). Coupling network for improving conversion efficiency of photovoltaic power source.*US4*.pp.873,480.

Luque, A. & Hegedus, S. (2003). "*Handbook of Photovoltaic Science and Engineering"*. John Wiley & Sons

Lee, D.-Y., Noh, H.-J., Hyun, D.-S. & Ick, C. (2003) .An Improved MPPT Converter Using Current Compensation Method for Small Scaled PV-Applications. *IEEE Ind. Electronics.* pp. 540-545, 0-7803-7768-0/03 IEEE

Luque, A. & Hegedus, S. (2003). *Handbook of Photovoltaic Science and Engineering.* 111 River Street, Hoboken; NJ 07030, USA John Wiley & Sons Inc.

Masoum, M. A. S., Dehbonei H. & Fuchs, E. F. (2002).Theoretical and Experimental Analyses of Photovoltaic Systems With Voltage- and Current-Based Maximum Power-Point Tracking. *IEEE transactions on energy conversion*, vol. 17, no. 4

Masoum, M.A.S. et al, (1998). Optimal power point tracking of photovoltaic system under all operating conditions. *17th Congress of the World Energy Council*, Houston, TX

Maheshappa, H.D., Nagaraju, J.& Murthy, M.V. (1998). An improved maximum power point tracker using a step-up converter with current locked loop. *Renew. Energy 13 (2)* .pp. 195–201.

Masoum, M.A.S. et al.(1999). Design, construction and testing of a voltage-based maximum power point tracker (VMPPT) for small satellite power supply. *13th Annual AIAA/USU Conference, Small Satellite.*

Masters, Gilbert M. (2004). *Renewable and Efficient Electric Power Systems*. pp 392-419. Hoboken NJ, USA: John Willey & Sons Incorporated,.

Markvart, T.,& Castafier, L.(2003). *Practical Handbook of Photovoltaic Fundamentals and Application*. Elsevier Ltd, Oxford UK, 589-621

Markvart, T. & Luis, C. (2003). *Practical Handbook of Photovoltaics: Fundamentals and Applications.* Elsevier Advanced Technology, The Boulevard. Langford Lane, Kidlington Oxford OX5 lGB, UK. pp.556

Mohan, N. Undeland, T. M. & Robbins, W. P. (1995). *Power Electronics: Converters, Applications, and Desig.,* 2nd ed., John Wiley & Sons, New York,

Messenger, R. A. & Ventre, J. (2005). *Photovoltaic Systems Engineering* (second ed.). London: Taylor & Francis

Mohan, N. Undeland, T.M., & Robbins,W.P (1995). *Power electronics*. (2nd Edn.). New York, USA. pp. 172–178. John Wiley & Sons Inc

Miyatake, M. Kouno, T. Nakano, M. (2002). A simple maximum power point tracking control employing fibonacci search algorithm for power conditioners of photovoltaic generators. *EPE-PEMC'02,* Cavtat & Dubrovnik

Messenger, R. A., & Ventre, J. (2004). *Photovoltaic Systems Engineering*. (2nd ed.). CRC Pres: New York.

Mukund, R. P. (1999). *Wind and solar power systems*. pp 155, Merchant Marine Academy Kings Point: New York, U.S.

Messenger, R. A., & Ventre J. (2005). *Photovoltaic Systems Engineering* (second ed.). London: Taylor & Francis

Neville, R.C. (1978). *Solar energy collector orientation and tracking mode*. pp. 7-11. Solar Energy 20

Nishioka, K. et al. (2003). Analysis of the temperature characteristics in polycrystalline Si solar cells using modified equivalent circuit model. *Jpn. J. Appl. Phys. 42 (12)*.pp.7175–7179.

Noguchi, T., Togashi, S. & Nakamoto, R. (2002). Short-current pulse-based maximum-power-point tracking method for multiple photovoltaic-and-converter module system. *IEEE Trans. Ind. Electronics*. *vol. 49*, pp. 217-223.

Noguchi, T., Togashi S. & Nakamoto, R. (2000). Short-Current Pulse Based Adaptive Maximum-Power-Point Tracking for Photovoltaic Power Generation System. *ISIE'2000*, pp.157-167.

Phang, J.C.H., Chan, D.S.H., & Phillips, J.R. (1984). Accurate analytical method for the extraction of solar cell. *Electron. Lett. 20 (10)* .pp. 406–408.

Perez R. (1991). *Things that Work*!. The Wattsun Two-Axis PV Tracker Home Power #25. Hornbrook,

Patel, M. R.(1999). *Wind and Solar Power Systems* (first Ed.) New York, CRC Press LLC.

Patcharaprakiti, N. Premrudeepreechacharn, S. Sriuthaisiriwong, Y. (2005). Maximum power point tracking using adaptive fuzzy logic control for grid-connected photovoltaic system. *Renew. Energy 30.* pp. 1771–1788.

Poulek, V.& Libra, M. *new bıfacıal solar trackers and trackıng concentrators. http://www.pvresources.com/en/arhiv/bifactracking.pdf*

Richard Perez,2004, '*to track or no to track'* 2007 from http://www.homepower.com/article/?file=HP101_pg60_Perez

Roger A. & Messenger J. V. (2005). *Photovoltaic Systems Engineering*. Taylor & Francis e-Library, pp.57-62,

Ross, J., Markvart, T., & He, W.(2000). *Modeling battery charge regulation for a stand-alone photovoltaic system*, Sol. Energy, 69,181–190.

Rashid, M. H. (1993). *Power Electronics*. pp.309-323. Upper Saddle River, NJ,USA. *Prentice Hall Inc.*

Ross, J., Markvart, T., & He, W.(2000). *Modeling battery charge regulation for a stand-alone photovoltaic system*, Sol. Energy, 69,181–190.

RASHID, Muhammad H. (2001): *Power Electronics Handbook*. (Academic Press Series in Engineering). San Diego, CA: Academic Press. A Harcourt Sciene and Technology Company.

Sedra S. A., & Smith C. K. (2004), "*Microelectronic Circuits"* ,fifth ed. pp.1266-1269 Oxfort University Press, New York, USA

Schoeman, J.J.& Wyk, J.D.V.(1982). A simplified maximal power controller for terrestrial photovoltaic panel arrays. *IEEE Power Electronics Specialists Conference. PESC '82 Record. New York, NY.* pp. 361–367.

Salas, V., Ol as, E., Barrado, A. & A. Lazaro, (2005). Review of the maximum power point tracking algorithms for stand-alone photovoltaic systems. *Elsevier*

Salas, V., Ol as, E., Lazaro, A. & Barrado, A. (2005). New algorithm using only one variable measurement applied to a maximum power point tracker. *Solar Energy Mater. Solar Cells 1–4* pp. 675–684.

Salas, V., Ol as, E., Lazaro, A. & Barrado, A. (2005). Evaluation of a new maximum power point tracker (MPPT) applied to the photovoltaic stand-alone systems. *Solar Energy Mater. Solar Cells 87 (1–4)* .pp. 807–815.

Schaefer, J.F.& Hise, L. (1984). An inexpensive photovoltaic array maximum-power-point-tracking DC-to-DC converter. *Number NMSEI/TN-84-1 New Mexico Solar Energy Institute*, Las Cruces, New Mexico 88003, Mayo

Salameh, Z., Dagher, F.& Lynch, W. (1991). Step-down maximum power point tracker for photovoltaic systems. *Solar Energy 46 (5)*.pp. 279–282.

Salameh, Z. & Taylor, D. (1990). Step-up maximum power point tracker for photovoltaic arrays. *Solar Energy 44 (1)*.pp.57–61.

Topology for Decentralised Solar Energy Inverters with a Low Voltage AC-Bus Björn Lindgren CHALMERS UNIVERSITY OF TECHNOLOGY Department of Electrical Power Engineering SE-412 96 Göteborg, Sweden 1633 from http://www.elkraft.chalmers.se

Tse, K.K. Chung, H.S.H. Hui, S.Y.R. Ho, M.T. (2001). A novel maximum power point tracking technique for PV panels. *IEEE Power Electronics Specialists Conference*, PESC. 2001 IEEE, vol. 4, pp 1970–1975.

Takashima, T., Tanaka, T., Amano, M. & Ando, Y. (2000). Maximum output control of photovoltaic (PV) array. *Intersociety Energy Conversion Engineering Conference and Exhibit (IECEC), 35th*. pp. 380–383.

Takehara, N. & Kurokami, S. (1997). Power control apparatus and method and power generating system using them. *Patent US5*.pp. 654-883.

UO Solar Radiation Monitoring Laboratory, 05/03/2007 http://solardat.uoregon.edu/SunChartProgram.html

Veerachary, M. Senjyu, T. Uezato, K. (2003). Neural-network-based maximum-power-point tracking of coupled inductor interleaved-boost-converter-supplied PV system using fuzzy controller. *IEEE Trans. Ind. Electron.* pp749–758.

Wilamowski, B.M. et al., (2001). Microprocessor implementation of fuzzy system and neural networks. *International Joint Conference on Neural Networks*, vol. 1, Washington, DC, pp. 234–239.

W.J.A. Teulings, J.C. Marpinard, A. Capel, A maximum power point tracker for a regulated power bus, in: Proceedings of the European Space Conference, 1993.

Won, C.-Y. Kim, D.-H. Kim, S.-C. Kim, W.-S. Kim, H.-S. (1994). A new maximum power point tracker of photovoltaic arrays using fuzzy controller. *25th Annual IEEE Power Electronics Specialists Conference*. PESC '94 Record, vol. 1, pp. 396–403.

Yamazaki, T., & Muramoto, K. (1998). *An advanced solar charging and battery discharge controller unit.* Renew. Energy., 15, 606–609.